Elucidating ribosome-dependent molecular mechanism of YchF

by

Kevin Ti Yen Lim

A Thesis submitted to the Faculty of Graduate and Postdoctoral Studies of the University of Manitoba in partial fulfilment of the requirements of the degree of

Master of Science

Department of Microbiology

University of Manitoba

Winnipeg, Manitoba, Canada

Copyright © 2026 by Kevin Ti Yen Lim

Abstract

Translation is the final step of gene expression in every living cell where proteins are assembled by the ribosome in a template-dependent manner. Guanosine triphosphatases (GTPases) act as molecular switches by hydrolyzing guanosine triphosphate (GTP) to regulate the ribosome's progression through the different steps of translation. A highly conserved protein sequence known as the G4 motif imparts guanine nucleotide specificity in nearly all GTPases. *Escherichia coli* YchF despite sharing structural and sequence similarities to other well-studied GTPases, contains a G4 motif that preferentially binds adenosine triphosphate (ATP) and has been shown in bacteria to be stimulated by the ribosome. Translational GTPases typically adopt distinct nucleotide-bound conformational states (GTP, GDP and unbound; *apo*), upon binding to their respective nucleotides. Yet, YchF's unique ability to bind to both adenine and guanine nucleotides has raised questions as to whether it operates as an ATP- or GTP-dependent molecular switch. Assessing the role that the G4 motif plays in the switch-like behavior of YchF will be crucial for deciphering YchF's molecular mechanism. Therefore, in this biochemical study, I investigated whether modifying YchF's G4 motif alters its nucleotide specificity and the nucleotide conformational states it adopts. Wild-type *E. coli* YchF and G4 motifs variants were overexpressed from recombinant plasmids and subsequently purified. The binding affinities were determined using equilibrium fluorescence titration with unlabelled and fluorescently labelled di/triphosphate nucleotides. I report that modifying the G4 motif to either retain or abolish adenine nucleotide specificity of YchF is reflect in the binding affinities. The presence of distinct nucleotide-bound states was probed using limited trypsinolysis and cleavage patterns analyzed on SDS-PAGE. Regardless of whether adenine nucleotide specificity is retained, I report that YchF adopts distinct 3-dimensional structure dependent on whether ATP or ADP is bound, showing first evidence that YchF does behave as an ATP-dependent switch.

Acknowledgements

I want to deeply thank my friends and family who has been with me throughout my life and instilling the beliefs that led me to pursue research in the first place. To my Mom for instilling love and morales that helped me see life full of colours. To my Dad who for his dedication to the family through hard work and labour. To my little sister, Victoria Lim for being my one and only sister who made sure I have someone to take care of. To my friend Ryan Sunga since junior high for sharing many laughs over games and our love for Star Wars. To my high school teachers Mrs. Malolos, Mrs. Nario, Mr. Dyer and Mr. Ottenbreit for helping me realize my passion for math and science when I was in high school. Lastly, to my cousin Benchmen Trieu for being my role model in school and your patience in tutoring me when I didn't know anyone better.

It was almost 4 years ago that I found my passion for academic research which ultimately led to the completion of my thesis. I would like to thank my amazing supervisor, Prof. Hans-Joachim Wieden for recognizing my potential and being with me each step of the way. Your expertise, guidance and patience helped me push past my limitations and to always strive for more.

Upon entering the Wieden lab group in summer 2023, I didn't know my capacity to operate as a researcher and what I could accomplish. Despite my doubts, the Wieden lab; both past and present, helped me realize that. You all have helped me develop myself professionally, but also emotionally at each step of the way and I wanted to thank you all individually. To Amanda Vazquez Gonzalez, for being my mentor when I started as a summer student and into my honour's thesis. You taught me everything you could to help me develop my own technical skills and prepare me for the M.Sc program. To Fabian Rhoden for your constructive criticism on my presentation and writing. Your charismatic personality helped me bolster my own well-being, more times than I could count and I am eternally grateful. I learned a lot from you and your experience made me realize my passion for scientific communications. To Jessica Semmelrock and Fan Mo for helping provide technical advice for me to troubleshoot my experiments. Although I still have much to learn, you both have been key mentors to me since the beginning of my M.Sc program and your continued support allowed me to develop my own problem-solving skills. Lastly, to Noah Boutang for brightening up the lab each day with funny jokes. You definitely went Glow Big or Go Home!

I would like to express my thanks to my committee members, Prof. Mazdak Kahjehpour and Prof. Denice Bay for their careful guidance, patience and continued support. A big thank you to Prof. Nediljko Budisa and your lab group for kindly mentoring me. Your whimsical personality and dedication to overseeing my development via Prairie iGEM help laid the foundations for my future as a graduate student and allowed me to meet Prof. Hans-Joachim Wieden. To all members of the Kothe lab; both past (Dr. Sarah Schultz, Timothy Vos and Dr. Runhua Han) and present (Daniel Rocca and Tirathjot Kaur), I thank you for your expertise and guidance throughout my project. I cherished the outings we had all together and hope you liked the Costco pizzas I brought!

Finally, I would like to thank all my funding sources (UMGF, NSERC, UM Faculty of Science, and the Innovation Hub), U of M staff members, Microbiology department and Mikey (the custodian staff). You all helped ensure that university operations occur smoothly everyday, ensuring me peace of mind!

Dedication

I wanted to dedicate this section to my Mom and Dad who worked so hard everyday to put food on the table and a house over our heads so that me and my little sister could rest with a peace of mind each night. Thank you from the bottom of my heart, I will return the favour a thousand-fold in my own way, so please continue to watch over me.

I also wanted to show my upmost appreciation to my friends and colleagues I recently met in the last year of my studies. To Linh Phan, Kristina Trieu, Brian Nguyen, Nguyen Hoang, Sanjana Fawziyah, Harry Vu, Linh Chi, Anh Truong and the rest of the Wesley and Leah team. You all watched me grow exponentially to become a better version of myself each day. Despite the hardships I faced in life, you all were there to comfort me during my times of need and accepted my shortcomings. From the bottom of my heart, I couldn't have asked for amazing friends.

Table of Contents

Abstract ..... **i**

Acknowledgements ..... **ii**

Dedication ..... **iii**

Table of Contents ..... **iv**

List of Tables ..... **vii**

List of Figures ..... **viii**

List of Abbreviations ..... **ix**

1. Introduction **1**

1.1. The ribosome **2**

1.1.1. Functional cycle **3**

1.1.2. Regulation of the functional cycle **3**

1.1.2.1. Initiation **4**

1.1.2.2. Elongation **5**

1.1.2.3. Termination **7**

1.1.2.4. Ribosome recycling **8**

1.1.2.5. Stress response **9**

1.1.2.5.1. Cold shock response **10**

1.1.2.5.2. Antibiotic stress response **11**

1.2. GTPases; the molecular switch of the cell **13**

1.2.1. G-domain **14**

1.2.1.1. G1-G5 motifs **16**

1.2.1.2. The G4 motif imparts GTP-binding specificity **21**

1.2.2. Functional cycle of GTPases **22**

1.2.2.1. GTPase-activating proteins/factors (GAP/Fs) **22**

1.2.2.2. Guanine nucleotide exchange proteins (GEFs) **24**

1.2.2.3. Distinct nucleotide-bound conformational states **24**

1.3. YchF – A universally conserved NTPase that binds to both ATP and GTP **27**

1.3.1. The wide-ranging cellular role of YchF 27
1.3.2. Potential role in translation 29
1.3.3. Structure of YchF 29
1.3.4. Non-canonical G4 motif confers dual-specificity nucleotide binding 30
1.3.5. Comparison of YchF's molecular switch-like behaviour to other GTPases 32
1.4. Research objectives 34
1.4.1. OBJECTIVE 1: Determine the nucleotide binding affinity of YchF and G4-motif variants 35
1.4.2. OBJECTIVE 2: Probe the structural dynamics of YchF to determine distinct and relevant nucleotide-bound states 35
2. Materials and Methods 36
2.1. Buffers and reagents 36
2.2. Overexpressing wild-type YchF and variants 36
2.3. Protein solubility test 37
2.4. Protein purification 38
2.5. Ethanol precipitation of RNA 39
2.6. Equilibrium fluorescence titration 39
2.7. Limited trypsinolysis 40
2.8. Virtual trypsin cleavage of YchF 40
2.9. Western blotting 40
2.9.1. Immunodetection of YchF 41
2.10. Molecular biology techniques 41
2.10.1. Sample preparation for SDS-PAGE 41
2.10.2. SDS-PAGE 42
2.10.3. Coomassie staining of proteins 42
2.10.4. Native PAGE 43
2.10.5. Denaturing PAGE 43
2.10.6. Ethidium bromide staining 44
2.10.7. Bis-Tris SDS-PAGE 44

2.10.8. Ponceau S staining 44

2.10.9. Silver staining of proteins 44

3. Results 46

3.1. Overexpression of YchF and G4 motif variants 46

3.2. Purification of YchF 48

3.2.1. Nickel affinity chromatography 49

3.2.2. Anion exchange chromatography 50

3.2.3. Size exclusion chromatography 51

3.3. Gel electrophoresis analysis for RNA bound to YchF 52

3.4. Equilibrium fluorescence titration to determine nucleotide binding affinity of YchF 54

3.5. Probing the structural dynamics of YchF via limited trypsinolysis 59

3.5.1. Protein fragment pattern analysis on Bis-Tris SDS-PAGE 60

3.5.2. Quantification of full-length YchF cleavage 62

3.5.3. Analysis of protein fragment obtained from limited trypsinolysis via Western blot 64

3.6. Probing the cleavage site of YchF 65

3.6.1. Probing for His-tagged YchF 65

3.6.2. Probing for the G-domain of YchF 65

3.6.3. Detection of cleaved protein fragment via silver staining 66

4. Discussion 67

4.1. Objective 1: Modifying the G4 motif leads to altered nucleotide binding specificity . 67

4.2. Objective 2: The molecular switch-like behaviour of YchF 71

5. Conclusions and future directions 73

6. References 75

7. Appendix 108

List of Tables

Table 1. Expression vectors encoding ychF that were used for protein overexpression 36

Table 2. Yields of YchF at each step of protein purification.....52

Table 3. Nucleotide affinities of WT YchF and G4 motif variants.....59

Table 4. Stability of YchF nucleotide-bound states in the presence of trypsin 63

Table 5. Virtual trypsin cleavage analysis of N-terminal 6xHis-tagged E. coli YchF.....64

Table A1. Fusion proteins used in this thesis.....108

List of Figures

Figure 1. Proteins consist of individual amino acid monomers joined together via peptide bonds 1
Figure 2. The functional cycle of the ribosome 4
Figure 3. EF-G catalyzed ribosomal subunit rotation during translocation 7
Figure 4. GTPases are found across all three domains of life 14
Figure 5. GTPases share a G domain that binds to both GDP and GTP 15
Figure 6. Typical GTP hydrolysis reaction 17
Figure 7. HAS-GTPases use alternative amino acid catalytic residues for GTP hydrolysis 20
Figure 8. The G4 motif is responsible for imparting guanine nucleotide specificity 21
Figure 9. The molecular cycle of GTPases 22
Figure 10. Difference between the 3-dimensional GTP- and GDP-bound structures of GTPases 26
Figure 11. The 3D structure of YchF 30
Figure 12. Proposed functional cycle of YchF 34
Figure 13. WT YchF and G4 motif variants expressed at 37°C in E. coli 47
Figure 14. YchF_NKMD is found in the insoluble fraction 48
Figure 15. Workflow of YchF purification 49
Figure 16. YchF purification from Ni-NTA affinity chromatography 50
Figure 17. YchF purification from anion exchange chromatography 51
Figure 18. YchF purification from anion exchange chromatography 52
Figure 19. YchF potentially co-purifies bound to 16S rRNA 54
Figure 20. Equilibrium fluorescence titration workflow 55
Figure 21. Emission spectra of YchF titrated with nucleotides 57
Figure 22. Determining the nucleotide affinities of YchF and G4 motif variants 58
Figure 23. Limited trypsinolysis workflow 59
Figure 24. YchF·ATP is the most stable nucleotide-bound state during limited trypsinolysis 62
Figure 25. YchF·ATP is degraded slower than YchF's other functional states 63
Figure 26. The cleaved 13-kDa fragment corresponds to the G domain and lacks a 6xHis tag 66
Figure A1. Assessing the inner filter effect on nucleotide binding 115

Abbreviations

ADP Adenosine diphosphate

APS Ammonium persulfate

ATP Adenosine triphosphate

CV Column volumes

DNA Deoxyribonucleic acid

DTT Dithiothreitol

E. coli *Escherichia coli*

EDTA Ethylenediaminetetraacetic acid

$\varepsilon_{260\ nm}$ Extinction coefficient at 260 nm

$\varepsilon_{280\ nm}$ Extinction coefficient at 280 nm

FRET Förster resonance energy transfer

GAP/F GTPase activating protein/factor

GDP Guanosine triphosphate

GEF Guanine nucleotide exchange factor

GTP Guanosine triphosphate

GTPase Guanosine triphosphatase

HAS Hydrophobic amino acid substitution

IPTG Isopropyl β-D-1-thiogalactopyranoside

K_D Dissociation constant

kDa Kilodaltons

LB Lysogeny Broth

Mant-ADP 2'-(or-3')-*O*-(*N*-Methylanthraniloyl)-ADP

Mant-ATP 2'-(or-3')-*O*-(*N*-Methylanthraniloyl)-ATP

Mant-GDP 2'-(or-3')-*O*-(*N*-Methylanthraniloyl)-GDP

MES 2-(N-morpholino)ethanesulfonic acid

mRNA Messenger RNA

Ni-NTA Nickel-nitrilotriacetic acid

OD_{600} Optical density at 600 nm

O/N Overnight

PMSF Phenylmethylsulfonyl fluoride

TEMED Tetramethylethylenediamine

TGS ThrRS, GTPase, and SpoT

tRNA Transfer RNA

RNA Ribonucleic acid

rRNA Ribosomal RNA

SDS-PAGE Sodium dodecyl sulfate – polyacrylamide gel electrophoresis

$t_{1/2}$ Half-life time

TAKM$_X$ 50 mM Tris-Cl pH 7.5, 70 mM NH_4Cl, 30 mM KCl, X mM $MgCl_2$

TBS Tris buffered saline

trGTPase Translational GTPase

WT Wild-type

1. Introduction

Proteins constitute a large class of biomolecules that are responsible for carrying out many cellular processes such as deoxyribonucleic acid (DNA) replication (Lehman *et al*., 1958), gene expression (Hurwitz *et al*., 1960), modulating cell death (Li *et al*., 1997), immune function (Hedrick *et al*., 1984 and Yanagi *et al*., 1984), maintaining cell structure (Gavara & Chadwick, 2016), metabolism (Teusink *et al*., 2000) and metabolite synthesis (Hollander *et al*., 1984). In 1901, Fischer and Fourneau discovered that proteins are comprised of amino acids monomers that are covalently held together by peptide bonds (Figure 1). This was documented in glycylglycine, a simple molecule comprised of two glycine monomers that is formed in the absence of water. The peptide bond formed between both glycine monomers can be hydrolyzed in the presence of water, depolymerizing the dipeptide. The term "polypeptide" would later be coined to describe the entire amino acid length of a protein (Fischer, 1903).

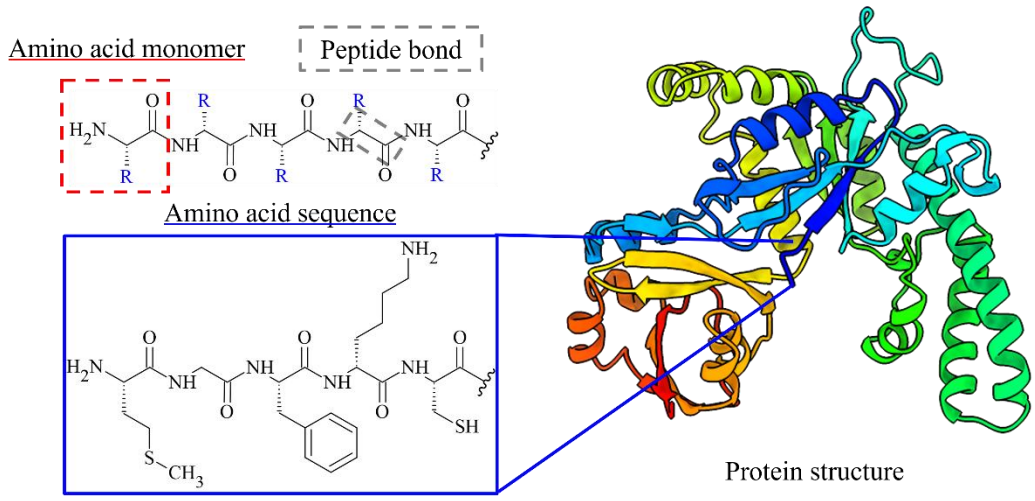

Figure 1. Proteins consist of individual amino acid monomers joined together via peptide bonds. All proteins consist of amino acids, as shown by an Alphafold prediction structure of *Escherichia coli* YchF (Uniprot ID: P0ABU2). The 3D structure of YchF was generated using Alphafold3 and visualized in ChimeraX. Amino acids share the same backbone structure but differ in their side chain residue (R-group). An amide bond (peptide bond: -OC-NH-) is formed between the hydroxyl oxygen of the carboxyl group (-COOH) from one amino acid and the amine group ($-NH_3$) of another amino acid. Repeating amino acids in the sequence interact with each other forming higher ordered 3-dimensional structures that impart the function of a protein.

Proteins are widely regarded as the workhorse of the cell and must be synthesized by a cell for it to live. The information that encodes proteins are stored in functional units of heredity called

genes. Genes are comprised of DNA sequences and are stored in the chromosome of all cells. A typical bacterial genome contains 5,000 protein-coding genes (Land *et al*., 2015) while a human cell contains four times as much (Nurk *et al*., 2022). Genes serve as genetic templates to synthesize an intermediate messenger ribonucleic acid (mRNA) molecule that encodes the respective protein. This step is carried out by RNA polymerases during the first stage of gene expression, known as transcription (Nakamoto *et al*., 1964). The ribosome then binds and decodes the mRNA to synthesize a protein in a template-dependent manner. This is the final step of gene expression, also known as translation (Hogland *et al*., 1958, Mcquillen *et al*., 1959 and Nirenberg & Matthaei, 1961).

A typical mRNA molecule encodes one protein, although there exist mRNAs that contain multiple coding regions (polycistronic) that each encodes a protein. Regardless, the entire mRNA molecule is flanked by two regulatory elements: a 5' and 3' untranslated region (UTR). The 5' UTR is involved in regulating mRNA stability, ribosome recruitment and translation efficiency (Jia *et al*., 2020). On the other hand, the 3' UTR mainly regulates mRNA stability (Shaw & Kamen, 1986). In prokaryotic systems, transcription and translation both occur in the cytoplasm (Miller *et al*., 1970). In eukaryotic systems, both steps of gene expression are separated by a membrane barrier, also known as the nucleus (Müller *et al*., 2024, Penman, 1966 and Rovera *et al*., 1970). The resulting mRNAs synthesized in eukaryotes undergo additional modifications to attach a 5' 7-methylguanosine cap (Wei *et al*., 1975) and a 3' poly-adenylic tail (Edmonds *et al*., 1971) to increase stability, before it is released into the cytoplasm to enter the translation cycle.

1.1. The ribosome

In the cytoplasm of both prokaryotes and eukaryotes, mRNAs are recognized by the ribosome and are decoded to synthesize proteins. The ribosome is a megadalton ribonucleoprotein complex that consists of a large ribosomal subunit (50S: prokaryotes and 60S: eukaryotes), a small ribosomal subunit (30S: prokaryotes and 40S: eukaryotes) (Ban *et al*., 2000, Wimberly *et al*., 2000, Yusupov *et al*., 2001). Both the large and small ribosomal subunits are comprised of ribosomal RNA (rRNA). The large ribosomal subunit consists of two species of rRNA (5S and 23S) in prokaryotes, but three in eukaryotes (5S, 5.8S and 28S). The small ribosomal subunit consists of only one rRNA (prokaryotes: 16S and eukaryotes: 18S) (Yusupov *et al*., 2001 and Natchiar *et al*., 2017). Together, these components are assembled to form a functional ribosome (70S in prokaryotes and 80S in eukaryotes). Each ribosomal subunit consists of a set of ribosomal proteins,

for a total of over 50 ribosomal proteins bound on the 70S/80S ribosome (Ban *et al*., 2000, Wimberly *et al*., 2000, Yusupov *et al*., 2001). During translation, the ribosome interacts with mRNA, transfer RNAs (tRNA) and accessory factors that regulate the progression of the ribosome throughout the translation cycle (Gabashvili *et al*., 2000, Spahn *et al*., 2001a, Schmeing *et al*., 2009 and Sashital *et al*., 2014). The 70S/80S ribosome is characterized by formation of three compartments within: the A-site for aminoacylated tRNA delivery (Nirenberg & Leder, 1964 and Ohta *et al*., 1968), the P-site where an RNA component (peptidyl transferase center) catalyzes the peptide bond of a growing polypeptide (Monro *et al*., 1968) and the E-site for tRNA dissociation off the ribosome (Rheinberger *et al*., 1981). The ribosome decodes a mRNA template from its 5' end to 3'end (Yusupova *et al*., 2006) in three nucleotide triplets, known as codons. There are 64 different codons and 61 of them encode for one of 20 standard amino acids that are delivered to the ribosome. The remaining three codons do not encode an amino acid but instead signals the end of the translation cycle and subsequent release of the polypeptide (Brenner *et al*., 1965 and Brenner *et al*., 1967). Amino acids are incorporated into the growing polypeptide chain until the stop codon is reached (Yusupova *et al*., 2006 and Demeshkina *et al*., 2012).

1.1.1. Functional cycle

The functional cycle of the ribosome is divided into four distinct steps: initiation, elongation, termination and lastly, ribosome recycling (Figure 2) (Rodnina, 2018 and Uematsu & Qian, 2025). Each step is sequential and characterized by different complexes that the ribosome forms with translation factors such as elongation factor thermounstable (EF-Tu) or EF-G (review by Rodnina, 2018). Translation is tightly regulated by translation factor guanosine triphosphatases (trGTPases) that hydrolyze guanosine triphosphate (GTP) to induce conformational changes in the ribosome, required to progress through its functional cycle (Agrawal et al., 1999 and Valle *et al*., 2003a). For the purposes of this thesis, the ribosome will be described in the prokaryotic system, with occasional comparisons to eukaryotes.

1.1.2. Regulation of the functional cycle

In addition to the critical role of the ribosome within the cell, translation in general is an immensely energy demanding cellular process. To synthesize proteins, many components are synthesized by the cell, such as the ribosome, mRNA, tRNA, translation factors and amino acids (Stark *et al*., 1997, Moazed *et al*., 1998 and Loveland *et al*., 2017). Additionally, energy in the

form of ATP is required to aminoacylate tRNAs for eventual delivery to the ribosome (Hoagland *et al*., 1956 and Berg & Offengand, 1958). The ribosome is tightly regulated by trGTPases, using GTP as an energy source. The following sub-sections will describe the key trGTPases that regulate each canonical step of translation.

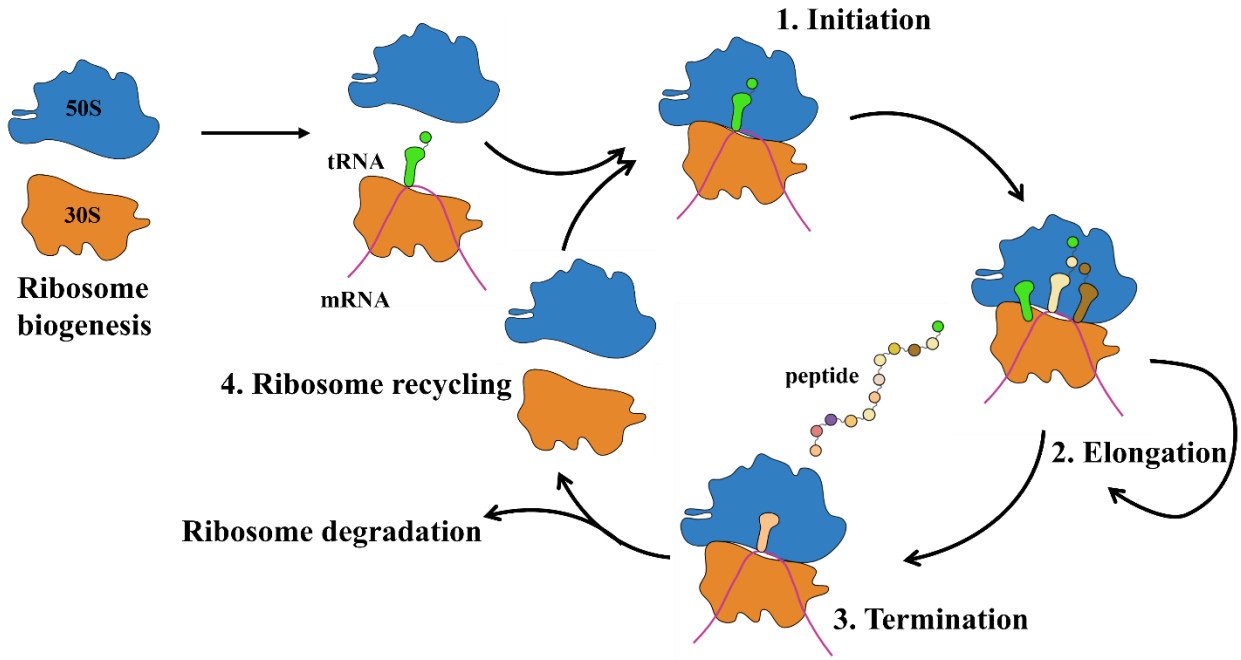

Figure 2. The functional cycle of the ribosome. After biogenesis and maturation of the ribosomal subunits (50S: blue and 30S: orange), the functional cycle of the ribosome is divided into four key steps: initiation, elongation, termination and ribosome recycling. During initiation, the 70S ribosome is fully assembled with a mRNA (pink) and fMet-tRNA^{fMet} (green). During elongation, amino acids are delivered to the ribosome via aminoacyl tRNAs. The termination step is entered when the ribosome decodes a stop codon in the mRNA, leading to subsequent polypeptide release. The ribosome is disassembled and recycled back into the ribosome pool. This figure was adapted from Brandon (2021), simplifying the functional cycle and colour coding scheme.

1.1.2.1. Initiation

The initiation step is tightly regulated by initiation factor 2 (IF2), a trGTPase that when bound to GTP, recruits N-formylmethionine (fMet)-tRNA^{fMet} (in prokaryotes) to the 30S subunit (Milón *et al*., 2010 and Milón *et al*., 2012). Eukaryotes instead utilize Met-tRNA^{Met}, while mitochondria and chloroplast utilize fMet-tRNA^{fMet} (Ranu & Wool, 1975 and Spencer & Spremulli, 2004). Recruitment of fMet-tRNA^{fMet} to the 30S subunit is governed by kinetics, occurring in one of two possible steps. Rapid kinetic techniques show that the most common

pathway occurs while IF2 is bound to an mRNA-programmed 30S subunit with its initiation factors (IF1 and IF3). Recruitment via an IF2 ternary complex (IF2·GTP·fMet-tRNA^{fMet}) has been shown to be unstable and short-lived (Milón *et al*., 2010). IF2-mediated initiator tRNA binding serves as a key checkpoint in initiation, preventing immature A-site tRNA binding and 70S ribosome assembly. IF1 and IF3 work respectively to block A-site tRNA binding and 50S large subunit association. All three initiation factors are transiently bound to the 30S subunit until the start codon (5' AUG 3') is recognized by fMet-tRNA^{fMet}. Upon codon-anticodon recognition with the start codon, fMet-tRNA^{fMet} induces a conformational change in the 30S subunit and subsequently shifts the conformational states IF3 samples towards a compact state ready for its dissociation (Elvekrog & Gonzalez, 2013). Binding by the large ribosomal subunit forms the GTPase-associated center (GAC) at the A-site, bringing the sarcin-ricin loop (SRL) within proximity of IF2 to stimulate GTP hydrolysis (La Teana *et al*., 2001 and Brandi *et al*., 2004). This irreversible step eventually leads to dissociation of the remaining initiation factors, forming a 70S initiation complex (Brandi *et al*., 2004, Tsai *et al*., 2012 and Goyal *et al*., 2015).

1.1.2.2. Elongation

During the elongation step, the ribosome decodes the mRNA template one codon at a time to synthesize polypeptides. This step is regulated by EF-Tu, a trGTPase that delivers aminoacyl-tRNA as part of a ternary complex (EF-Tu·GTP·aminoacyl-tRNA) in a codon-dependent manner to the ribosome. The ternary complex is docked at the GAC, located on the A-site of the 50S ribosomal subunit. The substrate tRNA is positioned inwards towards the decoding center of the 30S subunit (Stark *et al.*, 1997 and Schmeing *et al*., 2009). In both prokaryotes and eukaryotes, the EF-Tu ternary complex serves as an important checkpoint to determine whether the correct amino acids are incorporated into polypeptides. The ribosome possesses proofreading capabilities in the 16S/18S (prokaryotes/eukaryotes) rRNA to ensure that the correct aminoacyl-tRNA is recognized. In the decoding center of prokaryotes, G530, A1492 and A1493 are used to probe cognate codon-anticodon base-pairing via a selection process (Ogle *et al*., 2002). However, the 18S rRNA in eukaryotes uses G626, A1824 and A1825 (Brown *et al*., 2015). During the initial selection process, the nitrogenous bases of A1492/A1824 and A1493/A1825 "flip in" or "flip out" to recognize the cognate base-pairing. When the ribosome is in the resting state, both adenine bases are "flip out" of the decoding center, pointing inwards towards helix 44 of the 16S rRNA (Ogle *et al*., 2002 and Brown *et al*., 2015). Once the EF-Tu ternary complex is bound to the ribosome, both

adenines “flip in” to probe the minor grove of the mRNA-tRNA minihelix at the first two nucleotides of the codon-anticodon base pair. The first two nucleotides are probed stringently by hydrogen bonds, although the third nucleotide, known as the “wobble” position, is probed to a lesser extent. When a near or non-cognate tRNA is bound, the codon-anticodon interaction presents an energetically unfavorable interaction that is discriminated against by A1492/A1824 and A1493/A1825 (Ogle *et al*., 2001). In this case, EF-Tu still undergoes GTP hydrolysis to release near/non-cognate tRNA, but failure to recognize the codon leads to subsequent rejection of the tRNA (Thompson and Karim, 1982). Successful codon recognition with the cognate tRNA is achieved when A1492/A1824, A1493/A1825 and G530/G626 satisfies the geometry of the minor groove of the codon-anticodon base pair (Pape *et al*., 1999 and Ogle *et al*., 2001). The decoding center undergoes structural rearrangement that docks the EF-Tu ternary complex closer to the SRL, stimulating GTP hydrolysis (Loveland *et al*., 2017). Upon GTP hydrolysis, EF-Tu undergoes a conformational change that releases aminoacyl-tRNA deeper into the A-site. After the inorganic phosphate (P_i) is released, EF-Tu subsequently dissociates bound to guanosine diphosphate (GDP) from the ribosome (Dell *et al*., 1990 and Abel *et al*., 1996). EF-Tu·GDP dissociation serves as the final checkpoint to ensure that the ribosome recruits the correct aminoacyl-tRNA to proceed towards peptide bond formation.

After each successful incorporation of an amino acid into the polypeptide, the ribosomal subunits must rotate relative to each other to translocate the next codon into the A-site. Thermal energy drives the 30S subunit to rotate relative to the 50S subunit, allowing the pre-translocation ribosome to spontaneously shift between non-rotated and rotated states (Cornish *et al*., 2008). Spontaneous intersubunit rotation also allows the tRNA in A and P-site to shift between its classical (A/A and P/P; 30S/50S compartments) and hybrid states (A/P to P/E) (Figure 3) (Blanchard *et al*., 2004a). However, the codon-anticodon interaction presents an energetic barrier, preventing the ribosome from completing a successful intersubunit rotation. EF-G helps the ribosome overcome this energetic barrier by behaving as a molecular wedge to drive intersubunit rotation. EF-G·GTP binds to either rotation states of the ribosome, although it preferentially binds and stabilizes the rotated state (Cornish *et al*., 2008 and Rundlet *et al*., 2021). Docking occurs at the GAC and the similarity of EF-G’s Domain IV to the geometry of a tRNA allows EF-G to reach into the decoding center (Agrawal *et al*., 1998 and Rundlet *et al*., 2021). Through GTP hydrolysis, EF-G undergoes a ratchet-like motion that rearranges the decoding center and subsequently disrupts the codon-

anticodon interactions (Agrawal *et al.*, 1998 and Agrawal *et al.*, 1999). This massive conformational change irreversibly rotates the 30S subunit by about 3º-10º counterclockwise relative to the 50S subunit, lowering the energy barrier needed for the tRNA and mRNA to undergo coupled translocation (Frank & Agrawal, 2000, Gao *et al.*, 2003 and Valle *et al.*, 2003b). Interestingly, the P_i generated upon GTP hydrolysis remains bound to EF-G. P_i release is required for EF-G·GDP to dissociate from the ribosome, completing translocation (Carbone *et al.*, 2021). The ribosome enters a non-rotated state with the tRNAs in their post-translocation classical states (P/P and E/E) (Figure 3). The E/E state tRNA eventually dissociates, as the ribosome proceeds to the next round of codon decoding (Cornish *et al.*, 2008).

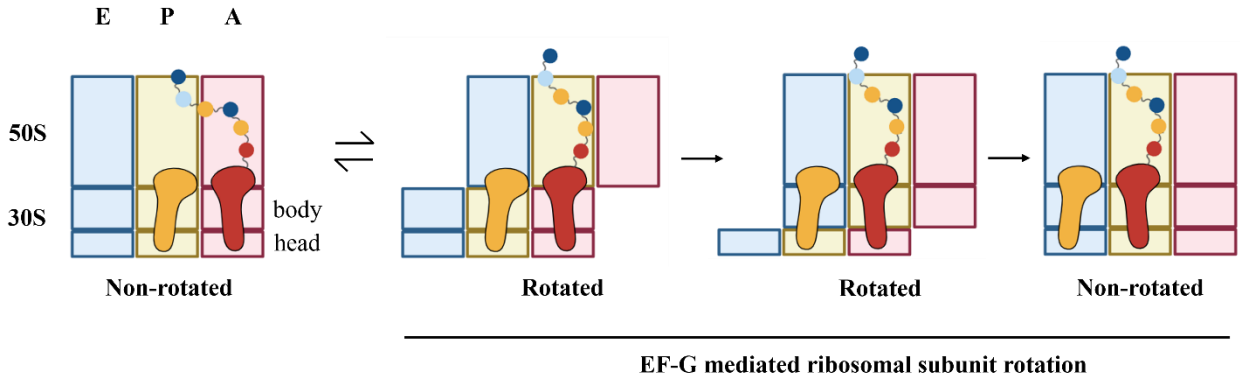

Figure 3. EF-G catalyzed ribosomal subunit rotation during translocation. After each elongation step, the ribosomal subunits must rotate relative to each other to position the deacylated and peptidyl tRNA into the next compartment. The nomenclature used to describe the tRNA states are the 50S/30S compartments. Ribosomes can spontaneously rotate between the non-rotated and rotated states. The corresponding tRNAs also shift between its pre-translocation classical states (A/A and P/P) and hybrid states (A/P and P/E). EF-G stabilizes the initial rotated state of the ribosome and disrupts the codon-anticodon base pair required for the tRNAs to shift to its classical post-translocation classical states (P/P and E/E). This figure was adapted from Noller *et al.*, 2017, indicating the progression of ribosomal subunit rotation and the steps mediated by EF-G.

1.1.2.3. Termination

After repeated rounds of elongation, the ribosome eventually decodes the stop codon. In prokaryotes, the A-site of the ribosome is accessible to release factors 1 or 2 (RF1 and RF2), which recognize UAG/UAA and UGA/UAA stop codons, respectively (Korostelev *et al.*, 2008). Interestingly, eukaryotes and archaea lack RF2 and instead utilize eukaryotic RF1 (eRF1) to recognize all three stop codons (Song *et al.*, 2000 and Vestergaard *et al.*, 2001). Both release factors

catalyze the hydrolysis of the ester bond of the peptidyl-tRNA and the subsequent release of the polypeptide from the ribosome yields the pre-70S/80S ribosome termination complex (Frolova *et al*., 1999, Korostelev *et al*., 2008). The dissociation of the release factors from the ribosome is facilitated by the trGTPase release factor 3 (RF3) (Zavialov *et al*., 2001, Gao *et al*., 2007a and Koutmou *et al.*, 2014). Unlike the previous trGTPase described, RF3 does not use GTP hydrolysis to regulate the progression of the ribosome through translation. Instead, RF3·GDP utilizes the nucleotide exchange step of a GTPase to facilitate RF1 and RF2 turnover (Zavialov *et al*., 2001 and Li *et al*., 2024). Recently, it has been elucidated in prokaryotes that the 70S ribosome termination complex allosterically regulates nucleotide exchange of RF3 through a salt-bridge interaction between RF3 and RF1/RF2 (Li *et al*., 2024). Li *et al*., (2024) identified that this salt-bridge interaction is disrupted in the 70S ribosome termination complex. Long-range structural rearrangement in RF3 from the loss of the salt-bridge to its G domain results in an invasion of the carbonyl oxygen of P22 into the nucleotide binding pocket. The carbonyl oxygen sterically clashes with the β-phosphate of GDP, catalyzing its dissociation. The 70S ribosome termination complex had previously been reported to accelerate nucleotide exchange by up to 250-fold (Peske *et al*., 2014). During which, rapid GTP binding induces a rotation in RF3 that disrupts its interactions with RF1/RF2. Additionally, the 30S subunit undergoes a rolling-like motion that docks RF3·GTP close to the SRL for GTP hydrolysis (Li *et al*., 2024). The rotation of the 30S subunit is also consistent with previous data that suggest that RF1/RF2 dissociates during this critical step (Zavialov *et al*., 2001, Gao *et al*., 2007a, Zhou *et al*., 2012 and Koutmou *et al.*, 2014). The final step of termination is ribosome-induced GTP hydrolysis to dissociate RF3 (Zavialov *et al*., 2001 and Zhou *et al*., 2012).

1.1.2.4. Ribosome recycling

Ribosomes are disassembled, following translation with the help of the ribosome recycling factor (RRF) and EF-G. Interestingly, the 3-dimensional structure of RRF closely resembles the "L-shaped" structure of tRNA. A similar feature is observed in other translation factors, such as the tRNA moiety of the EF-Tu ternary complex (EF-Tu·GTP·aminoacyl-tRNA) and domains III-V of EF-G. This phenomenon, known as molecular mimicry, suggests that translation factors and other biomolecules that share similar geometry to a tRNA will also share a similar binding site on the ribosome (Nissen *et al*., 1995 and Selmer *et al*., 1999). Indeed, biochemical and structural evidence has shown that RRF binds to the A-site of the post-termination ribosome complex

(Fujiwara *et al*., 2001 and Lancaster *et al*., 2002), just as EF-Tu (Stark *et al.*, 1997 and Schmeing *et al*., 2009) and EF-G (Agrawal *et al*., 1998 and Rundlet *et al*., 2021). However, RRF does not recognize any codons as a tRNA typically would, instead adopting a binding mode that is orthogonal in comparison. RRF interacts with the intersubunit bridge and is positioned towards the decoding site (Lancaster *et al*., 2002 and Weixlbaumer *et al*., 2007). EF-G shares a similar binding region at the decoding center as part of its role in translocation (Agrawal *et al*., 1998 and Rundlet *et al*., 2021). Based on structural and binding site similarity to EF-G, RRF has been hypothesized to function like a molecular wedge. Although RRF lacks GTPase activity, it recruits EF-G and utilize GTP hydrolysis by EF-G to drive ribosome dissociation (Hirashima & Kaji, 1972 and Yokoyama *et al*., 2012). GTP hydrolysis by EF-G facilitates rotation (~60º) in RRF disrupting intersubunit bridge, namely at B2a (helix 69 of 23S rRNA) and B3 (helix 71) (Peske *et al*., 2005 and Gao *et al.*, 2005 Gao *et al*., 2007b). Subsequently, the post-termination ribosome complex is disassembled into its large and small ribosomal subunits. With that, the 30S subunit remains bound to mRNA and deacylated tRNA. IF3 binds to the 30S subunit to facilitate deacylated tRNA dissociation and prevent pre-mature assembly of the 70S/80S ribosome (Karimi *et al*., 1999). After which, both subunits are recycled back into the ribosome functional state at the initiation step.

1.1.2.5. Stress response

Throughout its lifecycle, a cell has to respond to many cellular stresses that can lead to cell death, such as oxidative stress (McCord & Fridovich, 1969), temperature (Ritossa, 1962), starvation (Cashel & Gallant, 1969, Ashe *et al*., 2000 and Müller *et al*., 2015), DNA damage (Setlow R. & Setlow J., 1962 and Elledge & Walker, 1983), antibiotics (Dwyer *et al*., 2014), hypoxia (Wang & Semenza, 1995) and osmotic changes (Brewster *et al*., 1993 and Schüller *et al*., 1994). To defend or respond to these stresses, cells respond by reprograming the ribosome and biasing it toward a distinct class of mRNA. In prokaryotes, these are leaderless mRNAs which lack a 5' UTR (Vesper *et al*., 2011). In eukaryotes, these can either be mRNA containing upstream open reading frames (uORFs) or cap-independent mRNAs (Armstrong *et al.*, 2010 and Sun *et al*., 2011). These classes of mRNA encode stress response proteins involved in damage repairs and maintaining homeostasis (Armstrong *et al.*, 2010, Vesper *et al*., 2011 and Sun *et al*., 2011). The ability for the cell to "sense" and adjust its cellular processes is an important survival mechanism to prevent degradation of expensive components such the DNA, RNA, ribosomes and proteins. Much like the regulatory role of trGTPase, a handful of GTPase also regulates the ribosome in

response to a range of cell stresses. This section will focus on examples of GTPases that regulate the ribosome in response to cold-shock and antibiotic stress at the translational level.

1.1.2.5.1. Cold shock response

When a cell experiences cold (sub-optimal) temperatures, a series of problems occur that disrupt its growth. These include solidifying the lipid bilayer (Janiak *et al*., 1974), stabilizing inhibitory RNA secondary structure (Rissone *et al.*, 2024), slowing down enzymatic reactions (More *et al*., 1995) and translation (Das & Goldstein, 1968, Farewell *et al*., 1998) and impaired protein folding (Babu *et al*., 2004). To adapt to low temperatures, cells typically express cold shock proteins such as BPI-inducible protein A/tyrosine phosphoprotein A (BipA/TypA). BipA is a highly conserved bacterial trGTPase that has been reported to provide a fitness advantage during nutrient starvation (Freestone *et al*., 1997) and cold stress (Pfennig & Flower, 2001 and Choi *et al*., 2025). *bipA* is normally expressed at low basal levels, but its expression is induced under cold temperatures. The expression of BipA is positively regulated by cyclic adenosine monophosphate (cAMP) receptor protein (Choi & Hwang, 2018), a transcription factor that regulates expression of another cold shock proteins *cspE* (Uppal *et al*., 2011). In cold temperatures, expression of *bipA* increases BipA intracellular levels by ~3 to 10-fold (Choi & Hwang, 2018 and del Peso Santos *et al*., 2021).

Much like other well-studied trGTPase, BipA shares an N-terminal GTP-binding domain based on structural alignment with EF-G. As such, a cryo-EM structure of the BipA·GTP·70S complex, shows that BipA binds to the GAC of the 70S ribosome in a GTP-dependent manner. Interestingly, the ribosomal subunits are slightly rotated, resembling the pre-rotated state of the EF-G·GTP·pre-70S translocation complex (Kumar *et al.*, 2015). Preference for the 70S ribosome was also corroborated by immunoblotting assays, showing that BipA·GTP binds but not BipA·GDP (deLivron & Robinson, 2008 and Choi & Hwang, 2018). Additionally, BipA·GTP displayed weak binding towards individual subunits and polysomes, although BipA·GDP binds weakly to the 30S subunit (deLivron & Robinson, 2008 and Choi & Hwang, 2018). It is unsurprising for BipA to bind to both ribosomal subunits since it shares similar contact regions as EF-G (Gao et al., 2009). Despite biochemical and structural evidence that BipA interacts with the ribosome, its regulatory role once bound remains unclear. So far, GTP hydrolysis seems to play an important role in ribosomal maturation. This is supported by an accumulation of pre-50S subunit (44S), lacking L6 ribosomal protein in the absence of *bipA* (Choi & Hwang, 2018). Impaired

growth at 20ºC was observed in *bipA* knockout mutants, but supplementing plasmid-borne *bipA* rescues the wild-type phenotype (Pfennig & Flower, 2001, Kiss *et al*., 2004 and Choi *et al*., 2025).

During cell stress, the binding preference of BipA for the ribosome is modulated by the presence of the alarmone guanosine tetraphosphate (ppGpp) (deLivron & Robinson, 2008). One of the hallmarks of cell stress is a sharp decrease of intracellular GTP levels and increase in guanosine (penta)tetraphosphate (p)ppGpp levels (Lopez *et al.*, 1981 and Murray & Bremer, 1996, Bittner *et al*., 2014). (p)ppGp not only binds to GTPases (Corrigan *et al*., 2016) but also regulates the levels of GTP available for binding (Kriel *et al*., 2012), shifting the GTPase population towards GDP-bound and (p)ppGpp-bound. The structures of BipA·GDP and BipA·ppGpp have been solved via X-ray crystallography, revealing that both nucleotides occupy the nucleotide binding pocket and rules out the possibility that ppGpp regulates BipA allosterically (Fan *et al*., 2015). Interestingly, chaperone-like activity was discovered in BipA and that it was nucleotide-independent, suggesting a potential role off the 70S ribosome (Choi & Hwang, 2018). Current evidence suggests, however that *in vivo*, the majority of BipA exists in a ternary complex with the 30S subunit (BipA·GDP·30S) during cold shock. So far, it remains unclear how BipA·GTP populations are maintained during cellular stress and how this nucleotide-bound state regulates the 70S ribosome.

1.1.2.5.2. Antibiotic stress response

Ever since the discovery of antibiotics by Alexander Fleming (1929), they have seen widespread use to combat pathogenic microbes. In bacteria, antibiotics typically disrupt an essential cellular process that then leads to cell death. These includes, DNA replication (Shen *et al*., 1989 and Khodursky *et al*., 1995), cell wall synthesis (Wise & Park, 1965), membrane integrity (Silverman *et al*., 2003), metabolic pathways (Miller *et al*., 1972), transcription (McClure & Cech, 1978) and translation (Gale & Folkes, 1953 and Gottesman, 1967). However, overuse and misuse of antibiotics have led to the emergence of drug-resistant variants (Jevons, 1961, McGowan, 1983, Smith *et al*., 1999). These drug-resistant strains have been inadvertently selected by persistent antibiotic use and have acquired mutations that are beneficial to drug-resistance. Many of these variants possess mechanisms to combat current antibiotics and generally falls into three categories: degrading/modifying drugs (Abraham & Chain, 1940, Brzezinska *et al*., 1972 and Benveniste & Davies, 1973), reducing drug uptake (Neyfakh *et al*., 1993, Aínsa *et al.*, 1998 and Sanchez *et al*., 2013) or modifying the target site (Yoshida *et al.*, 1988 and Campbell *et al*., 2001).

Tetracycline is one such antibiotic that has seen widespread use for its role in inhibiting translation in bacteria. It typically binds to a pocket formed by helix 31 (residues 964–967) and 34 (residues 1054–1056 and 1196–1200) on the A-site of the 30S ribosomal subunit (Brodersen *et al*., 2000, Pioletti *et al*., 2001) with very high affinity (K_D ~ 1-20 μM), although it binds to several low affinity binding sites (< 1 mM) (Goldman *et al*., 1983). The primary binding site is situated behind the tRNA at the codon-anticodon interaction site on the 30S ribosomal subunit and occurs via hydrogen bond and salt-bridge interactions between the hydroxy groups of tetracycline and the phosphate oxygens of G966, C1054, G1197 and G1198. A Mg^{2+} ion coordinates a salt bridge interaction between tetracycline and the sugar backbone of G1197 and G1198. Additionally, the nitrogenous base of C1054 and U1196 bulge outwards, stabilizing the hydrophobic rings of tetracycline via base stacking (Brodersen *et al*., 2000, Pioletti *et al*., 2001 and Jenner *et al*., 2013). Once bound, tetracycline sterically blocks full accommodation of aminoacyl-tRNAs into the A-site, subsequently leading to ribosome stalling (Maxwell, 1967, Blanchard *et al*., 2004b and Jenner *et al*., 2013).

One of the mechanisms that drug-resistant variants utilize to combat tetracycline is to induce the expression of tetracycline resistance protein O (Tet(O)). Tet(O) restores translation *in vivo* and *in vitro* in the presence of tetracycline but does not inhibit tetracycline binding on the ribosome (Manavathu *et al*., 1990, Grewal *et al*., 1993 and Trieber *et al*., 1998). Analysis of the proteins sequence revealed that Tet(O) is classified as a trGTPase based upon the resemblance of its N-terminal region to a GTP-binding domain of other members such as EF-Tu and EF-G, suggesting a potential role in ribosome binding (Manavathu *et al*., 1990). An *in vivo* study by Grewal *et al*., (1993) documented that site-directed mutagenesis of D128, a key residue involved in GTP binding drastically reduced Tet(O)-mediated resistance. This study linked GTP-binding of Tet(O) to tetracycline resistance and established a foundation that led later studies to focus on elucidating the role of GTP hydrolysis in ribosomal regulation under tetracycline stress.

In vitro studies reported that Tet(O) has a higher binding affinity to GDP than GTP (K_D not measured), yet its GTPase activity is stimulated by 70S ribosomes (Taylor *et al*., 1995). A later study by Trieber *et al*. (1998) provided evidence that the ribosome potentially selects for Tet(O)·GTP by measuring the amount of GTP bound via guanosine 5'-O-[gamma-thio]triphosphate (GTPγS), a non-hydrolysable analog of GTP. Cryo-EM structures of the Tet(O)·GTP·70S complex not only revealed that Tet(O) is bound at the GAC, but also homology

modelling Tet(O) resembled structural features of domain IV of EF-G (Spahn *et al*., 2001b and Li *et al*., 2013). This finding is consistent with Manavathu *et al*., (1990) sequence homology predictions previously. The difference between Tet(O) and EF-G interactions with the 70S ribosome is the orientation of domain IV and the function of the three loops (438-, 465- and the 507-residue loop) found at its tip towards the 30S subunit (Thakor *et al*., 2008 and Li *et al*., 2013). Domain IV of TetO does not extend completely into the A-site compared to EF-Tu and does not occupy exactly the region of the anticodon stem of an aminoacyl tRNA. Additionally, the tips of domain IV do not contact the intersubunit bridge region B2a (Spahn *et al*., 2001b). Swapping the loop regions between Tet(O) and EF-G did not confer tetracycline resistance in EF-G variants, nor ribosome translocation activity in Tet(O) variants, suggesting specific functions of the loops in their respective trGTPase (Thakor *et al*., 2008). In Tet(O), the 438- and 507-residue loop closely occupies the location where the codon-anticodon normally occurs, while the 465-residue loop extends towards the primary tetracycline binding-site, near nucleotides 1055 and 1209 of helix 34. Introducing mutations into any of the three loops inhibits tetracycline resistance, conferred by Tet(O). The 507-residue loop is of particular importance as it would be sterically clashing with tetracycline if both were present on the ribosome (Li *et al*., 2013). This steric clash is avoided through GTP hydrolysis, in which TetO facilitates a conformational change of the stalled ribosome to restructure the primary tetracycline-binding pocket. This rearrangement disrupts the binding interactions between tetracycline for the 16S rRNA, leading to its subsequent dissociation. Furthermore, the conformational state the ribosome adopts prevents subsequent tetracycline molecules from binding long after TetO dissociates, while still allowing the EF-Tu ternary complex to bind (Spahn *et al*., 2001b, Connell *et al*., 2002 and Connell *et al*., 2003).

1.2. GTPases; the molecular switches of cells

GTPases are a class of enzymes that regulate many cellular processes such as translation and stress response. This class of enzymes hydrolyzes GTP as part of their function. In 1966, EF-Tu and EF-G were the first GTPases to be purified (Lucas-Lenard and Lipmann, 1966) and their regulatory roles would later be characterized in the context of the ribosome functional cycle (Miller, 1972) and the first members of the trGTPases family (Leipe *et al*., 2002). Other GTPases would later be discovered, purified and characterized, expanding the families/classes of GTPases currently known (reviewed by Caldon & March, 2003 and Verstraten *et al*., 2011) such as the TRAFAC (Translation Factor Association) and SIMIBI (Signal Recognition Particle, MinD, and

BioD) subclass (Leipe *et al*., 2002). Among the many different GTPases identified, many share a hydrophobic residue in place of the catalytic glutamine and are classified as hydrophobic amino acid substation GTPases (HAS-GTPase; explained further in section 1.2.1.1.) (Mishra *et al*., 2005 and Anand *et al*, 2006 and Vithani *et al*., 2017). Interestingly, out of all GTPases identified, only eight members are universally conserved across the three domains of life. These include the well studied TRAFACs (ex. IF2 and EF-Tu/G) and the HAS-GTPases (FtsY, HflX, YihA and YchF) (Figure 4) (reviewed by Caldon and March, 2003).

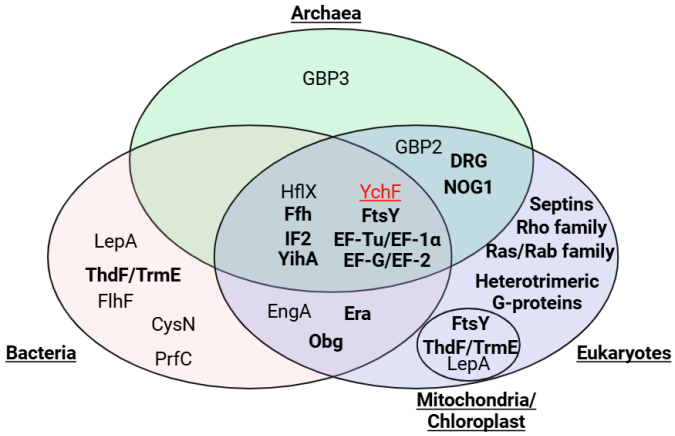

Figure 4. GTPases are found across all three domains of life. GTPases and families bolded indicate that they are essential to the cell. Only eight GTPases are universally conserved across the three domains of life. Over half are classified as translation factor GTPases. YchF (red) is an interesting trGTPase such that despite having a G domain with the hallmarks of the five G-motifs, it is one of the few members that can bind to both ATP and GTP. This figure was adapted from Caldon and March (2003) to include a colour coding scheme, bolding essential GTPases and highlighting YchF.

1.2.1. G domain

Members of the GTPase families share a highly conserved core domain, known as the G domain. The G domain is the functional unit of a GTPase that binds to either GTP or GDP and is responsible for converting GTP into GDP and P_i. The length of the G domain typically ranges between 160 and 260 amino acids, as seen in small GTPases (ex. Ras: 166 amino acids), or larger members (ex. dynamin: 261 amino acids). The 3-dimensional structure adopt an α/β-fold, that consist of a central β-sheet surrounded by α-helices, demonstrated with EF-Tu, EF-G and YchF (Figure 5A-C). The central β-sheet typically consist of 6 β-strands that are generally parallel to each other and flanked on both side by α-helices (Pai *et al*., 1990, Niemann *et al*., 2001 and reviewed by Verstraten *et al*., 2011). Contained within the G domain are five highly conserved amino acid motifs (G1-G5 motif) that form the active site for GTP hydrolysis (Bourne *et al*., 1991).

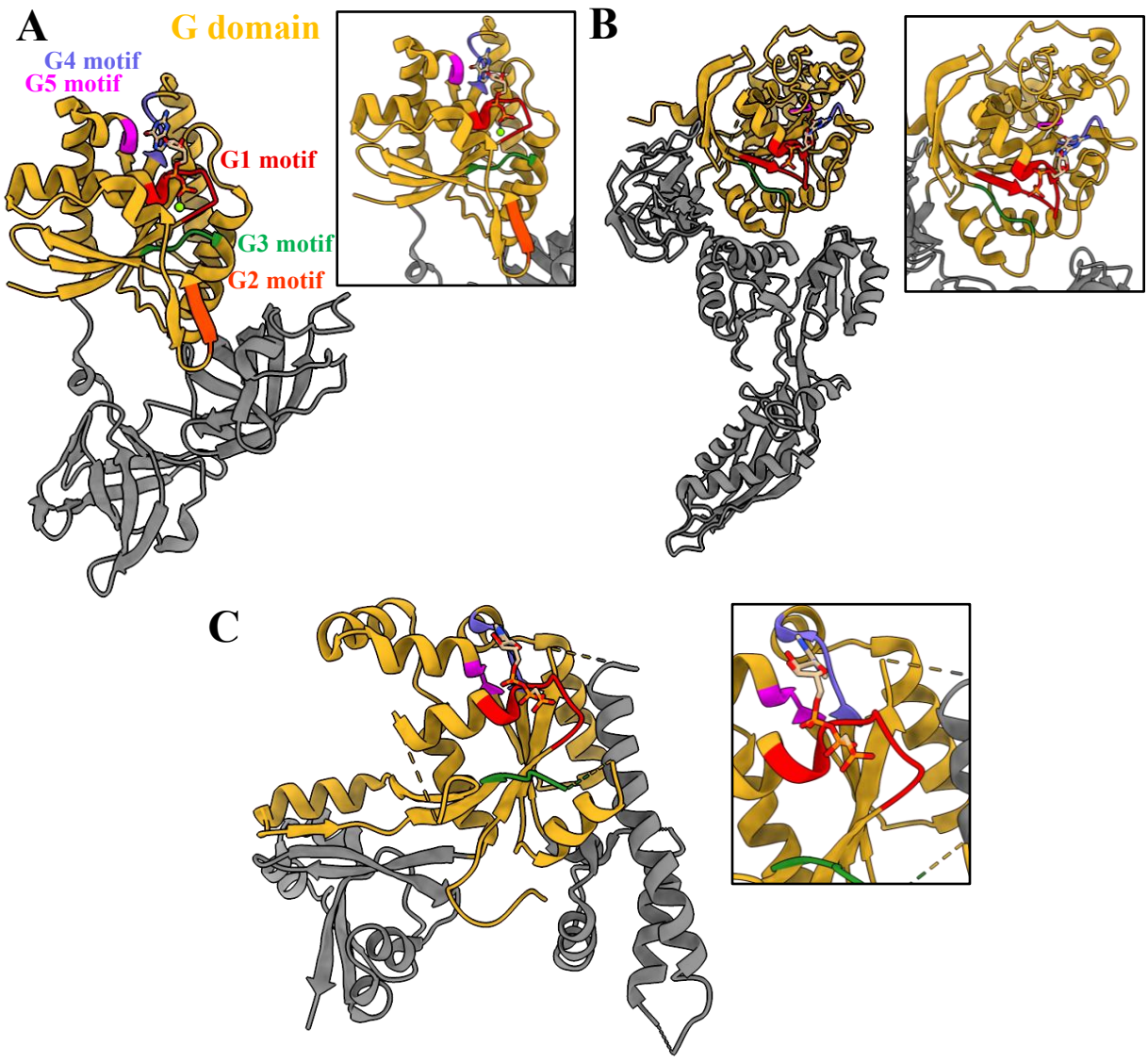

Figure 5. GTPases share a G domain that binds to both GDP and GTP. **A)** EF-Tu (PDB: 1DG1; Abel *et al*., 1996) and **B)** EF-G (PDB: 7PJZ; Petrychenko *et al*., 2021) are two well-studied GTPase that hydrolyze GTP using the G domain (yellow). The other protein domains are coloured grey. Within the G domain are five highly conserved amino acid sequences (G1-G5 motif) that forms the catalytic site for GTP hydrolysis and are as follows: G1 (Binds to phosphate groups; red), G2 (serine/threonine) and G3 (glutamine) (interacts with the β- and γ-phosphate group and coordinates a Mg^{2+} ion (neon green) for GTP hydrolysis; orange and green, respectively), G4 (discriminates GDP/GTP from other nucleotides; light purple) and G5 (aids in guanine nucleotide specificity; pink). **C)** YchF (PDB: 2OHF; Koller-Eichhorn *et al*., 2007) shares a G domain with the five highly conserved G-motifs and can bind to both ATP (adenosine 5'-(β,γ-methylene)triphosphate is shown; AMPPCP) and GTP.

1.2.1.1. G1-G5 motifs

The discovery of many GTPase families eventually led to an observation that they all shared a common glycine-rich protein sequence (GXXXXGK(T/S), where "X" is any amino acid) (Dever *et al*., 1987 and Saraste *et al*., 1990). Known as the G1 motif, it forms a binding interface that interacts with the phosphate groups of guanine nucleotides to properly position them within the nucleotide binding pocket. As shown from a crystal structure of H-ras p21, the amide backbone of several amino acid residues (G13-A18) helps stabilize the α- and β-phosphate group of non-hydrolysable GTP analog guanosine-5'-[(β,γ)-imido]triphosphate (GppNp). A single lysine residue (K16) forms a hydrogen bond between the β- and γ-phosphate group (Pai *et al*., 1990). This amino acid residue has been shown to be essential for nucleotide binding, based on single amino acid substitution in adenylate kinase. Substituting K16 reduced its ATP binding affinity (~16-fold) and completely abolished its catalytic activity (Reinstein *et al*., 1990). Interestingly, mutations in the G1 motif have been linked to oncogenic variants of K-Ras, such as G12C (~41% in non-small cell lung cancer) and G12D (~40% in pancreatic adenocarcinoma and ~27.5% in colorectal adenocarcinoma) (Huang *et al*., 2021). A later study would propose that mutations to glycine 12 results in lower intrinsic GTP hydrolysis of up to 20-fold, suggesting that the G1 motif plays a role in GTP hydrolysis (Song *et al*., 2025). The G1 motif had previously been identified in several families of adenosine triphosphatase (ATPase) and is also known as the Walker A motif (Walker *et al*., 1982). As a result, a new classification system called the phosphate-binding loop nucleotide triphosphatase (P-loop NTPase) was developed to unify both GTPase and ATPase families (Saraste *et al*., 1990). Within this new classification system, the P-loop NTPase are further divided into the TRAFAC and SIMIBI subclass based on signature protein sequences and function (Leipe *et al*., 2002).

The TRAFAC sub-class is defined by a highly conserved threonine or serine (G2 motif) that plays a key role in GTP hydrolysis (Bourne *et al*., 1991 and Leipe *et al*., 2002). GTP hydrolysis is initiated via a nucleophilic attack by a hydrolytic water molecule on the phosphoanhydride bond between the β- and γ-phosphate (Figure 6). Both the G2 and G3 motif (DXXGQ; Walker B motif) properly position a hydrolytic water molecule within 2.9 Å to 3.4 Å of the phosphoanhydride bond for cleavage. The presence of the γ-phosphate is detected by the sensory component of the G domain and is comprised of the G2 and G3 motif (Pai *et al*., 1990, Bourne *et al*., 1991 and Privé *et al*., 1992). Additionally, the surrounding region of both motifs are flexible and typically undergo

massive conformational changes depending on whether GTP or GDP is bound. For example, the EF-G·GTP·70S ribosome ternary complex has its G2 motif region buried inside the ribosome cavity near helix 14, forming an α-helix secondary structure. The G3 motif region is tightly packed within the G domain core, also adopting an α-helix secondary structure near the P-loop and the SRL of the 50S subunit. After GTP hydrolysis, the loss in the γ-phosphate results in the G2 motif region undergoing a massive 20 Å movement and results in its secondary structure becoming disordered. Additionally, the G3 motif region becomes relaxed and its secondary structure partially becomes disordered (Connell *et al*., 2007 and Ticu *et al*., 2009). It is for this reason that the G2 and G3 motif are also known as the switch I and II region, respectively. To discriminate between GTP binding andGDP, the backbone carbonyl group of threonine/serine (G2 motif) and backbone amide of glycine (G3 motif) recognizes the γ-phosphate by forming hydrogen bonds. Together, the threonine/serine residue of the G2 motif and an aspartate residue in the G3 motif coordinate the magnesium cation that is responsible for weakening the phosphoanhydride bond between the β- and γ-phosphate (Pai *et al*., 1990). During GTP hydrolysis, the conserved glutamine in the G3 motif helps coordinate a catalytic water molecule and stabilizes the GTP transition state via forming a hydrogen bond with the γ-phosphate (Privé *et al*., 1992 and Gavriljuk *et al*., 2012). A number of GTPases lack the conserved glutamine and which is instead replaced by another amino acid that still fulfils its function. TRAFACs such as EF-Tu generally contains a catalytic histidine in the switch II region (DXXGH) that acts in a similar way to glutamine (Daviter *et al*., 2003). HAS-GTPases contain a hydrophobic residue (DXXGh, where "h" is a hydrophobic residue) and must utilize a different catalytic residue, typically found either the switch II region or elsewhere in the protein (discussed later) (Mishra *et al*., 2005 and Anand *et al*, 2006).

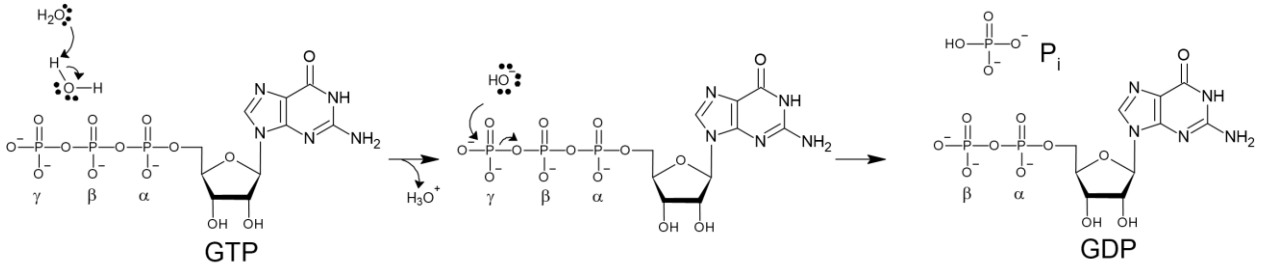

GTP + H_2O → GDP + P_i

Figure 6. Typical GTP hydrolysis reaction. GTP is hydrolytically cleaved between the β- and γ-phosphate, resulting in the formation of GDP and P_i.

Many GTPases play a regulatory role and are thus inactivated upon GTP hydrolysis. It is therefore unsurprising that mutational hotspots can occur within the protein sequence that can lead to impaired or abolished GTP hydrolysis. For instance, G3 motif mutations have also been linked to impaired GTP hydrolysis (like the G1 motif), such as Q61H/K/L in K-Ras. These side chain disrupts proper orientation of the hydrolytic water molecule, essentially "locking" GTPases in a biologically active conformational state (Mishra *et al*., 2005 and Song *et al*., 2025). So far, the role of GTP hydrolysis in TRAFAC GTPases has been reported to regulate translation, signal transduction, cell motility, and intracellular transport (reviewed by Verstraten *et al*., 2011).

The SIMIBI sub-class encompasses GTPases and other NTPases that differ from TRAFACs, based on three key elements in the protein sequence; the G1 motif, G2 motif and the lack of a conserved threonine or serine within. Despite sharing a G1 motif with TRAFAC class GTPases, members of the SIMIBI class contain an extra highly conserved glycine in the G1 motif (GxxGxGK(S/T)). The SIMIBI class also shares a G2 motif, although it is less conserved ((V/I/L)N(L/M)D(T/P)) than members of the TRAFAC class. Moreover, the G2 motif lacks the signature threonine or serine residue and instead contains a highly conserved aspartate residue that functions similarly (Leipe *et al*., 2002 and Gras *et al*., 2007). Members of the SIMIBI class have been reported in co-translationally target proteins to the cell membrane or secretion, cell division and biotin synthesis (Leipe *et al*., 2002).

Interestingly, a class of GTPase has been identified from across the TRAFAC and SIMIBI sub-class in which the catalytic glutamine within the switch II region is substituted for a hydrophobic amino acid. The HAS-GTPase class typically has one of the following amino acids such as: leucine, isoleucine, valine, methionine and phenylalanine (Mishra *et al*., 2005 and Anand *et al*, 2006 and Vithani *et al*., 2017). As previously discussed, this catalytic glutamine is essential for GTP hydrolysis. In GTPases such as Ras, the active conformational state is associated with the catalytic glutamine and therefore the switch II loop — pointed inwards towards the nucleotide binding pocket. However, all HAS-GTPases have been observed to have their switch II loop pointed outwards to avoid interactions with the γ-phosphate, arising from the hydrophobic properties of the HAS in members such as HflX and YchF (Mishra *et al*., 2005 and Anand *et al*, 2006). The HAS is stabilized by a hydrophobic pocket formed by residues from two regions: a hydrophobic residue prior to the P-loop (G1 motif) and from helix α3 (G3 motif). Yet, all HAS-GTPases are still capable of catalyzing GTP hydrolysis as efficiently as others and typically utilize

catalytic residues from outside the switch II region (Mishra *et al*., 2005). These amino residues typically are glutamate (FeoB and MnmE), aspartate (Era), the amide backbone of glycine (HflX; Figure 7A) and histidine (YchF; Figure 7B). For the purposes of this thesis, the SIMIBI sub-class will not be discussed further.

Nearly all GTPase identified to date specifically bind to GTP and GDP. Although, the G1-G3 motif is primarily responsible for discriminating between triphosphate and diphosphate nucleotide, GTPase are well known to only bind to guanine nucleotides. Both the G4 motif ((N/T)(K/Q)XD) and G5 motif (SAX) are responsible for imparting guanaine nucleotide specificity (Dever et al., 1987 and Bourne *et al*., 1991). Within the G4 motif, a highly conserved asparagine and aspartate residue interacts with the keto group and amine protons of the guanine

ring, respectively (Figure 8A) (la Cour *et al*., 1985). Both amino acid residues form hydrogen bonds with their respective recognition elements at the Watson-Crick face of a nitrogenous base. A hydrophobic pocket is formed between the G4 motif lysine residue and G5 motif (SAX) that helps position the guanine base in the proper orientation. In an X-ray structure of EF-Tu·GDP, a close-up view of this hydrophobic pocket shows that K136 forms a hydrophobic cavity together

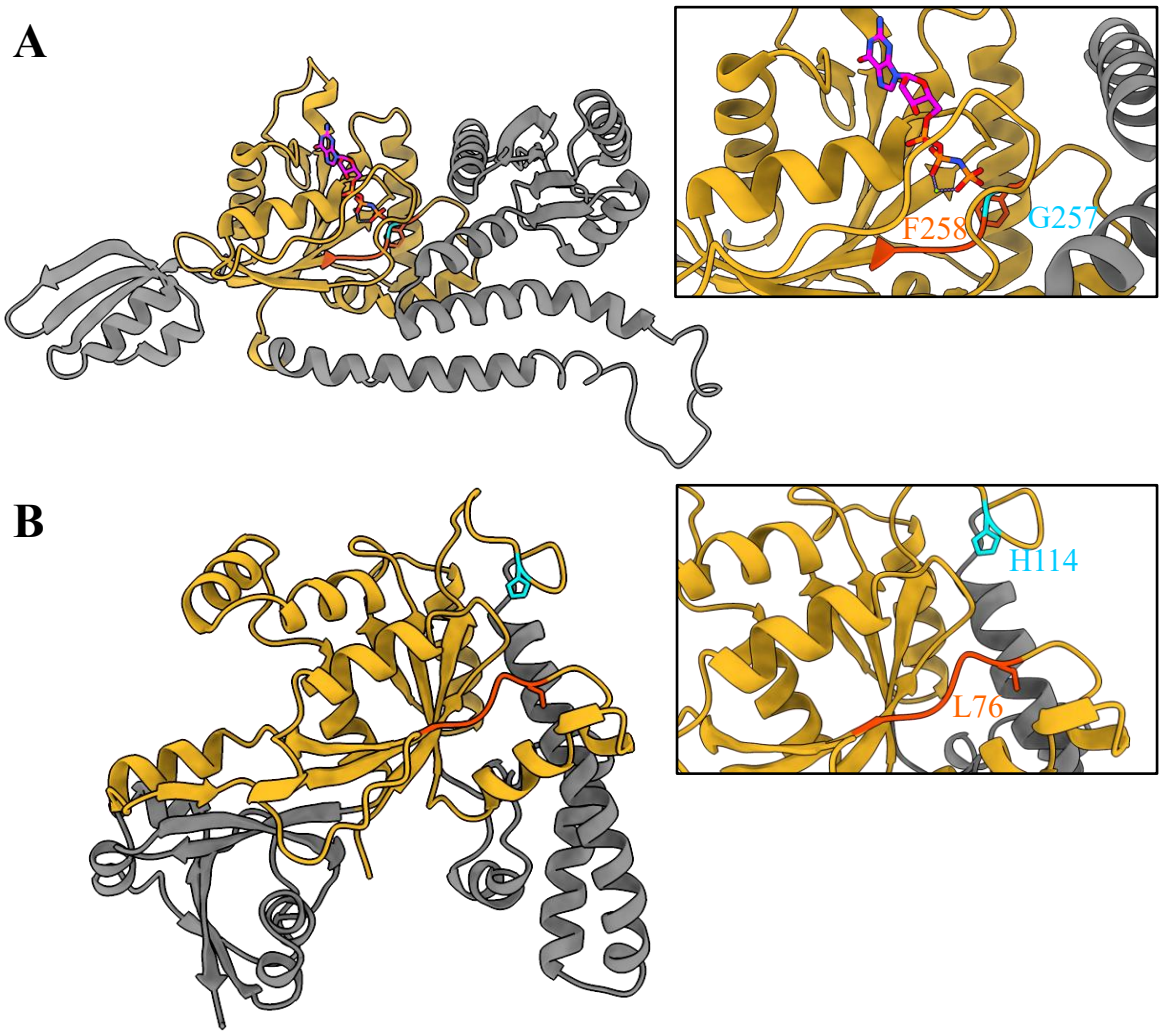

Figure 7. HAS-GTPases use alternative amino acid catalytic residues for GTP hydrolysis. In HAS-GTPases, the glutamine in the switch II region (orange) of many GTPases is replaced with a hydrophobic amino acid (side chain and label shown) and a catalytic residue (cyan) must be move from elsewhere to carry out GTP hydrolysis. **A)** HflX (PDB: 8A57) is shown sourcing a catalytic amide group from the peptide backbone of glycine, within the switch II region. A non-hydrolyzable analog of GTP is shown (phosphoaminophosphonic acid guanylate ester; pink) bound in the nucleotide binding pocket. **B)** On the other hand, an Alphafold prediction of YchF (Uniprot ID: P0ABU2) is shown sourcing a catalytic histidine from a nearby flexible loop, outside the switch II region (Rosler *et al*., 2015). ChimeraX was used to visualize the 3D structure.

with L175 and T26, stabilizing guanine ring via hydrophobic interactions (Figure 8B) (la Cour *et al*., 1985 and Andersen *et al*., 2000).

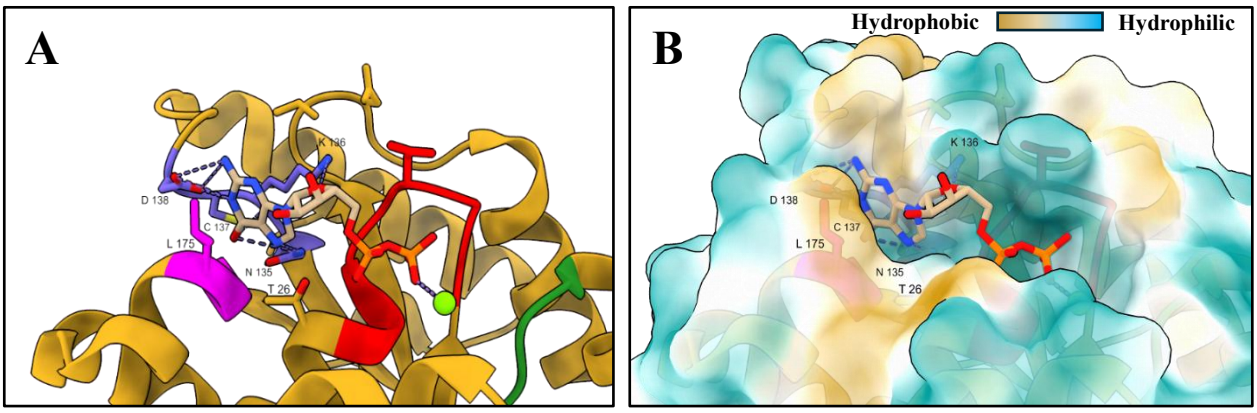

Figure 8. The G4 motif is responsible for imparting guanosine nucleotide specificity. **A)** EF-Tu is shown bound to GDP (PDB: 1DG1) near the G4 motif (purple). The G1 (red), G3 (green) and G5 (pink) motif are shown for proximity to the G4 motif. **B)** Lysine from the G4 motif forms a hydrophobic binding pocket for the guanine ring with T26 (G1 motif) and L175 (G5 motif). ChimeraX was used to visualize the 3D structure.

1.2.1.2. The G4 motif imparts GTP-binding specificity

Although the G4 and G5 motif both impart nucleotide specificity, the former contributes the most to nitrogenous base recognition. The specificity of the G4 motif is driven primarily by hydrogen bonds between the side chain and the Watson-Crick face (la Cour *et al*., 1985) (Figure 8A). Mutational studies that replaced either the asparagine or aspartate residue demonstrated reduced GTP binding affinity (~100-fold) and abolish nucleotide binding, respectively (Clanton *et al*., 1986 and Feig *et al*., 1986). This observation is consistently reported across many GTPases such as Ras p21 (Clanton *et al*., 1986 and Feig *et al*., 1986), EF-Tu (Hwang & Miller, 1987) and FeoB (Marlovits *et al*., 2002). Shifts in nucleotide binding specificity away from GTP has also been reported in the case of EF-Tu and FeoB. Substituting the aspartate residue to asparagine introduces a positively charged functional group in the side chain that stabilizes the keto group of xanthosine triphosphate (XTP) at the C6 position, resulting in nucleotide specificity to XTP (Hwang & Miller, 1987 and Marlovits *et al*., 2002).

1.2.2. Functional cycle of GTPases

GTPases operate much like molecular switches and are typically activated when they are bound to GTP (Figure 9). The GTP-bound state is often referred to as the "on" state because they are functionally active. Upon hydrolysis of GTP into GDP and P_i, GTPases enter an inactivated "off" state. Subsequent nucleotide exchange occurs to reactivate GTPase, completing its functional cycle. Two accessory factors typically regulate the progression of a GTPase throughout its functional cycle. These are the GTPase activating protein/factor (GAP/F) and the guanine nucleotide exchange factor (GEF).

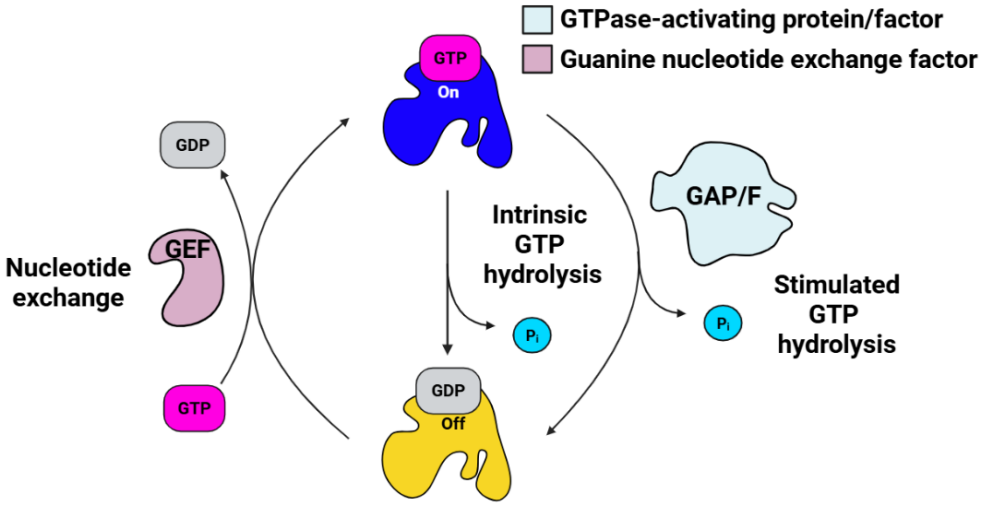

Figure 9. The molecular cycle of GTPases. GTPases share a common functional cycle, switching between GTP-bound ("on" state) and GDP-bound ("off" state) states. GTP hydrolysis separates both nucleotide-bound states and many GTPases interact with a GAP/F to accelerate this step. After GTP hydrolysis and subsequent release of P_i, nucleotide exchange occurs to replace GDP with GTP. This step is typically facilitated by the help of GEFs, accelerating nucleotide exchange and completing the functional cycle. The figure was made using BioRender.

1.2.2.1. GTPase activating proteins/factors (GAP/Fs)

GTP hydrolysis is driven by the repulsive electrostatic forces between β- and γ-phosphate group of a nucleotide and can occur spontaneously in water (10^{-7} to 10^{-6} s^{-1}; Åqvist and Kamerlin, 2015) (Figure 6). The presence of a GTPase help accelerate hydrolytic cleavage via its G domain by about 100-fold, such as in the case of EF-Tu. It's intrinsic GTPase activity is typically between 10^{-5} to 10^{-4} s^{-1} (Maracci et al., 2014). Intrinsic GTPase activity is typically slow – often occurring in time scales of seconds to hours (Ahmadian *et al.*, 1997, Martemyanov *et al.*, 2000 and

Grigorenko *et al*., 2008). Overcoming this rate limiting step is especially important in the context of the cell where cellular processes such as translation occur in the time scale of microseconds to milliseconds (Sakmann & Neher, 1984, Pape *et al*., 2009, Proshkin *et al*., 2010 and Silva *et al*., 2014). As a result, nearly all GTPases bind to a GTPase activating protein or factor (GAP/F) to accelerate nucleotide hydrolysis (Eccleston et al., 1993, Martemyanov *et al*., 2000 and Mohr *et al*., 2002). GAP/F can accelerate GTPase activity by about 10^5-fold, such in the case of Ras proteins (Eccleston *et al*., 1993). In translation, nearly all trGTPase are stimulated upon binding to the ribosome, typically by 10^7-fold (Martemyanov *et al*., 2000, Mohr *et al*., 2002 and Jain *et al*., 2009). As mentioned previously, many trGTPase follow a phenomenon known as molecular mimicry because they share similar structural features that mimic the geometry of a tRNA (Nissen *et al*., 1995 and Selmer *et al*., 1999). As a result, they generally dock at the A-site of the ribosome at the GAC with the assistance of the ribosomal stock proteins bL7/bL12 and stimulated by the SRL.

Recruitment of trGTPase to the ribosome is facilitated by the L7 and L12 ribosomal stalk proteins (Diaconu *et al*., 2005 and Helgstrand *et al*., 2007). Both stalk proteins are dimers of each other, but the only difference is that L7 is acetylated on a N-terminal serine (Gordiyenko *et al*., 2008). Two to three of the L7/L12 dimer can be found consecutively bound on the L10 anchor on the 50S subunit, forming the flexible ribosomal stalk that recruits trGTPases from the cytoplasm (Diaconu *et al*., 2005). Binding occurs at the C-terminus of L12 and is shared amongst many trGTPases, including IF2, EF-Tu, EF-G and RF3 (Helgstrand *et al*., 2007). Its role in stimulating GTPase activity is supported by a study that reconstituted ribosomes with purified L7/L12 observed accelerated GTP hydrolysis in EF-Tu (~2,500-fold) and EF-G (>4,000-fold), in comparison to the absence of dimers (Mohr *et al*., 2002). After recruitment, trGTPase are positioned close to the SRL to stimulate GTPase activity.

The SRL is a highly conserved ribosomal region, located in helix 95 of the 23S rRNA (50S ribosomal subunit in prokaryotes) or 28S rRNA (60S ribosomal subunit in eukaryotes). This short region (prokaryotes: nucleotides 2646–2674) adopts a compact hairpin secondary structure and contains an essential adenine (A2660) that interacts with trGTPase (García-Ortega *et al*., 2010 and Shi *et al*., 2012). Historically, the origins of the SRL's name stems from the fact that it is the target of two toxins: α-sarcin (Endo *et al*., 1983 and Endo & Tsuragi, 1987) and ricin. Both toxins cleave the nitrogenous base of A2660 (ricin) or phosphodiester bond between G2661 and A2662 (α-sarcin), impairing the interaction between the ribosome and trGTPases (García-Ortega *et al*.,

2010). Structural analysis reveals that phosphate oxygen of A2662 is in close proximity to the catalytic histidine of EF-Tu and EF-G, suggesting a potential catalytic role (Koch *et al*., 2015). Whether A2662 directly catalyzes GTP hydrolysis has been largely debated. An initial model was proposed that suggest that A2662 enables the catalytic histidine to be deprotonated and behave as a general base (Voorhees *et al*., 2010). Yet, biochemical and structural data suggests that the histidine must be protonated to stabilize the negatively charged β- and γ-phosphate of GTP (Liljas *et al*., 2011 and Zhou *et al*., 2012). Despite massive debate, the most recent literature suggests that SRL is not catalytically involved but instead serves as an anchor point for the G domain (García-Ortega *et al*., 2010, Shi *et al*., 2012).

1.2.2.2. Guanine nucleotide exchange proteins (GEFs)

Nucleotide exchange occurs following GTP hydrolysis to replenish the GTPase with a new molecule of GTP, completing the functional cycle (reviewed by Caldon & March, 2003 and Verstraten *et al*., 2011). Many GTPases are capable of nucleotide exchange on their own (Wilden *et al*., 2006, Jain *et al.*, 2009 and Shields *et al*., 2009). However, others require the assistance of GEFs to accelerate nucleotide exchange (Gromadski *et al*., 2002, Innocenti *et al*., 2002 and Li *et al*., 2024). Whether a GTPase requires a GEF depends on how fast GDP dissociates or if regulation at this step is required. Generally, a GDP dissociation rate above 1 s^{-1} is considered "fast", as cellular processes occur from microsecond to millisecond, as previously described (Sakmann & Neher, 1984, Pape *et al*., 2009, Proshkin *et al*., 2010 and Silva *et al*., 2014). For instance, even though EF-Tu and EF-G are paralogs of each other, only EF-Tu requires a GEF (EF-Ts) (Gromadski *et al*., 2002). The dissociation rate of GDP in the absence of a GEF ranges from 1.7×10^{-3} s^{-1} (Chau *et al*., 1981), but the assistance of EF-Ts increases the dissociation rate by a factor of 6,000-fold (Gromadski *et al*., 2002). EF-G for comparison has a rapid intrinsic GDP dissociation rate of 300 s^{-1} – a 10^5-fold difference than the intrinsic GDP dissociation of EF-Tu (Wilden *et al*., 2006).

1.2.2.3. Distinct nucleotide-bound conformational states

GTPases typically adopt distinct conformational states, depending on the nucleotides they are bound to (GTP, GDP and short-lived unbound state; *apo*). One of the most notable examples of massive conformational changes between GTP and GDP-bound states is EF-Tu. The G domain (also known as domain I) of EF-Tu undergoes approximately a 90º degree rotation during

nucleotide exchange from GDP to GTP, relative to the rest of its domains (II and III). A "hole", normally formed between the three domains in the GDP-bound state is closed in the GTP-bound state and the protein adopts a compact, globular structure (Figure 10) (Kjeldgaard *et al*., 1993 and Abel *et al*., 1996). In other words, the mechanism of EF-Tu conformational change is similar to a loaded spring mechanism, introduced by Vetter & Wittinghofer (review; 2001). The loaded spring mechanism describes how both switch regions store potential energy upon tightly binding to GTP which is released upon GTP hydrolysis. Conversely, transitioning from GTP-bound to GDP-bound induces the opposite effect (Figure 10A). Upon GTP hydrolysis, the loss of the γ-phosphate is detected by both switch regions, resulting in a relaxation of the "spring". During translation, EF-Tu·GTP forms a quaternary complex with the 70S ribosome and aminoacyl-tRNA. The ribosome stimulates GTP hydrolysis in response to codon recognition. EF-Tu undergoes a conformational change that disrupts the G domain interaction with the SRL, as well as the switch II region with the tRNA acceptor arm. This major conformation change lowers the binding affinity between EF-Tu and aminoacyl-tRNA, leading to aminoacyl-tRNA release deep into the ribosome A-site and subsequent EF-Tu dissociation from the ribosome (Schmeing *et al*., 2009). The loaded spring mechanism is shared across many GTPases such as EF-G. Similarly, EF-G·GTP adopts a closed and compact structure but, EF-G·GDP adopts an open and loose state (Figure 10B) (Connell *et al*., 2007). When bound to the ribosome, EF-G·GTP undergoes a massive conformational change at the switch I and II region upon GTP hydrolysis (Ticu *et al*., 2009). This conformational change is substantial enough to stabilize the ribosome rotational states; overcoming the energetic barriers needed to shift the mRNA one codon downstream during translocation (Connell *et al*., 2007).

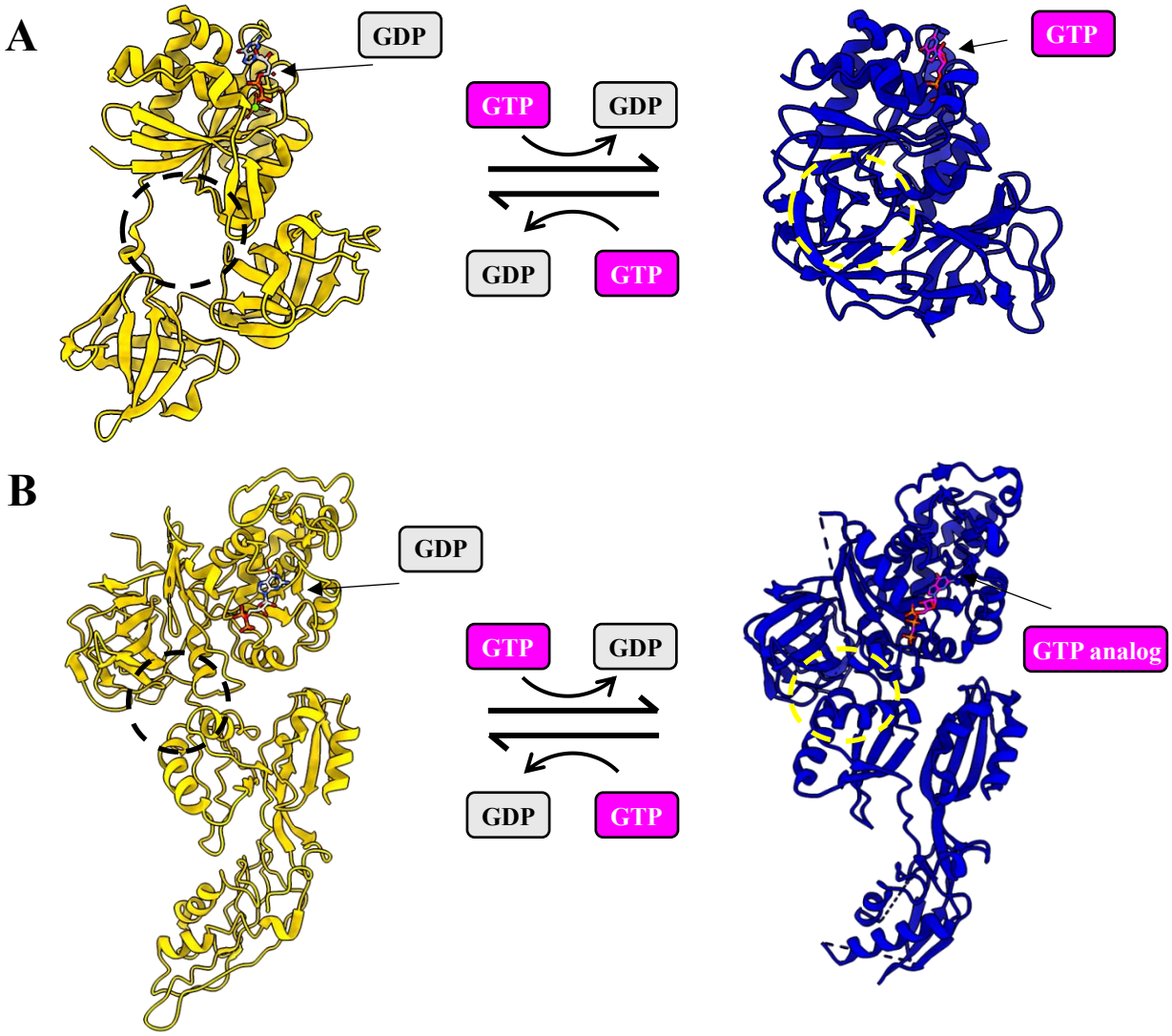

Figure 10. Difference between the 3-dimensional GTP- and GDP-bound structures of GTPases. The GDP-bound ("off"; yellow) and GTP-bound ("on"; blue) states are shown with their respective nucleotides; coloured grey and magenta, respectively. **A)** EF-Tu·GDP (PDB: 1DG1) adopts an open and loose structure, while EF-Tu·GTP (PDB: DWD8) adopts a closed and compact structure when bound to the ribosome and aminoacyl-tRNA. Similar structural features can be described for **B)** EF-G·GDP (PDB: 5OTZ) and EF-G·GCP (Phosphomethylphosphonic acid guanylate ester, PDB: 4V9H). The "hole" in the middle of the protein structure (as indicated by the circle) closes upon binding to GTP. The available 3D structures of both EF-Tu and EF-G were visualized using ChimeraX.

1.3. YchF – A universally conserved NTPase that binds to ATP and GTP

To date, only eight highly conserved GTPases that are shared across the three domains of life have been identified (Figure 4) (reviewed by Caldon & March, 2003). Of these eight GTPase, YchF is a GTPase that has seen growing interest over recent years for its potential role in translation (Becker *et al*., 2012, Rosler *et al*., 2015, Landwehr *et al*., 2021 and Yu *et al*., 2025). In the literature, YchF other names include: hOLA1, EngD, DOC45, GBP45, GTBP9, PTD004, YyaF, DugA and Ybr025c (Danese *et al*., 2004, Koller-Eichhorn *et al*., 2007, Kira & Nishikawa, 2008, Zhang *et al.*, 2009a, Sun *et al*., 2010 and review by Semmelrock & Wieden, 2026). YchF was initially identified in *Mycoplasma* spp., during attempts to engineer the smallest gene set possible that can sustain a living cell. In this experiment, *M. capricolum* was used as a host chassis for the reduced genome of *M. mycoides* (JCV-syn1.0). After removing non-essential genes, *ychF* remained as one of the core 901 genes (Lartigue *et al*., 2009). In the third iteration (JCV-syn3.0), the genome size was largely reduced to 473 genes, yet *ychF* was not removed during the selection process (Hutchison *et al*., 2016). Despite being a highly conserved GTPase, the deletion of *ychF* is not lethal to cells (Morimoto *et al*., 2002, Zhang *et al*., 2009b), yet other universally conserved GTPases such as EF-Tu have been demonstrated to be essential to cell viability (Figure 4) (Abdulkarim *et al*., 1991). As a result, it is currently unclear as to why YchF is widely distributed across all three domains.

1.3.1. The wide-ranging cellular role of YchF

YchF has been reported to be involved in a variety of cellular processes, suggesting it's a master regulator. These cellular processes include cancer progression (Sun *et al*., 2010 and Bian *et al*., 2022), cell proliferation (Kira & Nishikawa, 2008 and Matsuzawa *et al*., 2014), mitochondria function (Kira & Nishikawa, 2008), virulence (Fernebro *et al*., 2008 and Chen & Chung, 2011), cell stress (Wenk *et al*., 2012, Landwehr *et al*., 2021 and Jiang *et al*., 2024), protein degradation (Guerrero *et al*., 2006 and Gradia *et al*., 2009) and translation (discussed later in section 1.3.4.).

In cancer progression, YchF has been reported to be upregulated in tumors related to colon, rectum, ovary, lung, stomach, and uterus. The localization of YchF had been found to be in the nucleus and is downregulated in response to DNA damage (Sun *et al*., 2010). In breast and ovarian cancer cells, YchF is localized to the centrosome and γ-tubulin in spindle fibers during mitosis. YchF can also interact with the breast/ovarian tumor suppressor BRAC1 and its binding partner

BARD1 (Matsuzawa *et al*., 2014). BRAC1 and BARD1 forms a heterodimer that functions as a ubiquitin ligase (Brzovic *et al*., 2003) involved in DNA repair (Wu *et al*., 2023), transcription (Scully *et al*., 1997) and centrosome regulation (Hsu & White, 1998). This binding interaction with the heterodimer complex suggests a role for YchF in regulating the centrosome and therefore cell proliferation in cancer. Cytoplasmic YchF also seems to play a regulatory role via controlling expression levels of GSK3β and focal adhesion kinase (FAK), two cell signalling proteins involved in cellular pathways related to, for instance, hypoxia response in colorectal cancer (Liu *et al*., 2022), metastasis in oral cancer (Liu *et al*., 2020) and cell adhesion (Jeyabal *et al.*, 2014).

Other cellular pathways that YchF regulates can also target the mitochondria during oxidative stress. For example, in the absence of YchF, the MAPK/Pmk1 signalling pathway increases reactive oxygen species in the mitochondria and the cell responds by expressing two heat shock transcription factors: heat shock factor 1 (Hsf1) and Ssa1 (Luo *et al*., 2025). Reactive oxygen species arises because the mitochondrial electron transport chain can sometimes generate species such as superoxide and hydrogen peroxide at complex I (Liu *et al*., 2002). The same effect can be obtained with mitochondrial electron transport chain inhibitors (Koopman *et al*., 2005). YchF inhibits this feedback loop by directly prevent the upstream kinase Pek1 from phosphorylating Pmk1 (Luo *et al*., 2025). These recent findings support an earlier study in which functionally active YchF prevents cell death, induced by mitochondrial electron transport inhibitors (Kira & Nishikawa, 2008). In prokaryotes however, YchF has been reported to inhibit the catalase KatG in an ATP-dependent manner and is regulated by the stress response transcription factor OxyR (Wenk *et al*., 2012).

The role of YchF in virulence is limited and has been described in *Streptococcus pneumoniae*, *Vibrio vulnificus* and *Brucella melitensis*. *S. pneumoniae* is a Gram-positive extracellular, opportunistic pathogen that colonizes the nasopharynx (Weiser *et al*., 2018). It was demonstrated that YchF is required to obtain fast growth rates and efficient intranasal colonization (Fernebro *et al*., 2008). The role of YchF in virulence was later described in *V. vulnificus*, a Gram-negative flesh-eating bacterium. YchF is required for cytotoxicity against host macrophages and growth under iron-limiting mediums (Chen & Chung, 2011). The same finding was reported for *B. melitensis* under iron-limiting conditions (Danese *et al*., 2004).

During experiments to identify proteins bound stably or transiently to the proteasome, 64 potential proteins were identified. Of these 64 proteins, 42 were novel interactions and YchF was

discovered to be among of the novel proteins stably bound (Guerrero *et al*., 2006). A later study also confirmed that YchF was bound to the regulatory particle non-ATPase 10 (RPN10) proteasome subunit in *Trypanosoma cruzi* (Gradia *et al*., 2009).

1.3.2. Potential role in translation

YchF stands apart from nearly every other trGTPases for its ability to hydrolyze both GTP and ATP (Caldon & March, 2003; review, Becker *et al*., 2012, Rosler *et al*., 2015 and Cheung *et al*., 2016). ATP hydrolysis has been reported to be stimulated by ~10-fold (3.1 ± 0.2 min^{-1} from 0.36 ± 0.02 min^{-1}) upon binding to the 70S ribosome in bacteria (Tomar *et al*., 2011, Becker *et al*., 2012 and Rosler *et al*., 2015). To date, ATP binding has not been observed in other GTPases, aside the ribosome splitting GTPase HflX (Shields *et al*., 2009 and Dey *et al*., 2018). Ribosome binding has been shown biochemically and structurally in *E. coli* and *T. cruzi*, suggesting a potential role in translation (Gradia *et al.*, 2009, Landwehr *et al*., 2021 and Yu *et al*., 2025). Another line of evidence that links YchF to translation is that within the same operon, it is expressed co-transcriptionally with peptidyl-tRNA hydrolase (*pth*), a ribosomal auxiliary factor that hydrolyzes the ester bond of a peptidyl tRNA during ribosomal stalling (Schmitt *et al*., 1997, Cruz-Vera *et al*., 2002 and Ito *et al*., 2012). Typically, genes that are found within an operon are involved in related processes and share related roles. Currently, the exact role of YchF on the ribosome is unclear, but it is possible that the variety of phenotypes reported in the literature as described previously is linked to translation.

1.3.3. Structure of YchF

YchF exists as a monomeric, medium sized protein with a molecular weight of 40-45 kDa. The 3-dimensional protein structure is claw-like and divided into three key domains: N-terminal G domain, α-helical insertion domain (A-domain), followed up by a C-terminal ThrRS, GTPase, and SpoT (TGS) domain (Figure 11) (Becker *et al.*, 2012 and reviewed by Lin *et al*., 2023). A cleft (~20 Å) is formed between the A-domain and the TGS domain.

There currently exists structures of YchF bound to both guanine and adenine nucleotides, at the G domain (Koller-Eichhorn *et al*., 2007, Cheung *et al*., 2016, Cheung *et al*., 2022). The nitrogenous base of adenine and guanine nucleotides are orientated almost orthogonal to each other. YchF's classification as a HAS-GTPase positions the nucleotide within range of the catalytic histidine (H114), located in a flexible loop (Rosler *et al*., 2015). Interestingly, the G domain is

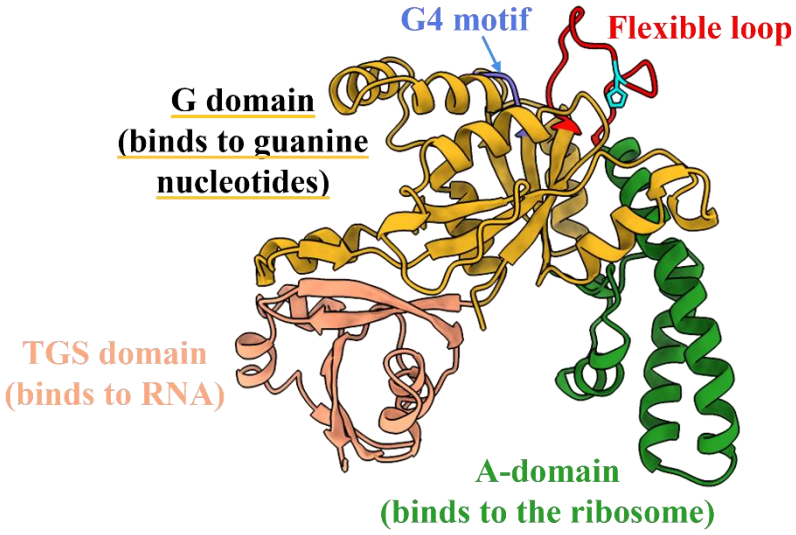

Figure 11. The 3D structure of YchF. The 3-dimensional structure of *E. coli* YchF was predicted using AlphaFold (Uniprot ID: P0ABU2) and contains: An N-terminal GTP-binding (G) domain (***yellow***) flanks an alpha helical domain (A-domain) (***green***) and ends with a C-terminal ThrRS, GTPase, and SpoT (TGS) domain (***pink***). The G4 motif is indicated (***purple***) and the flexible loop region (***red***) is shown with the catalytic histidine (***cyan***).

segmented (residues 1-118 and 203-278) due to the insertion of an α-helical domain (A-domain) (residues 119-202). A segmented G domain has only been identified in the Gα subunit of heterotrimer G proteins (Liu & Northup, 1998). Recent work by Yu *et al*., (2025) had elucidated that the A-domain is responsible for ribosome binding. The A-domain inserts into a groove, formed between ribosomal proteins L14 and L19 and helix 62 on the 50S subunit. Structural alignment between *apo* YchF and the 50S·YchF complex suggests that both the G domain and TGS domain undergoes a conformational change that narrows the cleft (Yu *et al*., 2025). Lastly, the C-terminal TGS domain (residues 279-363) has been reported to bind to the 3'CCA end of deacylated tRNA, as shown in RelA (Brown *et al*., 2016, Brandon, 2021).

Under oxidative stress conditions, YchF dimerizes via the formation of a disulfide bond at C35. The dimer (~90 kDa) exhibits reduced ATPase activity (~2-3-fold less) compared to monomers supplemented with strong reducing agents or thioredoxin 1 (Hannemann *et al*., 2016). It is possible that due to C35 proximity to the highly flexible G2 motif, formation of the disulfide bond impairs the loaded spring mechanism of YchF. The dimer does not form under optimal growth conditions, suggesting that the monomer plays an important role in the cell.

1.3.4. Non-canonical G4 motif confers dual-specificity nucleotide binding

YchF was initially identified as a GTPase based on sequence alignment and shared protein structural features (Teplyakov *et al*., 2003). However, its G4 motif deviates from the canonical sequence ((N/T)(K/Q)XD) in which the conserved lysine is lost and the aspartate is replaced with

a glutamate ((N/T)(M/L/V)XE). The loss of lysine and aspartate in YchF has resulted in some of species of YchF (ex. in *E. coli* and humans) preferentially binding to adenine nucleotides. Although in rice (*Oryza sativa*), YchF has been shown to have no preference for either nucleotide, based on binding studies (Cheung *et al*., 2016). Additionally, the crystal structure of *Thermus thermophilus* YchF has been solved with GDP bound (PDB: 2DBY; Kukimoto-Niino *et al*., unpublished), suggesting that this homolog of YchF is stable in the GDP-bound state. A combination of structural and biochemical studies on YchF later lead to it being reclassified as an ATPase, despite retaining guanine binding properties (Koller-Eichhorn *et al*., 2007, Becker *et al*., 2012 and Rosler *et al*., 2015).

In the literature, only a few GTPases have been identified to contain non-canonical G4 motifs similar to YchF. For instance, EngA (YphC/Der/YfgK) is a TRAFAC class GTPase, reported to be involved in ribosome assembly in bacteria and chloroplast (Bharat & Brown, 2014 and Suwastika *et al*., 2014). EngA is the only GTPase identified to possess two tandem G domains (GD1 and GD2), each with corresponding G4 motifs (Robinson *et al*., 2002). In cyanobactera and chloroplast homologs, GD1 contains a non-canonical G4 motif (NKCE), while the secondary G4 motif ((N/T)KXD) closely resembles the canonical sequence. The signature cysteine residue is found across cyanobacteria and plants, except *Gloeobacter* and reported to be involved in regulating redox signaling (Llop *et al*., 2023). Although no biochemical studies had been reported on the nucleotide binding specificity of cyanobacteria EngA to date, other bacterial homologs of EngA have been reported to still retain guanine specificity. In *E. coli* EngA, both G4 motifs (GD1 G4: NKAE and GD2 G4: NKXD) closely resemble the canonical G4 motif, suggesting both G domains can bind to guanine nucleotides. Interestingly, despite bearing similar 3-dimensional structure to other G domains, both play different roles. GD1 had been reported to regulate the orientation of GD2 to interact with specific ribosomal subunits (Hwang & Inouye, 2001 and Tomar *et al*., 2009). Both G domains still retain guanine nucleotide specificity even though the G4 motif of GD1 deviates from the canonical sequence.

Other GTPases have been identified to contain G4 motifs that resemble the canonical sequence, but interestingly lost guanine nucleotide specificity. *Vibrio cholerae* FeoB for example, despite sharing a similar G4 motif (NXXD) to the canonical sequence, has been identified to also bind to ATP for iron transport (Shin *et al*., 2019). *E. coli* FeoB in contrast is specific for guanine nucleotides. ATP hydrolysis was reported to be sufficient to carry out iron transport when GTP is

absent. To explain this dual-nucleotide specificity behaviour, Shin and colleagues examined the G5 motif that is also involved in imparting nucleotide specificity. Protein sequence alignment and phylogenetic analysis between *V. cholerae* FeoB, *E. coli* FeoB and other homologs reveal that the G5 motif is divided into either polar, or non-polar groups. The G5 motif of *E. coli* FeoB is non-polar, however *V. cholerae* FeoB is polar. In the latter, the authors identified and performed site-directed mutagenesis on S148 (S148V) and N150 (N150T) – two amino acid residues that potentially interacts with the adenine ring. Both S148V and N150T *V. cholerae* FeoB had greater affinity (Michaelis Menten constants: K_M) to GTP (S148V: 92.1 ± 32.7 μM and N150T: 261 ± 33.0 μM, respectively) than wild-type (648 ± 258 μM). The K_M constants reported were similar to wild-type *E. coli* FeoB (132 ± 57.1 μM). Despite sharing similar a G4 motif to the canonical sequence, the G5 motif can contribute significantly to nucleotide specificity as shown in *V. cholerae* FeoB.

1.3.5. Comparison of YchF's molecular switch-like behaviour to other GTPases

Even though GTPases have been identified with non-canonical G4 motifs or alter nucleotide specificities, one hallmark feature of GTPases is their molecular switch-like behaviour. As described previously, GTPases cycle between their functionally active ("On") and ("Off") inactive states (Figure 9). This feature is governed by the nucleotides that they are bound to, therefore GTPases are typically "turned on" when they are bound to GTP and "turned off" when bound to GDP or in the *apo* state.

YchF's cellular role is currently not well understood most likely because its switch-like behaviour has just begun to be elucidated. Early biochemical studies show promising results that the 70S ribosome behaves as an ATPase activating factor, analogous to the GAPs role for canonical GTPases (Tomar *et al*., 2011, Becker *et al*., 2012 and Rosler *et al*., 2015). Indeed, GTP hydrolysis serves to separate distinct conformational state associated with the three nucleotide-bound states (GTP, GDP and *apo*). Yet it remains to be shown if YchF adopts distinct conformational states in its ATP-dependent functional cycle, reflecting the switch-like behaviour observed in other GTPase (discussed in section 1.2.2.3.; Figure 10). Typically, GTPases adopt a closed and compact conformation when bound to GTP and become loose when bound to GDP or no nucleotides. Molecular dynamic studies by Rosler *et al*., (2015) have provided preliminary evidence that YchF does adopt an "open" and "closed" conformation. The dynamic region of YchF responsible for its "open" and "close" conformation is the extended flexible loop (residues 105-121) that contains the

catalytic histidine (Figure 11). In the available structures of YchF, only two (PDB: 7Y9I; Cheung *et al*., 2012 and 1NI3; Kniewel *et al*., unpublished) out of eight successfully resolved the loop, owing to its highly dynamic nature (Figure 5C for example). Rosler *et al*., (2015) reported that this flexible loop behaves as a hatch that closes upon ATP binding. Despite *in silico* analysis on the molecular switch behaviour of YchF, it has yet to be confirmed biochemically.

1.4. Research objectives

To date, only a few elements of the functional cycle of YchF have been elucidated. It is currently unclear whether YchF maintains the structural changes in response to the nucleotide di-/triphosphate bound that are typical for other trGTPase, despite altered nucleotide recognition motifs and associated nucleotide specificity. Determining whether YchF operates as a molecular switch will be critical information for deciphering YchF's molecular mechanism in other phenotypic traits reported in the literature. *I hypothesize that since YchF shares similar functional features with classical GTPases, and that modifying the G4 motif changes nucleotide specificity resulting in YchF being able to adopt distinct nucleotide-bound states reflecting the changed specificity for that particular nucleotide.* (Figure 12). To test this hypothesis, I will assess YchF's molecular switching behavior by first determining its binding affinities for di/triphosphate nucleotides. The binding affinities obtained will be used to select the optimal nucleotide concentration needed to obtain the respective saturated nucleotide-bound YchF complexes for structural probing via limited trypsinolysis .

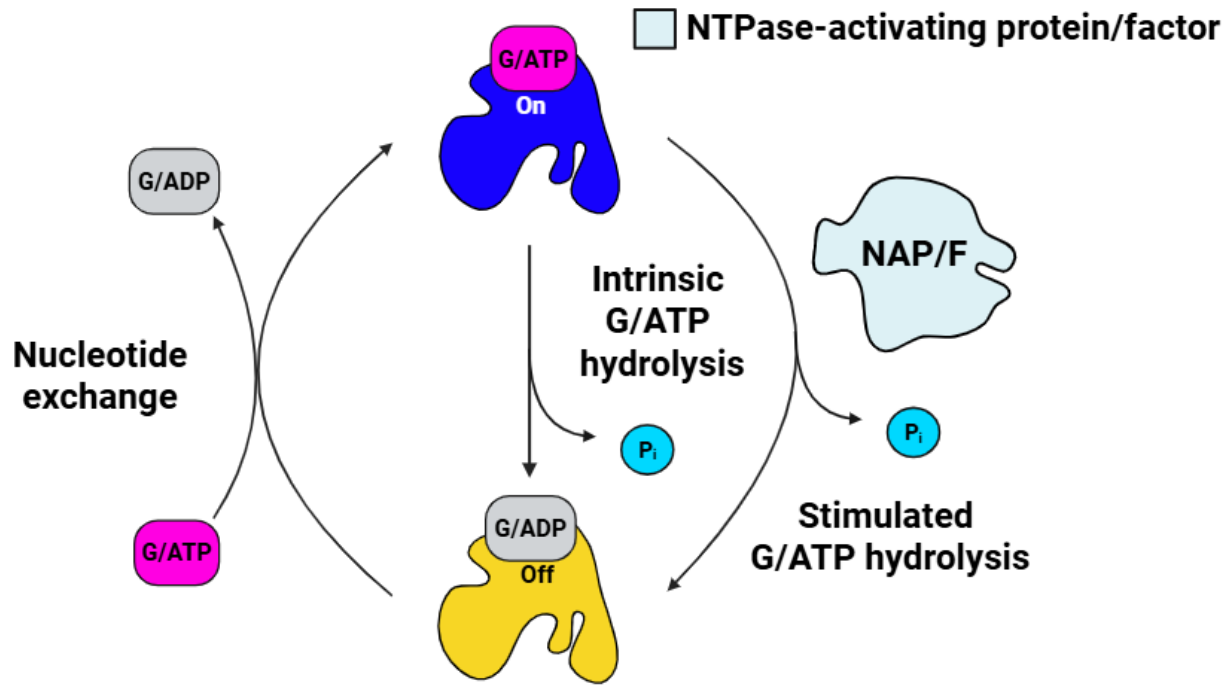

Figure 12. Proposed functional cycle of YchF. A G/ATP-dependent functional cycle for YchF is proposed based on the consensus switch-like behaviour of other GTPases. The figure was made using BioRender.

1.4.1. OBJECTIVE 1: Determine the nucleotide binding affinity of YchF and G4 variants

Wild-type *E. coli* YchF (G4 motif: NVNE) and its G4 variants (G4 motif: NLSS, NLSE and NKMD) were expressed with a N-terminal polyhistidine tag (6xHis) to facilitate protein purification via nickel-nitrilotriacetic acid (Ni-NTA) affinity chromatography. Anion exchange chromatography was carried out to separate YchF from RNA-bound populations and lastly size exclusion chromatography to separate based on size (Becker *et al*., 2012 and Rosler *et al*., 2015). YchF's nucleotide binding properties to ATP, GTP, ADP, GDP and their fluorescently labelled analog will be studied via equilibrium fluorescence titration to determine their binding affinities (K_D) (Becker *et al*., 2012). Obtaining the binding affinities can assess whether modifying the G4 motif plays a role in shifting the nucleotide-bound states YchF adopts in Objective 2.

1.4.2. OBJECTIVE 2: Probe the structural dynamics of YchF to determine distinct and relevant nucleotide-bound states

To probe the nucleotide-dependent structural dynamics of YchF for distinct nucleotide-bound states, limited trypsinolysis was performed to partially cleavage YchF. Fragments obtained at different stages of trypsin cleavage were analysed and quantified using sodium dodecyl sulfate-polyacrylamide gel electrophoresis (SDS-PAGE) followed by gel image densitometry, similar to previous a study designed to study the GTPase HflX (Fischer *et al*., 2012). If YchF is cleaved faster or slower for its ATP/GTP-bound states than its ADP/GDP/*apo* state, this suggests that YchF adopts distinct nucleotide-bound states, typically associated with the molecular switch function of GTPases. Additionally, assessing YchF G4 motif variants with for differences in nucleotide-bound states they adopt may establish a link between nucleotide specificity and inducing a conformational change.

2. Materials and Methods

2.1. Buffers and reagents

All solvents and reagents were purchased from Acro Organics, Becton Dickinson (BD), BioBasic, Bio-Rad, Sigma-Aldrich and Thermo Fischer Scientific. New England BioLabs. Nucleotides (ADP/ATP and GTP/GDP) were obtained from Sigma-Aldrich and their 2'/3'-O-(N-Methyl-anthraniloyl) (mant)-analogs were obtained from Jeana Bioscience. *E. coli* BL21(DE3) were purchased from New England BioLabs. All buffers were filtered and degassed using sterile 0.45 µm nitrocellulose membrane filters (Cytiva Whatman^{TM}) prior to use.

2.2. Overexpressing wild-type YchF and variants

All *E. coli* BL21(DE3) strains (Invitrogen; Cat. No. C6000–03) transformed with an expression vector (pET28a) encoding either wild-type (WT) YchF or its G4 motifs variants (YchF_NLSE/NLSS/NKMD; unpublished) were previously transformed by the lab group using New England Biolabs protocol (Cat. No. C2527) (Table 1). The plates were grown overnight at 37ºC (Forma Scientific CO_2 water jacketed incubator) and used the next day to prepare overnight cultures. The overnight cultures were prepared by selecting a bacterial colony to inoculate an Erlenmeyer flask containing 100 mL LB medium (pH 7.5) and 50 µg/mL kanamycin. Overnight cultures were grown at 37ºC, shaking at 100 rpm. The next day, cells were harvested (5,000 × g, 15 minutes) in a 50 mL Falcon tube (Sarstedt) and the resulting cell pellet was resuspended in 10-20 mL of fresh LB without antibiotics. The optical density at 600 nm (OD_{600}) was calculated based on UV-Vis measurements (Pharmacia Biotech Ultrospec 3000) and used to calculate the volume of starting culture used to inoculate protein expression cultures to initial OD_{600} of 0.1.

Table 1. Expression vectors encoding ychF that were used for protein overexpression.

Plasmid	**Plasmid backbone**	***ychF* gene**	**Resistance marker**	**Significance**
pET28a_YchF	pET28a	WT	Kanamycin	ATP-binding
pET28a_YchF_NLSE		YchF_NLSE		Hypothesized no binding
pET28a_YchF_NLSS		YchF_NLSS		Hypothesized ATP-binding
pET28a_YchF_NKMD		YchF_NKMD		Hypothesized GTP-binding

Protein expression cultures were prepared in 4 × 500 mL LB (pH 7.5, 50 µg/mL kanamycin) and inoculated to an OD_{600} of 0.1. Cultures were grown at 37 ºC with shaking at 225 rpm and cell density was monitored by OD_{600}. Protein expression was induced at $OD_{600} \approx 0.6$ with 1 mM isopropyl β-D-1-thiogalactopyranoside (IPTG) and continued for 3 h (37 ºC), except for YchF_NKMD, which was induced at 0.6 OD and incubated overnight at 15 °C to improve solubility. Sample volumes were collected at 0, 1 and 3 h (or after overnight induction) to an equivalent of 0.1 OD and were analyzed by 12% (v/v) SDS-PAGE to confirm overexpression (section 2.10.2.). After protein overexpression, all cell cultures were harvested (4,000 × g, 20 minutes, 4 ºC) (Thermo Scientific Sorvall Lynx 6000), typically yielding 6-10 g of cell pellets. Cell pellets were flash-frozen in liquid nitrogen and stored at −80 ºC until cell opening.

2.3. Protein solubility test

Small scale protein expressions in 500 mL LB media were carried out similarly to what was described previously (section 2.2.) to assess the solubility of YchF_NKMD under different growth temperatures (15ºC, 25ºC or 37ºC) or different IPTG induction concentrations (0.1 mM, 0.5 mM and 1 mM). As a positive control, WT YchF was treated to the same growth conditions. Typically, ~2 g of cells was obtained for cell opening. Cell opening was carried out at 4ºC wherever possible. During cell opening, the cell pellet was resuspended in 3 mL of lysis buffer (50 mM Tris-Cl pH 8.0, 1 mM EDTA pH 8.0 and 10 mM NaCl) with constant stirring in the presence of ~8 µM PMSF and 10 mg/mL lysozyme. This step was carried out for 1 hour, after which 4 mg of deoxycholate per gram of cells was added. To ensure complete cell opening, all cells were sonicated (2 x 15 s sonication at 50% amplitude, with 30 s rest on ice). All samples were centrifuged first (Thermo Scientific Sorvall X4R Pro-MD) (4,000 x g, 30 minutes) to remove unopened cells, then at (Thermo Scientific Lynx 6000) (30,000 x g, 30 minutes all at 4ºC) to remove cellular debris. To assess whether YchF_NKMD was soluble, components of the lysate were saved for SDS-PAGE analysis and are as follows. The supernatant (soluble fraction) obtained after centrifugation was saved, while the remaining pellet was resuspended in 1 mL of 0.1 M Tris-Cl pH 8.5, containing 5 M urea. After resuspending the pellet, the sample was centrifuged (Thermo Scientific X4R Pro-MD) (4,000 x g, 15 minutes, 4ºC) and the resulting supernatant was saved (insoluble fraction). The remaining pellet was resuspended in 1 mL H_2O and centrifuged once again (4,000 x g, 15 minutes, 4ºC) and the resulting supernatant was saved. All fractions obtained were stored at -20ºC until SDS-PAGE analysis (section 2.10.2.).

2.4. Protein purification

All YchF variants and wild-type protein were purified using the same protocol at 4 ºC. Cell pellets were resuspended in binding buffer (50 mM Tris-Cl pH 7.5, 60 mM NH_4Cl, 7 mM $MgCl_2$, 7 mM β-mercaptoethanol, 1 mM phenylmethylsulfonyl fluoride (PMSF), 300 mM KCl, 10 mM imidazole and 15% (v/v) glycerol) per gram of cells and lysed with lysozyme (BioBasic; 1 mg/mL) for 30 minutes with constant stirring. After 30 minutes, the resulting cell lysate was supplemented with 12.5 mg of sodium deoxycholate per gram of cells, together with 1 µL of DNase and the cell lysate was subsequently stirred for an additional 30 minutes. The crude cell lysate was then centrifuged (30 000 x g, 45 minutes) to remove cellular debris and the resulting supernatant was filtered via a 0.45 µm syringe filter (FroggaBio PES membrane). The processed supernatant was passed through a Ni^{2+}-Sepharose column (Ni-NTA resin) with a column volume (CV) of 7 mL to maximize protein binding. A constant flow rate of 1 mL/min was used to pass the supernatant through the column and the column was washed with 10 CV of 8% elution buffer (binding buffer with 250 mM imidazole) (20 mM imidazole) to remove unspecific proteins. Then a linear gradient (20 – 250 mM imidazole) was applied to elute YchF. Protein elution fractions that were confirmed on SDS-PAGE (section 2.10.2.) to contain YchF were pooled together and buffer exchange was carried out via a Amicon® ultra centrifugal filter with a 30 kDa molecular weight cut-off (MilliporeSigma). Elution buffer was exchanged to Q-Sepharose buffer A (50 mM Tris-Cl pH 7.5, 10 mM $MgCl_2$, 5 mM ethylenediaminetetraacetic acid (EDTA), 1 mM dithiothreitol (DTT)). YchF was then applied to a 60 mL Q-Sepharose column with a constant flow rate of 1 mL/min and allowed to bind in 1.8 CV. A linear gradient was applied to elute YchF in 4 CV (0 – 1 M KCl). The presence of RNA that co-elute with YchF was analyzed, following ethanol precipitation protocols (section 2.5.). Elution fractions that contained YchF were concentrated as described above and buffer exchanged with $TAKM_7$ buffer (50 mM Tris-Cl 7.5, 70 mM NH_4Cl, 30 mM KCl, 7 mM $MgCl_2$) containing 1 mM DTT. YchF was applied to a 200 mL Superdex 75 column with a flow rate of 1 mL/min and eluted out in 2 CV of $TAKM_7$, containing DTT. The resulting fractions that contained YchF were concentrated and subsequently quantified by UV-Vis. The absorbance at 280 nm was measured to utilize Beer-Lambert's Law and the calculated value of WT YchF's extinction coefficient ($\varepsilon_{280\ nm}$ = 39, 667 $M^{-1}cm^{-1}$) (obtained using Expast Protparam; Gasteiger *et al*., 2003) to measure protein concentration. Aliquots of purified YchF was prepared and were subsequently flash-frozen in liquid nitrogen for storage at −80 ºC.

2.5. Ethanol precipitation of RNA

Elution fractions from Q-Sepharose (section 2.4.) were pooled based on absorbance readings at 254 nm which corresponds to RNA. Typically, ~21 mL of pooled sample was obtained and subsequently mixed with 0.1 volumes of 3 M NaOAc pH 5.2 and 2 volumes of 100% (v/v) ethanol. RNA was precipitated for at least 24 hours at -20 ºC. After incubation, the precipitate was collected by centrifugation (Thermo Scientific Sorvall X4R Pro-MD) (5,000 x g, 5 min, 4ºC) and the resulting pellet, washed with 70% (v/v) ethanol. The RNA pellet was collected by centrifugation (5,000 x g, 5 min, 4ºC) and the obtained pellet was resuspended in no more than 1 mL of RNase-free Milli-Q H_2O. The concentration of RNA was subsequently determined by UV-Vis spectroscopy at 260 nm, using Beer-Lambert's Law. Since YchF has been shown to co-purify with tRNA (Brandon, 2021), the extinction coefficient of tRNA ($\varepsilon_{260\ nm}$ = 5.0 x 10^5 M^{-1} cm^{-1}) (calculated based on formula provided by Guéron & Leroy, 1978) was used to determine the concentration.

2.6. Equilibrium fluorescence titration

Purified YchF at a concentration of 1 µM was titrated in a 1 mm path length cuvette (Starna Cells Inc.), with increasing concentrations of nucleotides (ADP, ATP, GDP and GTP; wild-type was also titrated with mant-ADP (2'-(or-3')-*O*-(*N*-Methylanthraniloyl)-ADP), mant-ATP and mant-GDP). YchF was equilibrated for 1 minute at room temperature, then its tryptophan/tyrosine residues were excited using the PTI QuantMaster 8000 (Horiba) fluorometer to obtain the emission spectra. When YchF was titrated with ATP/GTP, the sample was excited at either 274 nm or 280 nm immediately without incubation. The following parameters were used depending on the nucleotide titrated: mant-nucleotide (274 nm, 1.5 nm excitation slits, 5 nm emission slits, 2 nm step size and 290 – 500 nm emission spectra) and unlabelled nucleotides (280 nm, 2 nm excitation slits, 5 nm emission slits, 1 nm step size and 295 – 400 nm emission spectra). In all experiments, binding between YchF and its di-/triphosphate nucleotides were carried out in biological triplicates. Each spectrum was corrected for the contribution of YchF dilution, resulting from the addition of the nucleotide and the excitation of free nucleotide. The fluorescence obtained was normalized by dividing by the intensity obtained at 0 µM nucleotide. The resulting fluorescence was plotted as a function of nucleotide concentration and subsequently fitted with a hyperbolic function (equation 1) to obtain the dissociation constant (K_D) – as a measure of binding affinity. In

equation 1, the parameters are described as follows: fluorescence observed (F), initial fluorescence (F_0), the change in signal intensity (ΔF_{max}) and K_D is the dissociation constant.

$$(1)\ F = F_o + \frac{\Delta F_{max}\ x\ [nucleotide]}{K_D + [nucleotide]}$$

2.7. Limited trypsinolysis

A master mix of 1 mg/mL trypsin (BioBasic) was prepared in $TAKM_7$ buffer and subsequently aliquoted for storage at -20ºC to prevent self cleavage. Purified YchF (wild-type or variants) at a final concentration of 2 µM in $TAKM_7$ buffer (50 mM Tris-Cl pH 7.5, 70 mM NH_4Cl, 30 mM KCl, 7 mM $MgCl_2$) was incubated with 1 mM, or 1.5 mM of nucleotide (ATP/ADP/GTP/ GDP/*apo*) in a total volume of 140 µL for 10 minutes at room temperature. The concentration of nucleotide was chosen to ensure 100% binding of the respective nucleotide. Subsequently, trypsin was added to a final concentration of 4.5 µg/mL and the reaction was incubated for 16 minutes at room temperature. To measure the time-dependence cleavage reaction, 20 µL aliquots were collected at various time points (0, 1, 5, 8, 10 and 16 minutes) and quenched in 6X SDS loading dye at 95ºC, 5 minutes. All samples were analyzed on either SDS-PAGE (section 2.10.2.) or Bis-Tris SDS-PAGE (section 2.10.7.).

2.8. Virtual trypsin cleavage of YchF

The protein sequence of N-terminal 6xHis tag wild-type *E. coli* YchF (Becker *et al*., 2015) was used as an input in the online Expasy PeptideCutter tool (Gasteiger *et al*., 2003). PeptideCutter, contains a model for trypsin that in addition to simulating the cleavage of YchF, also assigns the probability of cleavage. This setting was used instead of the default general model for trypsin. The setting for assembling a table of cleavage sites, sorted sequentially by amino acid number was selected to obtain (1) the amino acid sequence and (2) molecular weights of each peptide fragment predicted from the resulting cleavage simulation. Lastly, trypsin cleavage sites were predicted with at least 90% probability to obtain the peptide fragments with their corresponding molecular weights.

2.9. Western blotting

The Bio-Rad Trans-Blot Turbo Transfer system was used to transfer the protein from a Bis-Tris SDS-PAGE gel to a nitrocellulose membrane (Amersham™ Protran, 0.45 µm pore size) in semi-dry transfer buffer (48 mM Tris-Cl pH 8.3, 39 mM glycine, 0.037% (v/v) SDS and 20% (v/v)

ethanol) for 7 minutes (25 V and 1.3 A). The use of the FroggaBio BLUelf pre-stained protein ladder was used to qualitatively assess membrane transfer.

2.9.1 Immunodetection of YchF

After assaying protein transfer with Ponceau S (section 2.10.8.), the corner of the membrane was spotted with 1 µL of the primary and secondary antibody. The membrane was air dried for at least a minute before proceeding to the blocking step. The nitrocellulose membrane was blocked with 3% (w/v) skimmed milk powder (resuspended in 1X TBS) and subsequently incubated for at least 1 hour with constant shaking using an orbital shaker (Benchmark Orbi-Blotter^{TM}). After blocking the membrane, the milk solution removed and the membrane was washed once with 1X TBS buffer for 10 minutes. The membrane was then incubated overnight (~16 hours) at 4ºC using an orbital shaker (VWR standard analog shaker 3500) with primary antibody (either 1/5000 diluted monoclonal mouse anti His-tag IgG (epitope: HHHHHH) or 1/2500 diluted polyclonal rabbit anti-YchF IgG (epitope: CAAVEADIAELDDEERD)) Unbound primary antibodies were recovered for future use (stored at 4ºC) and the membrane was washed once with 1X TTBS buffer (TBS, supplemented with 0.05% (v/v) Tween 20) for 5 minutes, then twice with 1X TBS buffer for 10 minutes each. The nitrocellulose membrane was then incubated for at least 40 minutes at room temperature with the secondary antibodies (either 1/5000 diluted rabbit anti-mouse IgG or 1/5000 diluted goat anti-rabbit IgG) with constant shaking via the orbital shaker. The same procedure to wash away unbound antibodies was performed as described above. The presence of either the respective epitope was detected in an Amersham Imager 600 using the luminal reaction, after mixing solution 1 (0.033 mg/mL p-coumaric acid and 0.44 µg/mL luminol, in 1X TBS) and solution 2 (0.12% (v/v) H_2O_2, in 1X TBS) for 1 minute.

2.10. Molecular biology techniques

2.10.1. Sample preparation for SDS-PAGE

All samples to be analyzed for the presence of YchF were prepared in 600 µL Eppendorf tubes (Sarstedt) by first mixing 10 µL with 2 µL of 6X SDS loading dye (100 mM Tris base pH 6.8, 20 mM β-mercaptoethanol, 15 mM EDTA, 0.2% (w/v) bromophenol blue, 6% (v/v) glycerol and 6% (w/v) SDS). Cell lysates from overexpression were prepared slightly differently. Samples obtained to 1 OD from protein overexpression were centrifuged (12,000 x g, 5 minutes) using a IEC Micromax benchtop centrifuge. The supernatant was discarded and the cell pellet was

resuspended in 100 µL of denaturing buffer (75 mM Tris base pH 6.8 and 4 M urea) to 0.1 OD, prior to mixing with 20 µL od 6X SDS loading dye. All samples were heat denatured at 95ºC for at least 5 minutes; however, cell lysates were incubated for at least 8 minutes to ensure total denaturation. Water droplets that collected at the lid of the Eppendorf tube during heat denaturation were quickly recollected by centrifugation using the IEC Micromax benchtop centrifuge (12,000 x g, 1 s) and mixed.

2.10.2. SDS-PAGE

SDS-PAGE was used to detect for the presence of YchF during protein overexpression, purification, solubility testing and limited trypsinolysis. Considering that YchF has a molecular weight of between 40-45 kDa, analysis on 12% (v/v) resolving gel was selected. All SDS-PAGE gels were assembled with the Bio-Rad Mini-PROTEAN® tetra vertical electrophoresis cell apparatus and developed using the Thermo EC EC250-90 power supply. The Pierce™ unstained protein molecular weight ladder or FroggaBio BLUelf pre-stained protein ladder was used to assess the molecular weight of YchF. The development times were selected to ensure that only the dye front exited the gel before the proteins and are shown as follows. Proteins were migrated through 6% (v/v) stacking gel (375 mM Tris base pH 6.8, 6% (v/v) acrylamide/bis-acrylamide 29:1, 1% (w/v) SDS, 0.1% (w/v) ammonium persulfate (APS) and 0.1% (w/v) tetramethylethylenediamine (TEMED)) at 90 V for 30 minutes. Then in 12% (v/v) resolving gel (375 mM Tris base pH 8.8, 12% (v/v) acrylamide/bis-acrylamide 29:1, 1% (w/v) SDS, 0.1% (w/v) ammonium persulfate (APS) and 0.1% (w/v) tetramethylethylenediamine (TEMED)), proteins were migrated at 130 V for 75 minutes. The running buffer selected was 1X Tris-glycine-SDS (0.25 M Tris base, 1.92 M glycine, and 1% (w/v) SDS). The gel was stained, following Coomassie blue procedures.

2.10.3. Coomassie blue staining of proteins

After SDS-PAGE was performed, proteins were fixed onto the gel using dehydration buffer (50% (v/v) ethanol and 10% (v/v) acetic acid). All gels were submerged in dehydration buffer for 5 minutes. After which, all SDS-PAGE gels were transferred to staining buffer (5% (v/v) ethanol and 7.5% (v/v) acetic acid), supplemented with Coomassie blue (0.25% (w/v) Coomassie brilliant blue G-250 and 100% (v/v)) and staining was carried out for 1 hour or overnight to ensure complete staining. Once stained, the SDS-PAGE gels were destained in hot Milli-Q H_2O for at least 1 hour

or overnight until the gel background became transparent. The Bio-Rad ChemiDoc touch imaging system was used to image all SDS-PAGE gels.

2.10.4. Native PAGE

Based on previous findings that YchF co-elutes with tRNA during protein purification (Brandon, 2021), I attempted to detect for the presence of tRNA during protein purification of YchF. From the resuspended RNA pellet obtained from ethanol precipitation (section 2.5.), 10 µL of sample was mixed with 2 µL of DNA loading dye (1X TBE, 0.2% (w/v) bromophenol blue and 60% (v/v) glycerol) in a 600 µL Eppendorf tube. Considering that tRNA is a small RNA that adopts a distinct cloverleaf-like secondary structure, 12% (v/v) native PAGE was best suited to maintain its secondary structure and resolve its molecular weight (~75 nucleotides). Samples were analyzed on 12% (v/v) native PAGE (1X TBE, 12% (v/v) acrylamide/bis-acrylamide 29:1, 0.17% (w/v) APS and 0.08% (v/v) TEMED)) in 1X TBE (90 mM Tris base pH 8.3, 90 mM boric acid and 1 mM EDTA) running buffer at 100 V, for ~75 minutes. As a standard, purified $tRNA^{Phe}$ was analyzed together with my sample to assess for the presence of tRNA. Ethidium bromide staining (section 2.10.6.) was carried out to detect for the present of tRNA.

2.10.5. Denaturing PAGE

Based on previous findings that YchF binds to the ribosome (Tomar *et al*., 2011, Becker *et al*., 2012 and Rosler *et al*., 2015), I attempted to detect for the presence of ribosomes during protein purification of YchF. From the resuspended RNA pellet obtained from ethanol precipitation (section 2.5.), 10 µL of sample was mixed with 2 µL of RNA loading dye (1X TBE, 0.2% (w/v) bromophenol blue, 20 mM EDTA and 8 M urea) in a 600 µL Eppendorf tube and subsequently heat denatured for at least 5 minutes to ensure total denaturation of the ribosome. Water droplets that collected at the lid of the Eppendorf tube during heat denaturation were quickly recollected by centrifugation (IEC Micromax; 12,000 x g, 1 s) and mixed. Prior to analyzing samples, all denaturing PAGE gels were pre-ran for at least 1 hour at 300 V in hot 1X TBE running buffer. RNA samples were analyzed on both 5% and 12% (v/v) denaturing PAGE (1X TBE, 5% or 12% (v/v) acrylamide/bis-acrylamide 19:1, 2.5 mM EDTA, 8 M urea, 0.1% (w/v) APS and 0.1% (w/v) TEMED) to detect tRNA and ribosomes, respectively. Both gels were developed in 1X TBE running buffer at 300 V, 30 minutes. As a standard, purified $tRNA^{fMet}$/$tRNA^{Phe}$ and 16S ribosomal

RNA were analyzed together for both gels. Both gels were stained following ethidium bromide staining protocols (section 2.10.6.).

2.10.6. Ethidium bromide staining

Both native and denaturing gels (prepared in section 2.10.4. and 2.10.5.) were promptly submerged in an ethidium bromide bath for ~5 minutes. Destaining was carried out in Milli-Q H_2O for 20 minutes and all gels were subsequently imaged using the Axygen® gel documentation system.

2.10.7. Bis-Tris SDS-PAGE

A Bis-Tris gradient between 6-15% (v/v) was selected to detect for the presence of the cleaved fragments. To detect all protein fragments, 20 pmol of total protein were prepared (as described in section 2.10.1.) and analyzed on a 6-15% (v/v) Bis-Tris gradient SDS-PAGE gel, using 1X 2-(N-morpholino)ethanesulfonic acid (MES) running buffer. The gel was developed first at 90 V (30 minutes), then at 130 V (75 minutes). To visualize the protein fragments, all gels were either stained following Coomassie blue or silver staining protocols (section 2.10.3. and 2.10.9.). Alternatively for Western blotting, the staining step was skipped and the workflow for membrane transfer was followed (section 2.9.).

2.10.8. Ponceau S staining

After transferring the protein fragments from YchF onto the nitrocellulose membrane, the presence of protein was quickly assayed with Ponceau S stanning. The membrane was incubated with 0.1% (w/v) Ponceau S (prepared in 5% (v/v) acetic acid) for 1 minute with constant shaking, then excess Ponceau S was promptly washed with Milli-Q H_2O to visualize the intact fragments. Since Ponceau S stanning is reversible, the dye was washed twice with 1X Tris buffered saline (TBS) buffer (10 mM Tris-Cl pH 7.5 and 150 mM NaCl) for 10 minutes each. Immunodetection of YchF (section 2.9.1.) was carried out after removing Ponceau S.

2.10.9. Silver staining of protein

To assess of the presence of the missing 13-kDa fragment, samples obtained from limited trypsinolysis of *apo*-state wild-type YchF in the presence or absence of trypsin was analyzed on a 6-15% Bis-Tris gradient SDS-PAGE (section 2.10.7.). The gel was resuspended in 15 mL of fix solution I (30 % (v/v) ethanol and 10 % (v/v) acetic acid) for 15 minutes, after which the solution

was discarded. The gel was then resuspended for 30 minutes in 15 mL of fix solution II (30 % (v/v) ethanol, 0.5 % (v/v) acetic acid and 0.4 M sodium acetate) that was supplemented with 15 mg sodium thiosulfate and 150 µL of 50% (v/v) glutaraldehyde. After the fixing step, the gel was thoroughly washed and equilibrated three times with Milli-Q H_2O. Silver staining carried out by incubating the gel with 15 mL of staining solution (0.14 % (w/v) $AgNO_3$ and 0.018 % (v/v) formaldehyde) for 30 minutes. Milli-Q H_2O was used to thoroughly wash away the staining solution and gel development was commenced upon supplementing to a final concentration 25 mg/mL sodium carbonate and 0.0015% (v/v) formaldehyde. Development was carried out for up to 7-8 minutes, them immediately quenched in 5% (v/v) acetic acid. The cleaved protein fragments from *apo*-state wild-type YchF were imaged on top of a Variquest 100 white light transilluminator.

3. Results

In my thesis, I selected wild-type (WT) *E. coli* YchF because its binding affinities for di/triphosphate nucleotides had previously been measured by our lab group (Becker *et al*., 2012). This would allow me to compare its binding affinities I measured with the G4 motif variants to assess nucleotide specificity. The G4 motif variants selected to assess if solely modifying the G4 motif alters YchF's nucleotide specificity (Table A1). The K_Ds of some G4 motif variants had previously been measured by Dr. Binod Pageni (unpublished), allowing me to select the following for my thesis (Table 1). YchF_NLSE was predicted to retain ATP binding specificity because its G4 motif originates from the human homolog ATPase hOLA1 (Koller-Eichhorn *et al*., 2007). YchF_NKMD was selected because its G4 motif resembles the sequence ((N/T)(K/Q)XD)) of a typical GTPase (Dever et al., 1987 and Bourne *et al*., 1991), predicted to have GTP binding specificity. Lastly, YchF_NLSS was selected for its G4 motif was predicted to have abolished nucleotide binding based the K_D obtained by Dr. Pageni ($K_{D\ ATP} \approx 430 \pm 110$ μM, unpublished). Changing the G4 motif of a GTPase has been performed previously as an approach to studying nucleotide specificity (Hwang & Miller, 1987, Marlovits *et al*., 2002 and Shan & Walter, 2003). However, previous studies only report a shift in nucleotide specificity from guanine to xanthine nucleotides, but not adenine nucleotides (Hwang & Miller, 1987, Marlovits *et al*., 2002 and Shan & Walter, 2003). It is currently unclear in GTPases whether switching nucleotide specificity also affects their switch-like behaviour. YchF ability to bind to both adenine and guanine nucleotides provides a unique opportunity to assess if nucleotide specificity is linked to distinct nucleotide-bound states it adopts. If the nucleotide specificity can be changed, perhaps the switch-like behaviour of YchF can also be changed to depend on either adenine nucleotides, guanine nucleotides or neither. Therefore, I report the binding affinities for di/triphosphate nucleotides and investigated for distinct nucleotide-bound states.

3.1. Overexpression of YchF and G4 motif variants

E. coli BL21(DE3) cultures harboring either WT or G4 motif variants had similar growth behaviours during YchF protein overexpression, therefore only the WT YchF growth curve is shown as reference (Figure 13A). All bacterial cultures required an incubation time of 5-6 hours before protein expression was induced. Considering that *E. coli* has a doubling time of ~20-40 minutes (Helmstetter & Cooper, 1968), this was quite unexpected. Given the starting OD, YchF

induction should have occurred after 2.5 hours, assuming there was not leaky expression (later confirmed by SDS-PAGE). Generally, the OD_{600} obtained from overnight cultures exceeded 10 OD units, suggesting that the bacterial cultures had approached stationary phase. To potentially prevent the overnight culture from approaching death phase, the shaking rotation speed was reduced from 180 rpm to 100 rpm.

At the end of protein expression, bacterial cells were harvested to yield typically 6-10 g of cell pellet per 2 L of LB media. Analysis by SDS-PAGE revealed leaky expression of YchF (T_0), both in the WT and the G4 motif variants, prior to inducing protein expression (Figure 13B-E). Despite that, IPTG induction to a final concentration of 1 mM still led to overexpression of WT YchF and the G4 motif variants (Figure 13B-E).

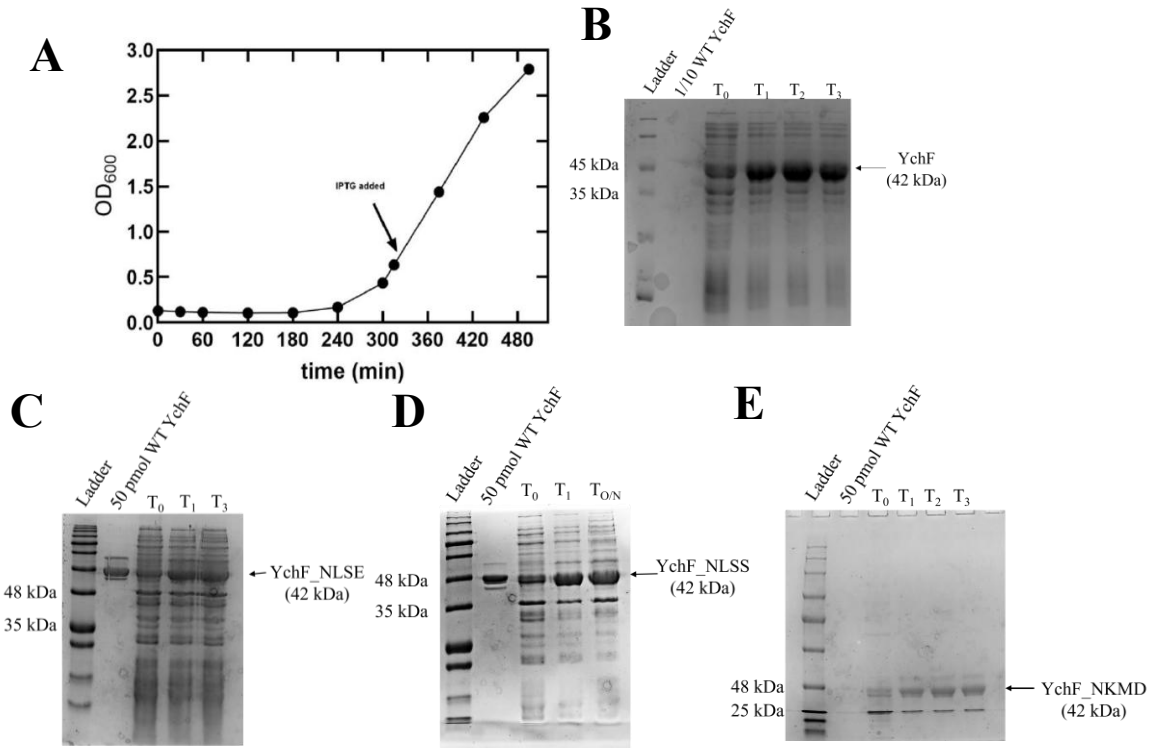

Figure 13. WT YchF and G4 motif variants expressed at 37ºC in E. coli. **A)** All *E. coli* BL21(DE3) strains harboring pET28a-encoded WT YchF or the G4 motif variants displayed similar growth behaviour and the WT is shown as a representative. Samples obtained before and hourly after IPTG induction were analysed on 12% (v/v) SDS-PAGE at 0.1 OD for **B)** WT, **C)** YchF NLSE **D)** YchF NLSS and **E)** YchF NKMD.

Although WT YchF is known to be soluble in the context of the cell (Figure 14A and 14B) (Becker *et al*., 2015 and Cheung *et al*., 2016), only YchF_NKMD was mostly found to be insoluble

in the cell at standard conditions (37ºC and 1 mM IPTG) (Figure 14A). YchF_NLSE and YchF_NLSS were still soluble since they were able to be successfully purified and analyzed on SDS-PAGE after Ni-NTA affinity chromatography. Expression conditions of YchF_NKMD were optimized as best as possible by reducing IPTG concentrations and incubating at colder temperatures (Figure 14B). However, its solubility only slightly improved when expressed at 15°C with 0.5 mM IPTG. Due to time constraints, attempts to improve the solubility of YchF_NKMD was discontinued.

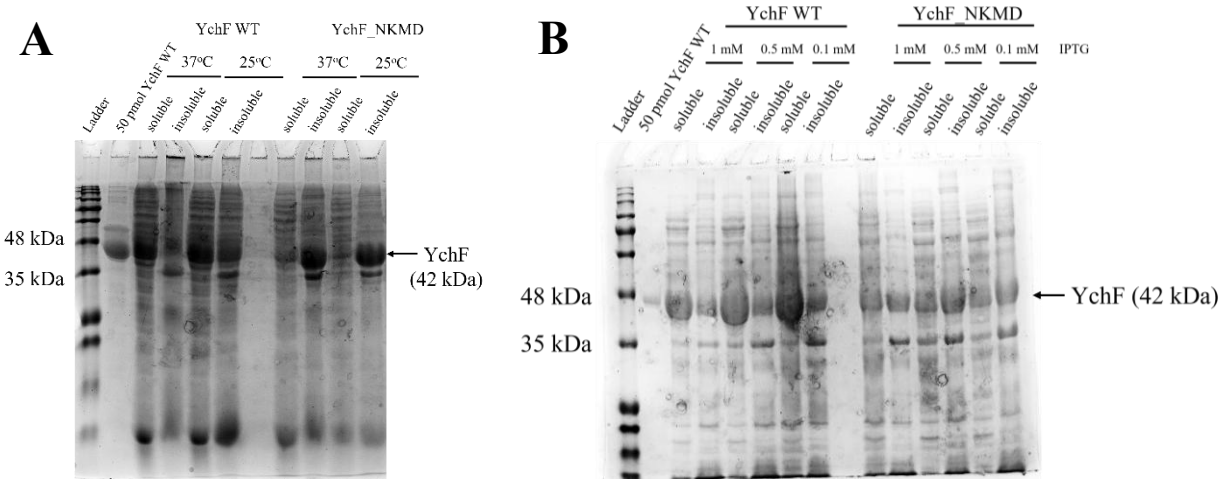

Figure 14. YchF_NKMD is found in the insoluble fraction. **A)** YchF_NKMD expression was induced in *E. coli* BL21(DE3) for three hours with 1 mM IPTG at either 25ºC or 37ºC. Protein solubility test was performed and analysed on 12% (v/v) SDS-PAGE for YchF_NKMD solubility. **B)** Expression was next induced and incubated at 15ºC and examined the effects of decreasing IPTG concentrations (1 mM, 0.5 mM and 0.1 mM) on its solubility. In both experiments, WT YchF was also expressed under the same conditions as a positive control.

3.2. Purification of YchF

A three-step protein purification procedure was used to purify WT YchF and the G4 motif variants, consisting of: Ni^{2+}-Sepharose, Q-Sepharose and Superdex 75 (Figure 15) (Becker *et al*., 2015). To separate YchF from the cell lysate, YchF was tagged with a N-terminal 6xHis tag to facilitate purification based on nickel affinity. YchF purified after Ni-NTA affinity chromatography may be bound to the ribosome (Tomar *et al*., 2011, Becker *et al*., 2012 and Rosler *et al*., 2015) and/or tRNA (Brandon, 2021). Therefore, YchF was separated from any RNAs using a salt gradient (0-1 M KCl) in anion exchange chromatography. If YchF was bound to the ribosome, any auxiliary factors bound to the ribosome, such as ribosomal proteins may co-elute and remain

during the purification step. To separate potential impurities, size exclusion chromatography was performed to separate YchF based on size. All three purification techniques were performed using the ÄKTA pure™ system. The detection of WT YchF by SDS-PAGE was also consistent for the G4 motif variant, therefore, only the purification procedure for the WT is shown.

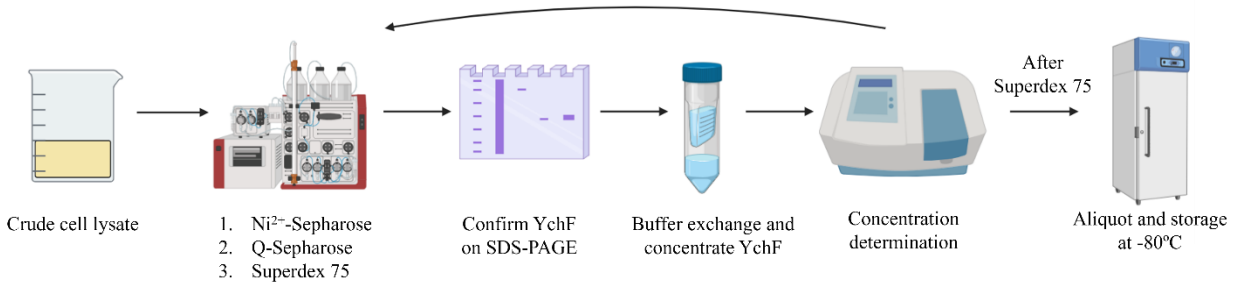

Figure 15. Workflow of YchF purification. WT YchF and its G4 motif variants were purified via the same procedure as shown. After each protein purification step, YchF was confirmed on 12% (v/v) SDS-PAGE. The resulting elution fractions that contain YchF was pooled for buffer exchange to prepare for the next purification step. The concentration of YchF was determined to determine the protein yield at each step of the purification procedure. After confirming YchF on SDS-PAGE from size exclusion chromatography, elution fractions were pooled, concentrated and subsequently aliquoted for storage at -80ºC.

3.2.1. Nickel affinity chromatography

A uniform elution peak was obtained at ~75 mM imidazole (Figure 16A) and the resulting elution fractions was subsequently analysed on 12% (v/v) SDS-PAGE to confirm the presence of YchF. YchF appears as a 42 kDa protein on SDS-PAGE together with a WT YchF standard from a previous purification batch, indicating successful purification (Figure 16B). Typically, a yield of ~ 3-6 mg of purified YchF was obtained per g of cell mass (Table 2). Although, the yield obtained are very likely be an overestimate given that there are other non-specific proteins are present in the pooled sample. The other impurities could possibly be ribosomal proteins, requiring YchF to be separated from RNA.

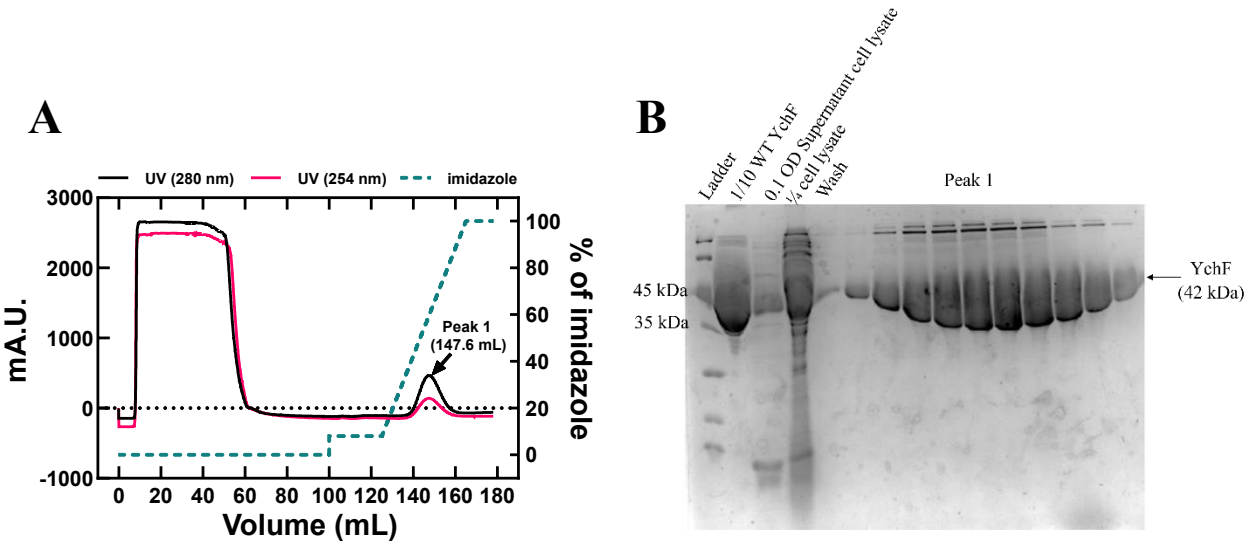

Figure 16. YchF purification from Ni-NTA affinity chromatography. **A)** After passing filtered cell lysate into Ni-NTA resin column and eluting from a linear gradient (20-250 mM imidazole), a uniform elution peak was observed at ~75 mM imidazole. **B)** In each lane on 12% (v/v) SDS-PAGE, 10 µL cell lysate, wash or elution factions were analyzed (90 V in stacking gel for 30 minutes; 130 V in resolving gel for 75 minutes) and successfully confirmed purified YchF. As a positive control, 368 pmol of previously purified WT YchF was analyzed to confirm the molecular weight of the current batch of YchF.

3.2.2. Anion exchange chromatography

The resulting chromatogram from nickel affinity chromatography revealed an elution peak measuring absorbance at 254 nm in the same fractions as YchF (Figure 16A). Nucleic acids absorb strongly at 260 nm (Ely & Ross, 1949 and Holden & Pirie, 1955) and RNA could be bound to YchF. To dissociate YchF from RNA, the ionic strength of the buffer can be increased. The ionic strength has an inverse relationship on the binding affinity of YchF for its RNA, by weakening the electrostatic interactions between them both (Record *et al*., 1976). To assess if RNA was present, a linear gradient from 0-1 M KCl was chosen to ensure total dissociation. As a result, two distinct elution peaks were obtained (Peak 1 and Peak 2). Peak 1 elutes at ~ 0.3 M of KCl and appears to have a higher protein content, as shown by a higher absorbance at 280 nm, than 254 nm. Peak 2 elutes later at 0.5 M KCl as a small peak and seems to consist primarily of RNA (Figure 17A). SDS-PAGE revealed that YchF was only present in Peak 1 (Figure 17B), therefore only elution fractions from Peak 1 were pooled together. Typically, ~20 mL of sample was obtained and a yield of 1-9 mg of purified YchF was obtained per g of cell mass (Table 2).

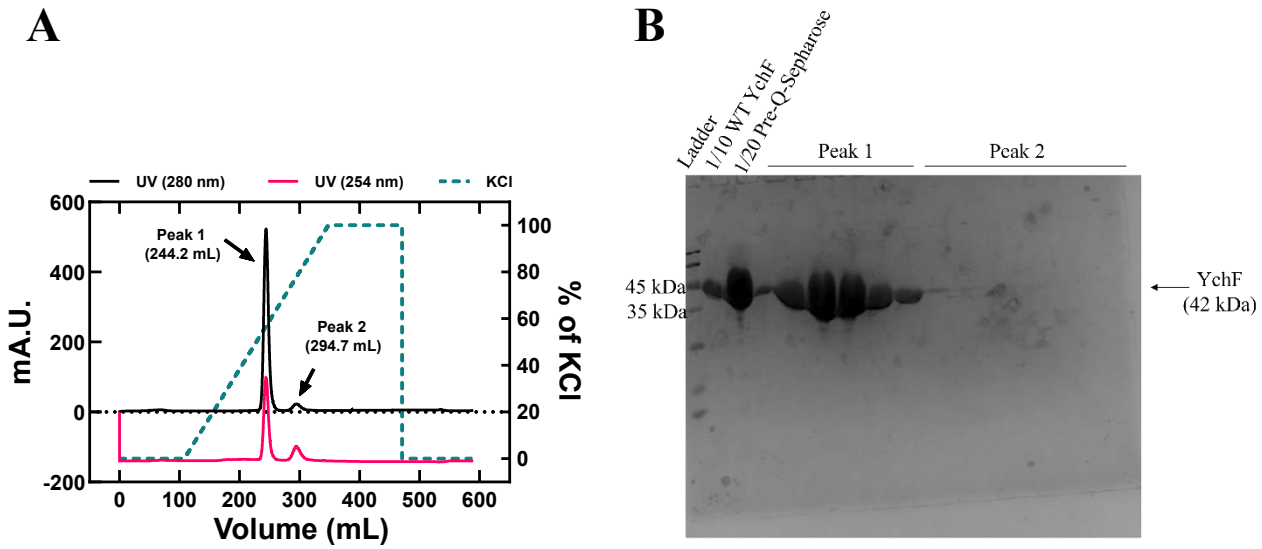

Figure 17. YchF purification from anion exchange chromatography. **A)** After passing concentrated YchF into a Q-Sepharose column and eluting from a linear gradient (0-1 M KCl), two distinct elution peaks were observed: Peak 1 and Peak 2. **B)** In each lane on 12% (v/v) SDS-PAGE, 10 µL of pre-elution and post-elution factions (Peak 1 and 2) were analyzed (90 V in stacking gel for 30 minutes; 130 V in resolving gel for 75 minutes) and only peak 1 successfully confirmed purified YchF. As a positive control, 36.8 pmol of previously purified WT YchF was analyzed to confirm the molecular weight of the current batch of YchF.

3.2.3. Size exclusion chromatography

YchF obtained after passing through a Q-Sepharose column was found to co-elute with 16S rRNA (see section 3.3.). The 16S rRNA and by extension the 30S ribosomal subunit binds up to 21 ribosomal proteins (Hardy *et al*., 1969). Even though no ribosomal proteins were detected via Coomassie blue staining (Figure 17B), there could be trace amounts present and must be separated. To separate YchF, size exclusion chromatography was performed. A uniform elution peak was observed after passing YchF through a Superdex 75 column, corresponding to purified YchF (Figure 18). Typically, a yield of ~1-6 mg of purified YchF was obtained per g of cell mass.

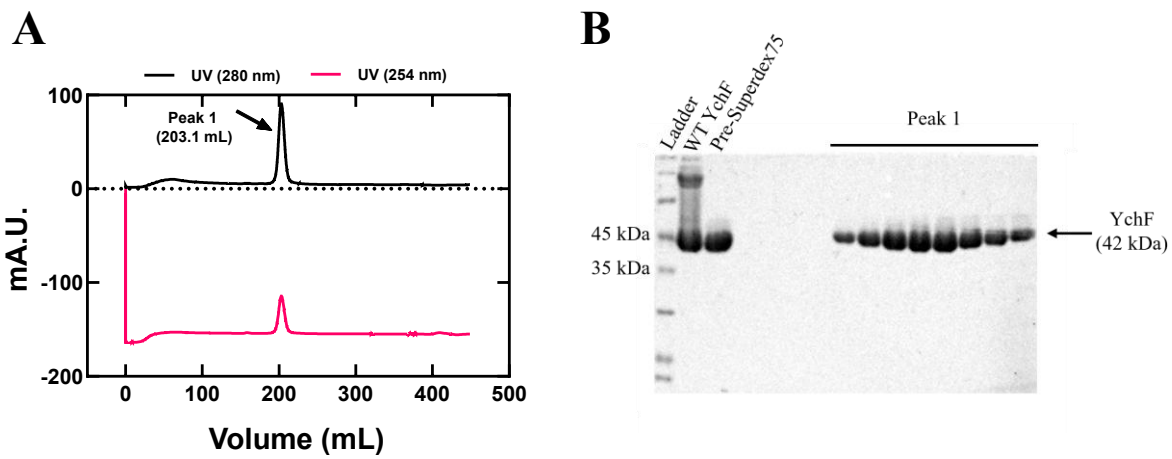

Figure 18. YchF purification from size exclusion chromatography. **A)** After passing concentrated YchF into a Superdex 75 column and eluting in TAKM$_7$ buffer, a uniform elution peak was observed. **B)** In each lane on 12% (v/v) SDS-PAGE, 10 µL of pre-elution and post-elution factions were analyzed (90 V in stacking gel for 30 minutes; 130 V in resolving gel for 75 minutes) and successfully confirmed purified YchF. As a positive control, 551 pmol of previously purified WT YchF was analyzed to confirm the molecular weight of the current batch of YchF.

Table 2. Yields of YchF at each step of protein purification.

YchF	Cell Mass	Yield from Ni^{2+}-Sepharose[a]	Yield from Q-Sepharose[a]	Yield from Superdex 75[a]
WT	6.71 g	5.73 mg/g cell	8.90 mg/g cell	5.91 mg/g cell
YchF_NLSE	9.12 g	5.73 mg/g cell	2.60 mg/g cell	1.18 mg/g cell
YchF_NLSS	10.85 g	3.05 mg/g cell	1.45 mg/g cell	0.69 mg/g cell

[a] The yields were calculated by dividing the mass of YchF obtained at each purification step by the cell mass obtained from protein overexpression. The mass of YchF was calculated using the concentration obtained from Beer-Lamberts Law and contribution of the buffer was accounted for using the flow through obtained from concentrating YchF as a blank.

3.3. Gel electrophoresis analysis for RNA bound to YchF

YchF has been reported in the literature to interact with nucleic acids such the ribosome (Becker *et al*., 2012, Landwehr *et al*., 2021 and Yu *et al*., 2025) or tRNA (Brandon, 2021). As a result, YchF may co-elute with either RNAs and needs to be separated to ensure that they do not affect YchF's nucleotide binding affinities or trypsin cleavage in subsequent experiments. Therefore, YchF was purified from anion exchange chromatography and the resulting elution fractions from Peaks 1 and 2 (Figure 18A) analyzed on SDS-PAGE. YchF was only found in Peak 1 (Figure 18B) suggesting that only nucleic acids were present in Peak 2. To assess for nucleic acids, denaturing-PAGE in the presence of 8 M urea was performed (Summer *et al*., 2009). A single

band was detected in Peak 2 for YchF_NLSE (shown for reference in Figure 19A) and YchF_NLSS. The molecular weight observed was larger than a typical tRNA (~75 nucleotides) and no band for tRNA was detected. Given that the nucleic acids are diluted, as shown by the faint single band detected by ethidium bromide staining (Figure 19A), other less abundant nucleic acids would be virtually undetectable. To potentially reveal other nucleic acids that could be present, ethanol precipitation (Green *et al*., 2020) was performed to collect and concentrate all nucleic acids in Peak 2 for reanalysis on denaturing PAGE. A white precipitate was observed after overnight ethanol precipitation (Figure 19B) and the amount of nucleic acid collected ranged from 27.7-29.0 μg. It is important to note that after measuring the absorbance at 254 nm, the extinction coefficient of tRNA was used to calculate the mass. At the time I hypothesized that based on previous findings that YchF co-elute with tRNA (Brandon, 2021), that the nucleic acid species was pre-dominantly tRNA. After concentrating the nucleic acid sample, analysis on native and denaturing PAGE potentially suggest that 16S rRNA was present with YchF after purification from Ni-NTA affinity chromatography (Figure 19C and 19D). Because this subsection falls outside the scope of my project, I did not continue to investigate and confirm the identity of the nucleic acid present. However, future studies could confirm whether the nucleic acid purified is 16S rRNA using RNA probes specific to the target through Northern blotting analysis.

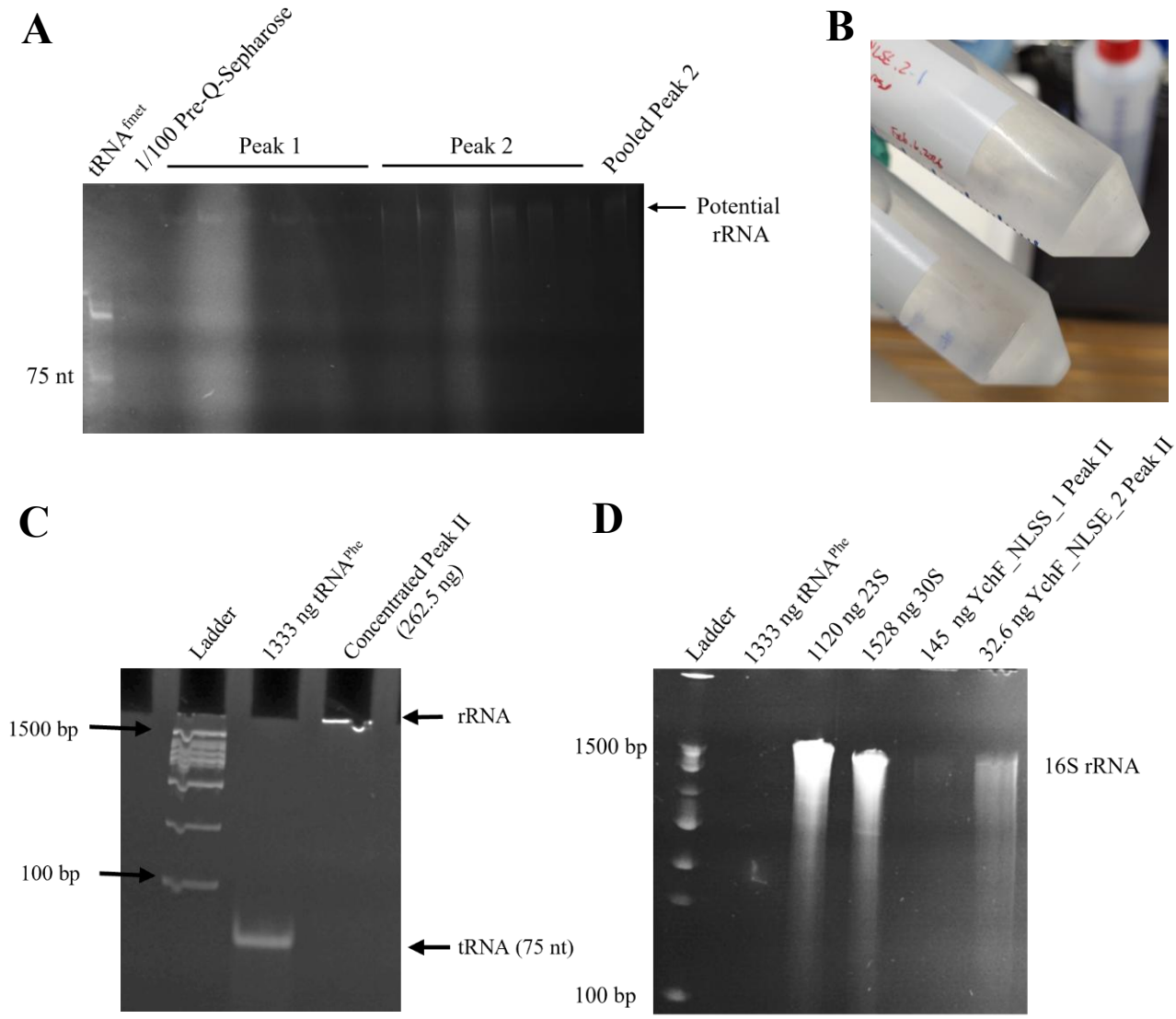

Figure 19. YchF potentially co-purifies bound to 16S rRNA. **A)** Elution fractions obtained from anion exchange chromatography from were analyzed on 12% (v/v) denaturing PAGE for the presence of rRNA (300 V for 30 minutes) in 1X TBE buffer. RNA bands were observed in both peaks, but higher levels were detected in Peak 2. **B)** Nucleic acids were precipitated with 100% (v/v) ethanol in 3 M NaOAc pH 5.2 **C)** Analysis on 12% (v/v) native PAGE (100 V in for 30 minutes) in 1X TBE buffer could not detect tRNA present. **D)** Analysis on 5% (v/v) denaturing PAGE (300 V for 30 min) in 1X TBE buffer, suggests that YchF co-elutes with 16S rRNA.

3.4. Equilibrium fluorescence titration to determine nucleotide binding affinity of YchF

To date, nearly all trGTPase have been identified to bind to guanine nucleotides (Dever *et al*., 1987 and Bourne *et al*., 1991). In doing so, they adopt distinct conformational states depending

on whether they are bound GTP or GDP (Kjeldgaard *et al*., 1993 and Abel *et al*., 1996). In order to probe for different conformational states of YchF, there must be detailed understanding of its binding affinities for adenine/guanine nucleotides. To measure nucleotide binding, equilibrium fluorescent titration (EFT) was performed for both WT and G4 motif variants (Figure 20).

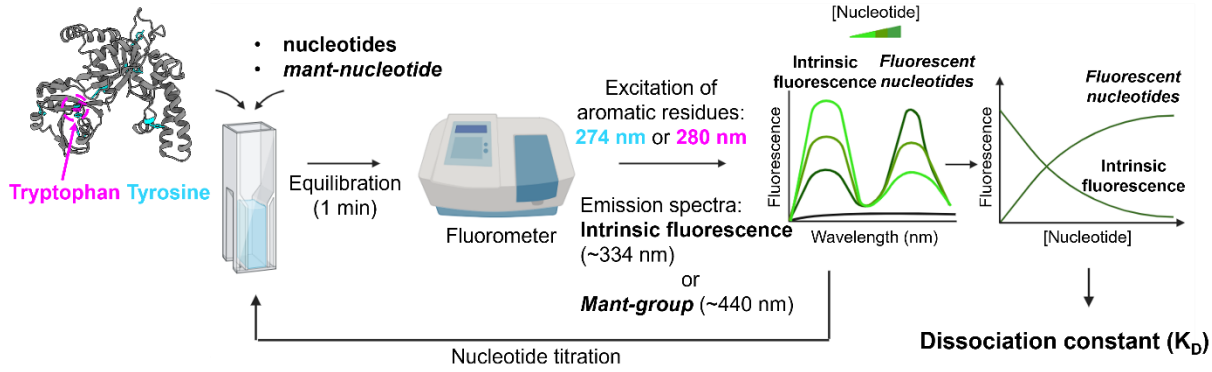

Figure 20. Equilibrium fluorescence titration workflow. EFT is an approach to measure binding affinity between a protein and its ligand (Becker *et al*., 2019). The ligands can vary and in the case of YchF, the ligands used were either non-fluorescently labelled nucleotides or their mant-group analogs. Titrating nucleotides at increasing final concentrations eventually saturates the available YchF molecules in the cuvette and if binding occurs, the following information can be gained based on the nucleotides used. Non-fluorescent nucleotides report potential conformational changes of YchF based on the environment of tryptophan and tyrosine residues. Mant-analogs report proximity between the nucleotide and YchF based on Förster resonance energy transfer.

This experiment probes the local environment of tryptophan and tyrosine residues of YchF in response to nucleotide binding (Figure 21A). Both tryptophan and tyrosine are sensitive to the polarity of their environment and if nucleotide binding occurs, this may trigger a conformational change in the protein structure that could be reported by intrinsic tryptophan/tyrosine fluorescence (Burstein *et al*., 1973 and Ghisaidoobe & Chung, 2014). YchF fortunately contains one tryptophan residue located in its TGS domain and seven tyrosine residues spread across the protein structure (G domain: 3, A-domain: 1 and TGS domain: 3). The G4 motif variants used in my thesis also contain the same set of tyrosine and tryptophan residues, given they are variants of WT *E. coli* YchF. Alternatively, fluorescently labelled mant-analogs of the di/triphosphate nucleotides can be used to assess the distance between the nucleotide and YchF via Förster resonance energy transfer (FRET) (Figure 21B). The emission wavelength of tryptophan (~337 nm) overlaps with the excitation wavelength of the mant-group (330-350 nm), allows for FRET to occur (Burstein *et al*., 1973 and Hiratsuka, 1983).

Unlike the WT, the G4 motif variants generally bind just as weak to adenine nucleotides as their guanine counterparts (Figure 22 and Table 3). Guanine nucleotide binding affinities did not appear to change between WT and variants, even though the inner filter effect was accounted for via titrating tryptophan with GDP (Figure A1). Interestingly, nucleotide binding was still observed in YchF_NLSS despite previously being predicted to have no binding (Figure 22D, Table 3). Fluorescence intensities generally plateaued at high micromolar ranges (100-1000 μM) instead of sub- to mid-ranges (1-100 μM) (Figure 22C and 22D). The only exception was YchF_NLSE which achieved mid-micromolar binding affinity for ATP (60 ± 30 μM). Another key difference between variants and WT is that the binding affinities for ADP were ~40-fold weaker than WT. Additionally, a measurable K_D could be obtained for ATP that previously was unmeasurable in WT. YchF_NLSE and YchF_NLSS both had a K_D of 60 ± 30 μM and 830 ± 340 μM, respectively. The latter measurement indicates very poor binding to ATP. When both K_D measurements were compared to the WT binding affinity for mant-ATP – a proxy for ATP binding affinity, YchF_NLSE and YchF_NLSS were ~60-fold and over 800-fold worse.

When comparing K_D measurements between mant-ADP, mant-ATP and mant-GDP for WT YchF, two K_Ds are generally obtained because of the FRET donor (tryptophan/tyrosine emission) and acceptor (mant-group) pair. Both K_Ds should generally match considering it is an inverse relationship; decrease in tryptophan/tyrosine emission and increase in mant-group emission as increasing mant-nucleotides are titrated. A pair of K_Ds are obtained when WT YchF was titrated with mant-ADP/ATP, however the mant-group emission could not be detected from mant-GDP to its respective K_D. Instead, only the K_D obtained from the tryptophan/tyrosine emission was reported (Table 3). Overall, the K_Ds obtained suggest that guanine nucleotide specificity is unaffected by modifying the G4 motif in YchF. Additionally, adenine nucleotide binding specificity is retained even in the G4 motif variants to a lesser extent and ATP specificity is lost in YchF_NLSE.

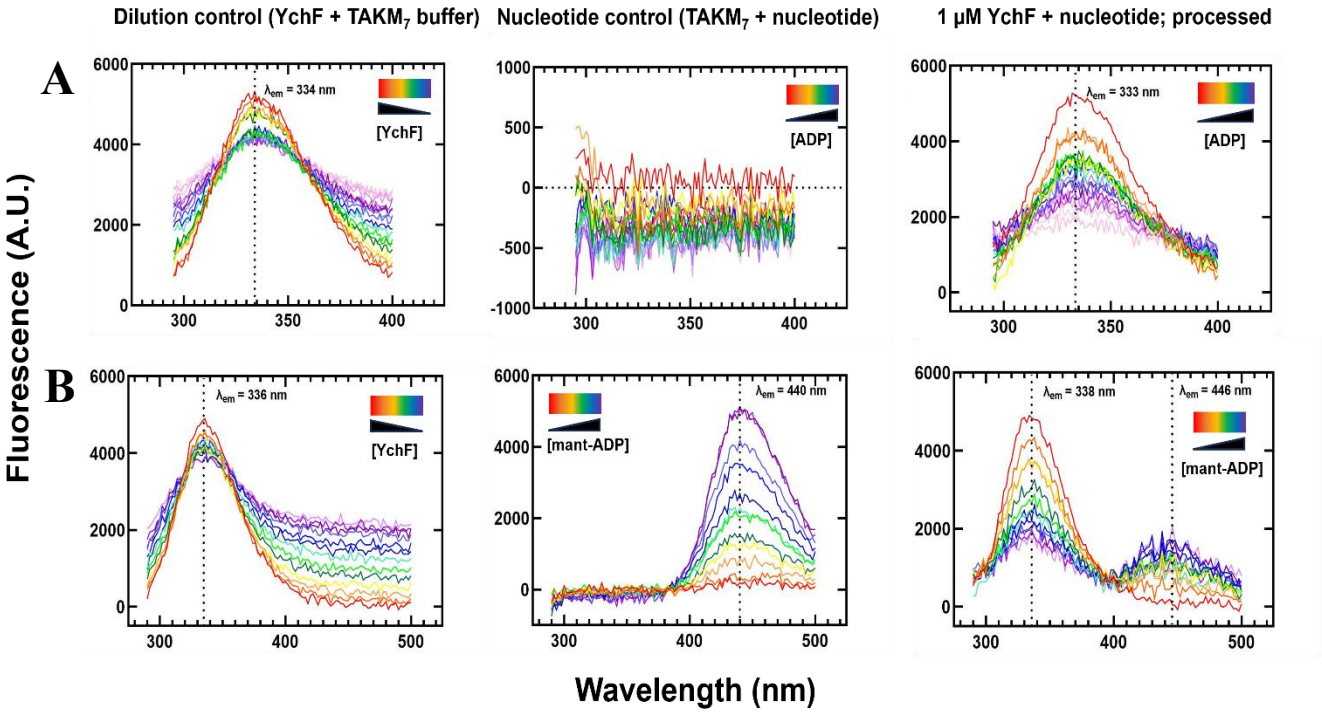

Figure 21. Emission spectra of YchF titrated with nucleotides. As a representation of the emission spectra obtained WT *E. coli* YchF and its G4 motif variants, only WT YchF is shown titrated with **A)** ADP and **B)** mant-ADP. YchF (1 µM) was titrated with increasing concentrations of nucleotides in a cuvette with 1 mm pathlength. For WT YchF, adenosine nucleotides were titrated from 0-50 µM, while guanosine nucleotides were titrated from 0-1500 µM. The G4 motif variants were titrated from 0-250/500/1000 µM with ADP/ATP/GDP/GTP. The concentration range chosen was based on previous binding affinities measured by Dr. Binod Pageni (unpublished). YchF was equilibrated with nucleotides for 1 minute at room temperature, then excited at 274 nm or 280 nm to obtain the emission spectra. When YchF was titrated with triphosphate nucleotides, the sample was excited immediately without incubation. YchF dilution at each titration step was accounted for in the final calculations, as was the excitation of the nucleotide.

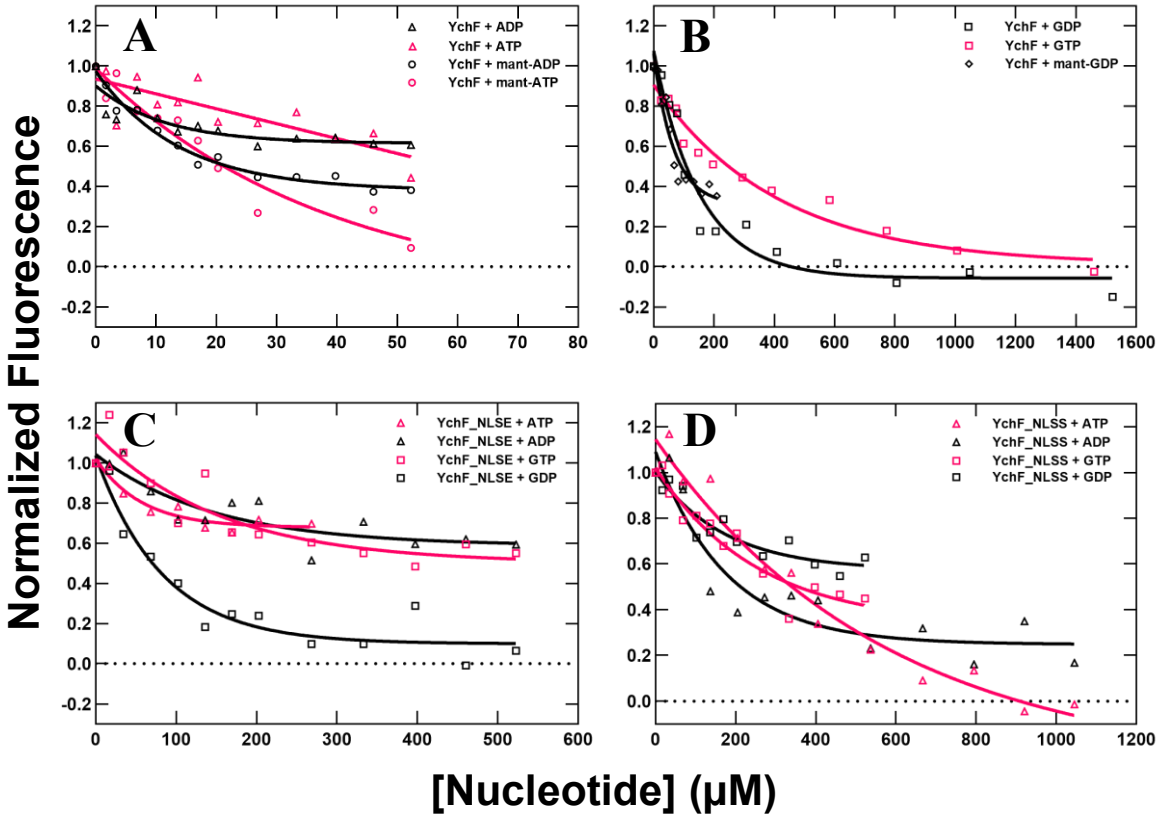

Figure 22. Determining the nucleotide affinities of YchF and G4 motif variants. WT *E. coli* YchF (1 μM) was titrated with increasing concentrations of nucleotides in a cuvette with 1 mm pathlength **A)** ADP, ATP, Mant-ADP (0-50 μM), **B)** GDP, GTP and mant-GDP (0-1500 μM) in $TAKM_7$ buffer. The sample was equilibrated for 1 minute at room temperature, then excited at 274 nm or 280 nm to obtain the emission spectra. When YchF was titrated with triphosphate nucleotides, the sample was excited immediately without incubation. YchF dilution at each titration step was accounted for in the final calculations, as was the excitation of the nucleotide. For the G4 motif variants, **C)** YchF_NLSE and **D)** YchF_NLSS, both were titrated with unlabelled nucleotides and excited at 280 nm to obtain the emission spectra. The G4 motif variants were titrated from 0-250/500/1000 μM with ADP/ATP/GDP/GTP. The concentration range chosen was based on previous binding affinities measured by Dr. Binod Pageni (unpublished).

Table 3. Nucleotide affinities of WT YchF and G4 motif variants.

Nucleotide	WT YchF K_D	YchF_NLSE K_D	YchF_NLSS K_D
ATP	Not detected[a] (337 nm)	***60 ± 30 μM (334 nm)***	***830 ± 340 μM (334 nm)***
ADP	4 ± 2 μM (337 nm)	***160 ± 120 μM (334 nm)***	***160 ± 80 μM (334 nm)***
Mant-ATP	60 ± 40 μM (332 nm) 1.1 ± 0.7 μM (440 nm)	Not measured[b]	Not measured[b]
Mant-ADP	13 ± 3 μM (338 nm) 5 ± 3 μM (446 nm)	Not measured[b]	Not measured[b]
GTP	360 ± 90 μM (337 nm)	***180 ± 130 μM (334 nm)***	***270 ± 140 μM (334 nm)***
GDP	130 ± 40 μM (337 nm)	***70 ± 20 μM (334 nm)***	***180 ± 130 μM (334 nm)***
Mant-GDP	***82 ± 36 μM (334 nm)*** ***Not detected[a] (440 nm)***	Not measured[b]	Not measured[b]

The K_D constants were obtained by fitting a hyperbolic data to normalized fluorescent intensities as a function of nucleotide concentration.
[a] No change in fluorescent intensity was detected over the course of nucleotide titration.
[b] The nucleotide was not yet tested for binding.
All K_D measurements that are bold and italicized indicate that they have not been reported in the literature (Becker *et al*., 2015).

3.5. Probing the structural dynamics of YchF via limited trypsinolysis

After obtaining the K_D constants in section 3.4. (Table 3), the structural dynamics of YchF in each of its nucleotide-bound states can be assessed. Since YchF binds to its nucleotide stoichiometrically 1:1, the Hill-Langmuir equation (Langmuir, 1918) can be used to calculate the percentage of nucleotide-bound YchF. Based on the Hill-Langmuir equation, a majority population of YchF in a nucleotide-bound state can be obtained, typically this is accomplished by supplementing nucleotides at a concentration at least three times over the K_D constant (>75% bound). One approach to assess for differences between nucleotide-bound states of YchF is limited trypsinolysis, because trypsin cleaves basic residues based on cleavage site accessibility on the protein surface (Figure 23). N-terminal 6xHis WT YchF contains a total of 38 possible cleavage sites based on the Expasy PeptideCutter tool. However, given that GTPase adopts different conformational states depending on whether they are bound to GTP or GDP, each nucleotide-bound state will have a unique set of cleavage sites accessible to trypsin. If this assumption is true for YchF, then each nucleotide-bound state (*apo*/ADP/ATP/GDP/GTP) should have their own set

of accessible cleavage sites. This approach has been used before to probe the molecular switch behaviours of trGTPases such as HflX (Fischer *et al*., 2012) and EF-G (Ticu *et al*., 2009).

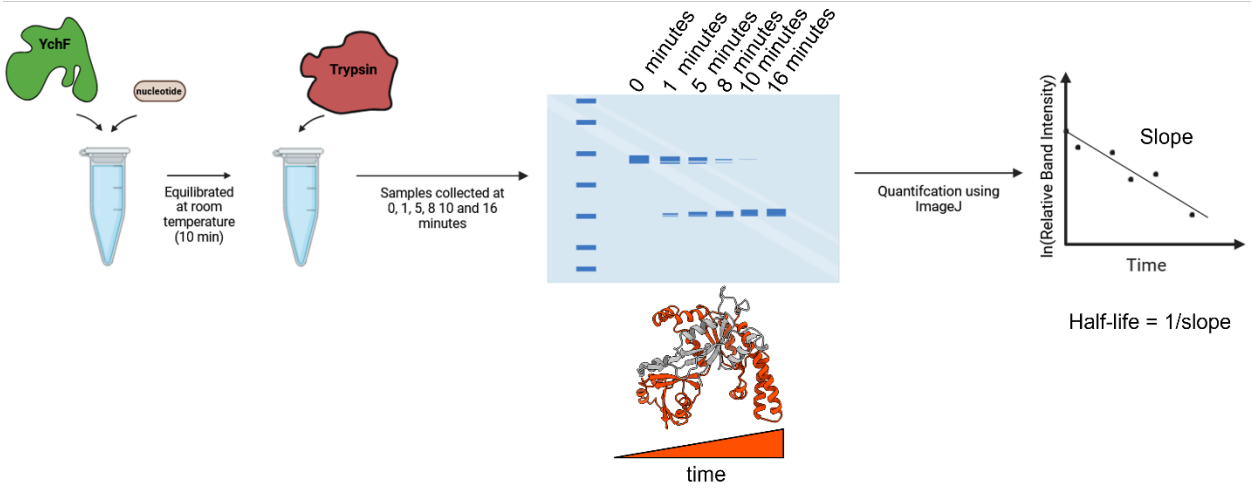

Figure 23. Limited trypsinolysis workflow. YchF is incubated with either adenine or guanine di/triphosphate nucleotides, supplemented at concentrations over three times the K_D to obtain its nucleotide-bound state. GTPase typically adopt distinct 3D structures that are either closed and rigid (GTP-bound) or open and loose (GDP-bound/*apo* state) as part of their molecular switch-like behaviour. The protein surface of each nucleotide-bound state may be different and can be probed using trypsin to cleave basic amino acid residues. Time point samples obtained are analyzed on SDS-PAGE and subsequently quantified using gel densitometry to obtain a parameter called the half-life to assess the cleavage patterns for each nucleotide-bound state.

3.5.1. Protein fragment pattern analysis on Bis-Tris SDS-PAGE

On SDS-PAGE, full-length YchF appears as a ~42-kDa protein (later shown on Bis-Tris SDS-PAGE; Figure 24), with cleavage occurring between 1-8 minutes post-exposure to trypsin. When bound to ATP, cleavage is delayed and occurs between 5-8 minutes after trypsin was supplemented. When bound to GTP, GDP, ADP or in the *apo* state, cleavage occur earlier, between 1-5 minutes. Aside the ATP-bound state, the fragmentation patterns between all other nucleotide-bound states appeared similar to the *apo* state. Cleavage resulted in the emergence of a 31-kDa peptide fragment, although the 13-kDa fragment could not be detected by standard Coomassie staining. Considering that 12% (v/v) SDS-PAGE is unable to resolve proteins below 17 kDa, any small proteins will exit the gel. Therefore, Bis-Tris SDS PAGE was selected to prevent the 13-kDa fragment from prematurely exiting the gel and produce sharper protein bands. Additionally, a pre-

stainned protein ladder was used to track protein migration and indicates when to stop the development of the gel before small peptides can exit the gel. Analysis on Bis-Tris SDS-PAGE unfortunately could not detect the 13-kDa peptide fragment. Immunoblotting and silver staining (section 3.6.) was performed to identify the missing fragment. On Bis-Tris SDS-PAGE, full-length YchF appears as a ~44-kDa protein and similar cleavage patterns were reported on the gel for all nucleotide-bound states (Figure 24). Both G4 motif variants were cleaved similarly to WT and were most stable when bound to ATP than ADP/*apo*. Similar to SDS-PAGE, cleavage of the ATP-bound state occurred between 5-8 minutes after trypsin was supplemented, whereas all other nucleotide-bound states were cleaved between 1-5 minutes. There was very little difference observed in the cleavage patterns when YchF was bound to GTP/GDP/*apo*. Taken together, binding to ATP appears to trigger a conformational change in YchF that is resistant to trypsin cleavage.

To control for YchF self-cleavage, time-point samples were obtained prior to addition of trypsin (T_0) and was analyzed together with the rest of the cleaved samples on Bis-Tris SDS-PAGE (Figure 24). Interestingly, a secondary protein band with a molecular weight on the upper end of the 31-42 kDa range was consistently observed in all Bis-Tris SDS-PAGE gel analysis of both WT and G4 motif variants. This protein was not resolved previously during the purification of YchF because elution samples were overloaded on SDS-PAGE. However, the identity of this protein was further analysed using Western blot and later identified to be YchF without its N-terminal 6xHis tag (~40 kDa; see section 3.6.1. and 3.6.2.). Taken together, this suggest that when YchF is purified, there will be a sub-population that lost its N-terminal 6xHis tag. It is very likely that over time, the N-terminal 6xHis tag is self-cleaved. For analysis of trypsin cleavage, this protein band was ignored.

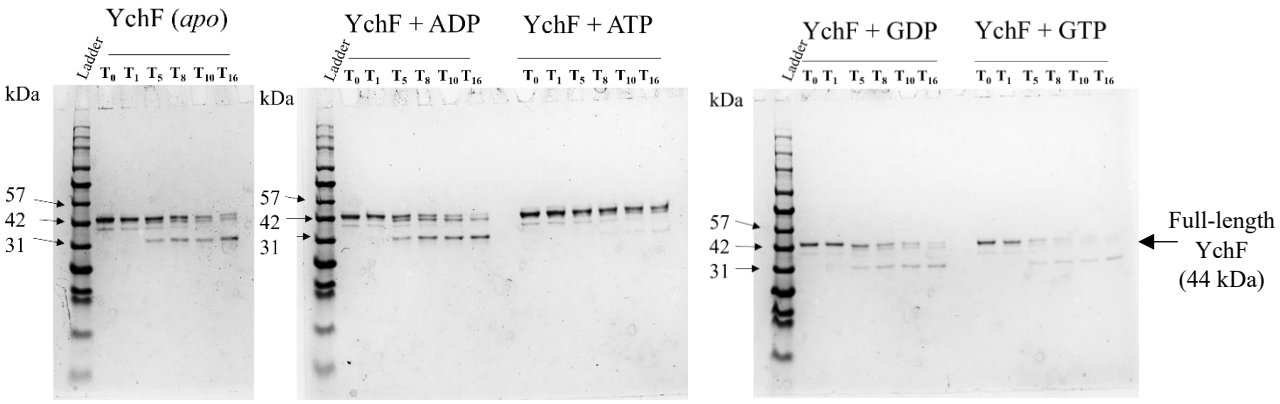

Figure 24. YchF·ATP is the most stable nucleotide-bound state during limited trypsinolysis. 2 µM of YchF was incubated with 1 mM nucleotide (ATP/ADP/GTP/ GDP/*apo*) for 10 minutes at room temperature in $TAKM_7$ buffer. After which, trypsin was added (4.5 µg/mL) and the reaction was incubated for 16 minutes at room temperature. 20 µL aliquots of the reaction was removed at various time points (0, 1, 5, 8, 10 and 16 minutes) and quenched with 6X sodium dodecyl sulfate loading dye (95ºC, 5 minutes). All samples were analyzed on 6-15% (v/v) Bis-Tris SDS-PAGE. The experiment was performed in biological triplicates and a representative gel shown for all nucleotides tested. The rate of trypsin cleavage was quantified as described in Figure 25 and Table

3.5.2. Quantification of full-length YchF cleavage

Assessing the time-dependent behaviour of full-length YchF cleavage on SDS-PAGE gives qualitative information to assess for distinct conformational states. An extra step can be taken to further quantify YchF cleavage by measuring the band intensity of full length YchF (42 kDa) as a function of time. All variants of YchF·ATP were cleaved the slowest by trypsin and the half-life time ($t_{1/2}$) obtained was over 3-fold slower than YchF·ADP and *apo* state (Figure 25 and Table 4). The GTP- and GDP-bound states achieved similar $t_{1/2}$ as the *apo* state, although there is a slight difference between YchF_NLSS·GTP (6 ± 1 min) and YchF_NLSS·GDP (4 ± 1 min) states.

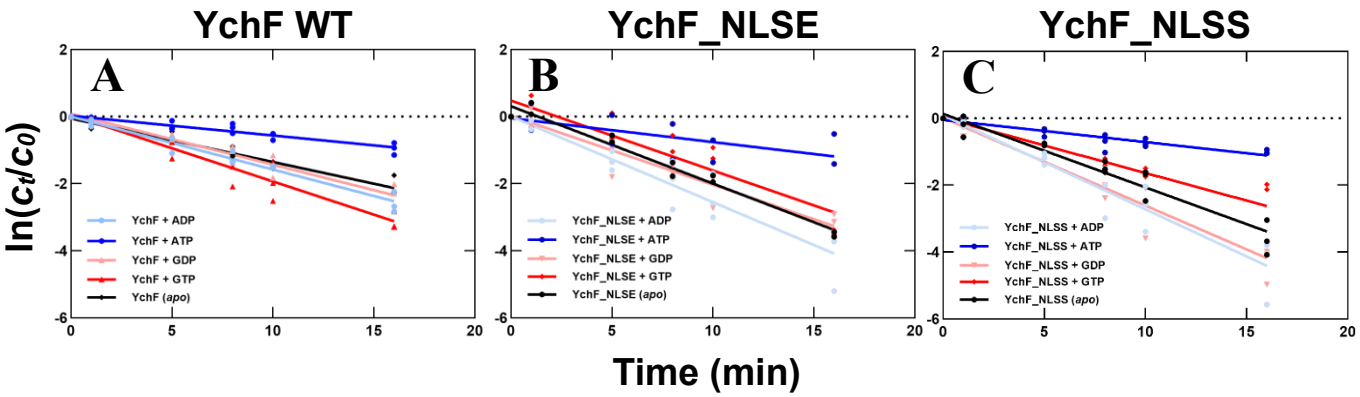

Figure 25. YchF·ATP is degraded slower than YchF's other functional states. The band intensity of full-length **A)** WT YchF (44 kDa) was quantified using the ImageJ software. The natural logarithm of the band intensity at time t, (c_t), relative to the band intensity at t = 0 (c_0) was plotted as a function of time. The same data analysis was carried out for **B)** YchF_NLSE and **C)** YchF_NLSS. As indicated in Table 4, the slope obtained is the rate of degradation and its reciprocal is the half-life ($t_{1/2}$).

Table 4. Stability of YchF nucleotide-bound states in the presence of trypsin.

YchF variant	Nucleotide-bound state of YchF[a]	Slope (min^{-1})	Half-life $t_{1/2}$ (min)
WT YchF (Hypothesized ATP-binding)	ATP	0.06 ± 0.01	17 ± 3
	ADP	0.16 ± 0.01	6 ± 1
	apo	0.13 ± 0.02	8 ± 1
	GDP	0.15 ± 0.03	7 ± 1
	GTP	0.20 ± 0.02	5 ± 1
YchF_NLSE (Hypothesized ATP-binding)	ATP	0.07 ± 0.02	15 ± 5
	ADP	0.26 ± 0.06	4 ± 1
	apo	0.23 ± 0.01	4 ± 1
	GDP	0.21 ± 0.02	5 ± 1
	GTP	0.21 ± 0.01	5 ± 1
YchF_NLSS (Hypothesized no binding)	ATP	0.07 ± 0.01	15 ± 2
	ADP	0.28 ± 0.04	4 ± 1
	apo	0.22 ± 0.05	5 ± 1
	GDP	0.26 ± 0.04	4 ± 1
	GTP	0.16 ± 0.04	6 ± 1

[a] The colours used for each nucleotide are based on Figure 25.

3.5.3. Analysis of protein fragment obtained from limited trypsinolysis via Western blot

The trypsin-dependent cleavage of YchF resulted in a ~13-kDa and a 31-kDa fragment. It was unclear which region of YchF this cleavage occurs at. Previous work (Kyla Kristobal, unpublished), identified that the N-terminal region was cleaved first. Expasy PeptideCutter (Gasteiger *et al*., 2003) also revealed a 13-kDa fragment (residues 1-125) (Table 5) that was mapped to the N-terminal region of 6xHis tagged YchF (Figure 26A). Even though the 13-kDa fragment also contains cleavage sites, it was unclear whether this fragment remained intact. To confirm the results obtained *in silico*, the fragment had to first be identified using alternative detection techniques (section 3.6.).

Table 5. Virtual trypsin cleavage analysis of N-terminal 6xHis-tagged E. coli YchF.

N-terminal fragment	Peptide sequence	Peptide Mass (kDa)	Cleavage probability
1-17	MGSSHHHHHHSSGLVPR	1.9	100%
18-24	GSHMGFK	0.7	100%
25-35	CGIVGLPNVGK	1.1	90.7%
36-44	STLFNALTK	1.0	100%
45-70	AGIEAANFPFCTIEPNTGVVPMPDPR	2.7	100%
71-82	LDQLAEIVKPQR	1.4	100%
83-98	TLPTTMEFVDIAGLVK	1.7	94.4%
99-102	GASK	0.4	93.9%
103-115	GEGLGNQFLTNIR	1.4	98.5%
116-125	ETEAIGHVVR	1.1	100%
126-138	CFENDNIIHVSGK	1.5	94.2%

Virtual trypsin cleavage was performed using the Expasy PeptideCutter tool with at least 90% cleavage probability. PeptideCutter assess the protein sequence of YchF for potential cleavage sites and does not consider protein folding as a factor. Only cleavage in the N-terminal region is shown based on previous findings that this region is first cleaved by trypsin (Krystobal, unpublished). The cleavage of WT YchF is shown since the proposed 13-kDa fragment shares the same amino acid sequence across the G4 motif variants.

3.6. Probing the cleavage site of YchF

Despite accounting for the missing 13-kDa fragment exiting the Bis-Tris SDS-PAGE gel, it could not be detected by Coomassie blue staining. One of the disadvantages of this staining technique is that the amount of Coomassie blue G-250 that is available to bind is proportional to the molecular weight of the protein. Small proteins like the missing 13-kDa fragment would be difficult to detect using this technique. Therefore, other techniques were explored to confirm the presence of the missing fragment. Western blotting is one of the best techniques available to probe for a target molecule. This technique utilizes antibodies that specifically bind to a target protein and exploits the luminol–H_2O_2–horseradish peroxidase reaction to detect protein in the picogram range (review by Khan *et al*., 2014). Given that the fragmentation patterns were similar across all nucleotide-bound states of YchF, only the *apo* state of the WT was examined in the presence or absence of trypsin.

3.6.1. Probing for His-tagged YchF

The N-terminal 6xHis tag was chosen to be probed because if the predicted 13-kDa fragment sequence is between amino acid residues 1-125 (~13 kDa, Table 5), then it should still retain the tag after the first initial cleavage. If this is true, a cleavage site found at position 17 would result in the loss of the 6xHis tag because the resulting fragment would be easily accessed by trypsin. Immunodetection revealed that only the cleavage of full-length of YchF (42 kDa) could be detected using primary monoclonal anti 6xHis antibodies. Interestingly, the N-terminal 6xHis tag could not be detected as well as the secondary ~40-kDa protein initially observed on Bis-Tris SDS-PAGE (Figure 26B).

3.6.2. Probing for the G domain of YchF

To determine the region of the intact 31-kDa fragment, the G domain was probed using primary polyclonal antibodies with an epitope against residues 237-253 (G domain) of YchF. This region lies outside of the predicted cleavage site, serving as a positive control to only detect full-length YchF (42 kDa) and the 31-kDa fragment (Figure 26B). As expected, both full-length YchF and the 31-kDa fragment were detected upon imaging. Due to the cross-reactivity of polyclonal anti-G domain YchF, other non-specific target were detected. These include the secondary ~40-kDa protein observed on Bis-Tris SDS-PAGE (Figure 26B) and a faint protein band with a molecular weight on the upper end of the 24-31 kDa range before trypsin was added (Figure 26B).

3.6.3. Detection of cleaved protein fragments via silver staining

Coomassie staining and Western blot analysis were unable to detect the presence of the 13-kDa band (Figure 26B). Western blot, despite being a very sensitive technique, it may not detect the fragment if the primary antibody does not bind. Considering that 13 kDa is a very small peptide, the next technique to consider was silver staining. Silver staining is 30-100x more sensitive than Coomassie blue and able to detect low nanogram amounts of protein (Neuhoff *et al*., 1988). After performing silver staining, a faint 13 kDa band could be observed (Figure 26C).

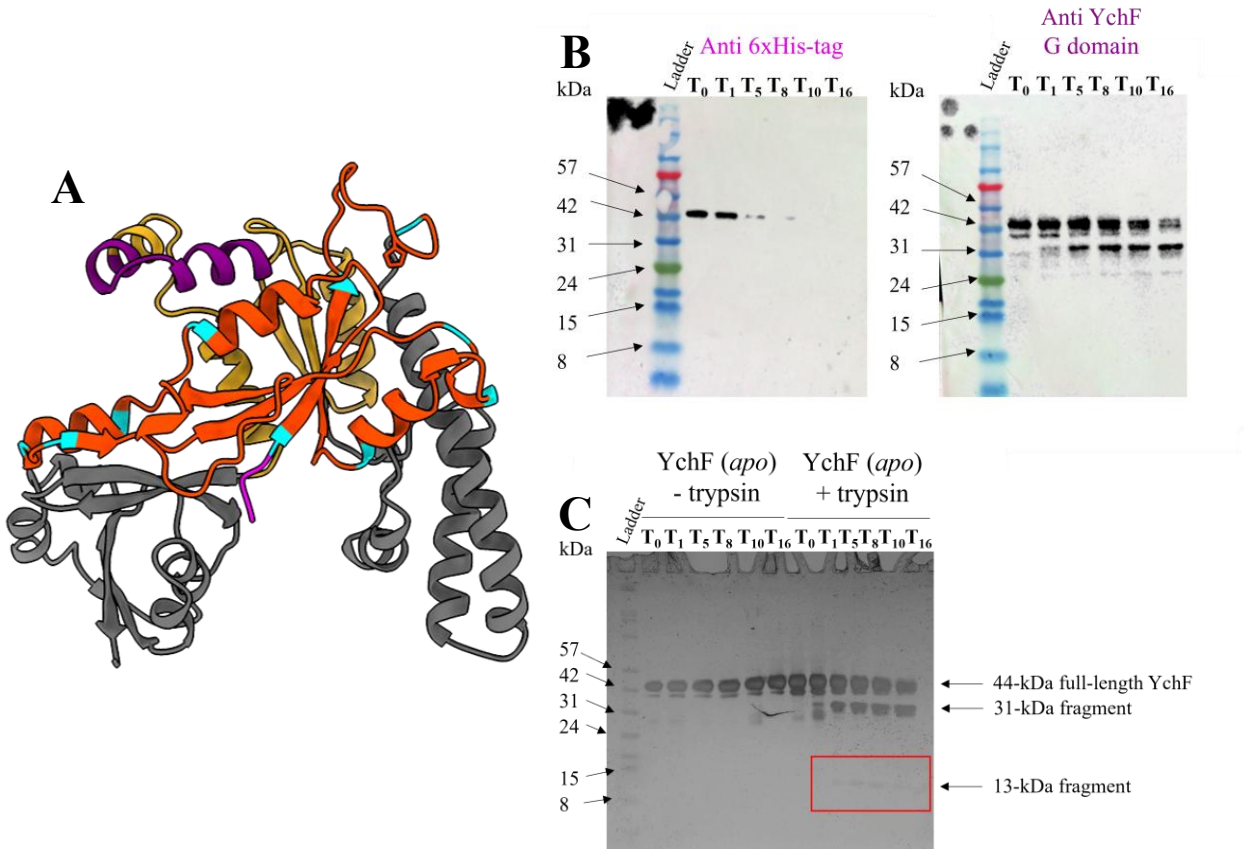

Figure 26. The cleaved 13-kDa fragment corresponds to the G domain and lacks a 6xHis tag. **A)** Probing the structural dynamics of YchF that is bound to its different nucleotides (*apo*/ADP/ATP/GDP/GTP) revealed a major 13-kDa cleavage (orange: cleaved region and cyan: cleavage sites) is believed to be part of the N-terminal G domain (yellow) region. **B)** Western blot was performed to probe the N-terminal region at the 6xHis tag (pink) and an epitope outside the proposed cleavage site (residues 237-253; purple). **C)** Samples of *apo* state YchF was cleaved with or without trypsin and subsequently analyzed on 6-15% (v/v) Bis-Tris SDS-PAGE. The gel was developed at 50 V (45 minutes), then 150 V until the dye front exited the gel. Silver staining was carried out the gel developed for 8 minutes.

4. Discussion

The canonical molecular switch behaviour of GTPases assumes that guanine nucleotides are involved in their functional cycle. YchF shares properties with classical GTPases, even though it has been reclassified as an ATPase. These properties include a highly conserved G domain (Becker *et al.*, 2012 and review by Lin *et al*., 2023), its stimulation by an ATPase activating factor (the ribosome) and adopting distinct "open"/"closed" states (Becker *et al*., 2012 and Rosler *et al*., 2015). YchF is highly conserved across the three domains of life (Caldon & March, 2003) and despite numerous cellular roles reported, there does not seem to be a clear consensus as to the underlying mechanism that describes YchF function. Describing the ATP-dependent functional cycle may be the first step to understanding the cellular role of YchF on the molecular level.

Potential differences in the ATP-dependent functional cycle between bacterial YchF and its human homolog hOLA1 could be utilized to identify future antibiotic targets that selectively inhibits bacterial homologs. For example, fusidic acid has been identified to selectively inhibit bacterial EF-G, but not the eukaryotic homolog eEF2. Fusidic acid occupies the space between the interface of the switch II region and domains II and III of EF-G in the 70S·EF-G·GDP post-translocation complex. Upon binding, the dissociation of EF-G is prevented, leading to ribosome stalling (Agrawal *et al*., 1999, Stark *et al*., 2000 and Gao *et al*., 2009). Both EF-G·GDP and *apo* eEF2 share similar 3-dimensional structure (Jørgensen *et al*., 2003), however the amino acid sequence similarity between *Homo sapiens* eEF2 and *E. coli* EF-G is very low at ~34-39%. Similarly, hOLA1 and *E. coli* YchF share 45% sequence identity (Landwehr *et al*., 2021). If the amino acid sequence difference between EF-G and eEF2 is substantial enough such that antibiotics like fusidic acid can discriminate between EF-G and eEF2, then perhaps the same approach could be exploited between bacterial YchF and hOLA1.

4.1. Objective 1: Modifying the G4 motif leads to altered nucleotide binding specificity

To date, the effects of altering the G4 motif in YchF has yet to be determined. Typically, altering the G4 motif in other GTPases such as p21 Ras or EF-Tu have resulted in either abolished binding (Clanton *et al*., 1986) or a shift in specificity from guanine to xanthine nucleotides (Hwang & Miller, 1987, Marlovits *et al*., 2002 and Shan & Walter, 2003). YchF's ability to bind to guanine or adenine nucleotides presents a unique opportunity to assess whether it is possible to shift binding

preference towards one nucleotide or the other. For this reason, the YchF_NLSE (predicted adenine nucleotide binding) YchF_NLSS (predicted no binding) and YchF_NKMD (predicted guanine nucleotide binding) variants was selected to study their nucleotide binding properties

Out of all YchF variants purified, YchF_NKMD remained insoluble and could not be purified via the same procedure as the rest. The only difference between it and the others is its G4 motif sequence. The G4 motif closely resembles the canonical motif ((N/T)(K/Q)XD)) (Dever et al., 1987 and Bourne *et al*., 1991) and is shared by EF-G and some species of IF2 (Leipe *et al*., 2002, Borges *et al*., 2007 and Verstraeten *et al*., 2011). The insolubility of YchF_NKMD may have arisen in part because the nucleotide binding pocket was destabilized by the methionine in the third position. However, hydrophobic residues in the third position of the G4 motif have been shown in many GTPases such as isoleucine (LepA, HflX and Obg), leucine (Ffh, FtsY and PurA) and even bulky residues like tryptophan (EngA in G domain 2) (Leipe *et al*., 2002, Borges *et al*., 2007 and Verstraeten *et al*., 2011) – all of which still result in a soluble GTPase. It was unexpected that simply altering the G4 motif of YchF towards a classical guanine nucleotide binding motif results in an insoluble protein. One possible reason is that because evolution has selected YchF to behave as an ATPase, the G domain chassis had been optimized to recognize adenine nucleotides. This suggests additional elements in the G domain beyond the G4 motif is needed for nucleotide specificity and identified in the 3-dimensional structure because guanine nucleotides are not the optimal ligand.

WT YchF, YchF_NLSE and YchF_NLSS potentially avoids the solubility issues encountered by YchF_NKMD in the cell because they still retain adenine nucleotide specificity and are stabilized by ATP. The intracellular ATP/GTP ratio of *E. coli* is typically high in mid-log phase to facilitate YchF stability (~2-fold difference; calculated based on Buckstein *et al*., 2008). Considering that the calculated intracellular WT YchF concentration (~3.8 μM) (Becker *et al*., 2012) and given the intracellular nucleotide concentrations of *E. coli* mid-log phase (ATP: 3,600 μM, ADP: 120 μM, GTP: 1,700 μM and GDP: 200 μM) (Buckstein *et al*., 2008) and the corresponding K_Ds measured (Table 3), over 99% of WT YchF molecules will be bound to ATP. Only a small sub-population of WT YchF can exist bound to GTP (~0.8%). In the case of YchF_NLSE, ~96% and 3.6% would be bound to ATP and GTP, respectively. For YchF_NLSS, ~81% and 16% would be bound to ATP and GTP, respectively.

The protein structures of YchF have been solved with guanine (PDB: 2DBY; Kukimoto-Niino *et al*., unpublished and 5EE9; Cheung *et al*., 2016) and adenine nucleotides (PDB: 5EE3; Cheung *et al*., 2016 and 2OHF; Koller-Eichhorn *et al*., 2007) bound to the G domain. Yet, FRET experiments titrating WT YchF with mant-analogs may suggest otherwise. Namely, the mant-group emission from mant-GDP was not detected compared to its adenine nucleotide counterparts. Even though the only difference between guanine and adenine nucleotide binding at the G domain is the orientation of the nitrogenous base, this binding orientation should not be detected by FRET. This is because the following factors govern if FRET is achieved: (1) short distance between a FRET donor and its acceptor, (2) good alignment of their transition dipole moment (κ^2), (3) good overlap between the emission spectrum of the FRET donor and absorption spectrum of the acceptor and lastly, (4) a high quantum yield of the FRET donor (Förster, 1948 and Schneckenburger, 2019). The EFT experimental setup uses tryptophan/tyrosine as a FRET donor and the mant-group as the respective acceptor. The Förster radius (R_0) between tryptophan and the mant-group is ~20 Å, although energy transfer also occurs with tyrosine as the FRET donor (Cheng *et al*., 1998 and Robertson *et al*., 2005). Since there currently does not exist a nucleotide-bound structure of *E. coli* YchF, an Alphafold prediction of WT *E. coli* YchF was structurally aligned to the ACP-bound hOLA1. *E. coli* YchF contains a single tryptophan in the TGS domain, located ~38 Å away from the 2'/3'-hydroxyl oxygen of a nucleotide where the mant-group is covalently bound. This distance falls outside the R_0 range of the tryptophan-mant-group FRET pair to be feasible for energy transfer. Therefore, the mant-group emission observed for the mant-ATP/ADP are contributed primarily by the three tyrosine residues found in the G domain (Y204: ~24 Å, Y218: ~18-19 Å and Y274: ~32 Å). The absence of the mant-group emission reported by the tyrosine-mant-GDP FRET pair could suggest that orientation of the mant-group leaves it exposed to the aqueous environment. Exposure to polar solvents such as water can quench the fluorescence emitted from FRET (Maillard *et al*., 2021). But closer analysis of the 2'- and 3'-hydroxyl group of both nucleotides in the solved structures reveal that they are generally oriented outwards of the G domain. Therefore, another factor is responsible for the differences in mant-group fluorescence observed between mant-GDP and mant-ADP/ATP.

If both adenine and guanine nucleotides bind at the G domain, then the mant-group fluorescence should have been observed in all cases. For only mant-GDP to lack a detectable mant-group fluorescence, my results suggest that guanine nucleotides potentially bind elsewhere on

YchF. Modifying the G4 motif of YchF does not seem to change its binding affinity for guanine nucleotides. For instance, YchF_NLSS still retains the ability to bind to ADP, GDP and GTP despite being predicted to have abolished binding. The fourth position in the G4 motif is typically an aspartate in other GTPases and is responsible for recognizing the guanine Watson-Crick face. However, in YchF it is replaced with glutamate, allowing for adenine recognition.

The TGS domain could serve as a secondary binding site since it has been shown in RelA to bind to the 5' -CCA 3' end of deacylated tRNA. Located about 40 Å from the 2'/3' OH group of the nucleotide ribose sugar, this could explain the lack of a mant-group fluorescence observed for mant-GDP. In the literature, three interactions govern RelA's interaction with deacylated tRNA. The first is via an interface between β4-strand and 3'OH group of the ribose sugar. The second is inserting a positively charged α-helix into the minor groove to interact with the phosphate backbone. Lastly, the CCA residues are stabilized by pi stacking interactions with the TGS domain (Brown *et al*, 2016 and Loveland *et al*., 2016). Given that GTP/GDP were titrated at mid-high micromolar concentrations, it is possible that non-specific interactions may occur. The TGS domain contains pockets of positively charged regions that may bind to the negatively charged phosphate groups of nucleotides. Binding at this domain may prevent the mant-group from being efficiently buried enough into its hydrophobic core to prevent quenching by water. However, this explanation assumes that the binding affinity of nucleotides to the TGS domain is weaker than the G domain and no conformational changes is induced. Additionally, binding at the TGS domain positions the nucleotide far closer to the only tryptophan residue in *E. coli* YchF (~15 Å) that has a higher quantum yield than tyrosine. This would result in ~85% FRET efficiency and therefore mant-group fluorescence compared to ~1.5% FRET efficiency if bound at the G domain. However, the latter is supported by my FRET experiments.

This leaves the A-domain as the only possible candidate to explain the FRET results obtained. Located ~40-50 Å from the 2'/3' OH group of the nucleotide ribose sugar, the A-domain also fulfils the distance criteria previously described for the TGS domain. Additionally, the A-domain contains a single tyrosine residue that is exposed to the aqueous solvent. If mant-GDP binds at the A-domain, poor FRET efficiency could occur if the transition dipole moment between the tyrosine donor and mant-group acceptor are misaligned. Recent experimental evidence from Yu *et al*., (2025) have shown that the A-domain facilitates YchF's interaction with the ribosome and therefore a role in nucleic acid binding. Future studies could assess the role of the A-domain

in nucleotide binding by comparing the K_D constants between purified YchF A-domain, purified YchF G domain and truncated YchF lacking either domain.

4.2. Objective 2: The molecular switch-like behaviour of YchF

Although HAS-GTPases utilize an alternative catalytic residue to the switch I glutamine present in canonical GTPases, it is currently not well understood how it influences their 3-dimensional structural rearrangements in response to nucleotide binding. Pre-steady state kinetics suggests that YchF follows a two-step process when it binds to ATP. The first step is fast and characterized by nucleotide binding, followed by a slower step, potentially related to a structural rearrangement of YchF (Rosler *et al*., 2015). Additionally, molecular dynamic simulations predicted that the different conformational changes YchF can adopt are nucleotide-dependent (Rosler *et al*., 2015). Based on the classical behaviour of GTPases, I wanted to investigate whether YchF adopts different conformational states by probing its 3-dimensional structure.

Limited trypsinolysis revealed two specific fragments resulting for cleavage and was subsequently mapped onto the protein sequence of YchF. The first major cleavage occurs at the flexible loop, suggesting that the G domain is sensitive to trypsin. This observation was most likely possible if the cleavage sites were buried on the protein surface. In all YchF variants analyzed, the rate of cleavage was slower for YchF·ATP, than it was for YchF·ADP/*apo* (Table 4). Similar stabilities between YchF·ADP and *apo* state could be a result of purifying ADP-bound state. Given the K_Ds obtained previously, the intracellular nucleotide concentrations and YchF's intrinsic ATPase activity, it is unlikely that the *apo* state was purified. YchF would predominately be in the ATP-bound state upon cell harvest but considering that YchF purification is a multi-day procedure, ATP would be slowly hydrolyzed to ADP over the course of protein purification.

HflX is another HAS-GTPase and its GTP-bound state was also identified as the most stable conformation. However, the cleavage patterns observed in YchF was not reflected in HflX. Instead, cleavage in HflX occurred at its N-terminal domain, rather than its central G domain (Fischer *et al*., 2012). This is unsurprising considering that the catalytic residue of HflX (protein backbone amide group of glycine) is in the switch II region, deep within the nucleotide binding pocket (Figure 7A) (Huang *et al*., 2010). Although the switch II region is also flexible, it is not as exposed to the aqueous solvent as YchF's catalytic flexible loop. MnmE, YqeH and FeoB also source their catalytic residues from the switch II region (Q282, D57 and G56, respectively) (Scrima & Wittinghofer, 2006, Anand *et al*., 2010 and Ash *et al*., 2011). If HflX is used as a basis

of describing the structural rearrangements of similar HAS-GTPases, then rearrangements outside the G domain (ex. its N-terminal domain) are responsible for the differences between their conformational states. Therefore, structural rearrangements of the G domain serves as the difference between the different conformational states of YchF.

Interestingly, similar stabilities between *apo*, GTP- and GDP-bound states were observed. GTP binding does not appear to stabilize YchF against trypsin cleavage. Trypsin cleavage resulting in the formation of the first fragment, indicates that GTP did not trigger a conformational change as observed for ATP. This could support a potential secondary binding site for GTP elsewhere on the protein structure. However, it is also possible that guanine nucleotide binding may result in conformational changes that are not "detected" by trypsin. A comparison between GTP- and GDP-bound structures of YchF with the flexible loop resolved can help rule this possibility out. This is not possible since out of the eight currently available structures in the Protein Data Bank (PDB: 7Y9I, 1NI3, 2OHF, 1JAL, 2DBQ, 2DBY, 5EE3 and 5EE9), only two successfully resolved the flexible loop. At best, comparisons between GMPPNP-bound *O. sativa* YchF (PDB: 5EE9; Cheung *et al*., 2016) and GDP-bound *Thermus thermophilus* YchF (PDB: 2DBY; Kukimoto-Niino *et al*., unpublished) reveal that switch I and II are positioned closer to the GMPPNP. Therefore, it is likely that the flexible loop is exposed regardless of the guanine nucleotide-bound state.

Interestingly, YchF_NLSS·ATP was found to be just as stable as the WT. It is likely that G4 motif is still capable of imparting some adenine nucleotide specificity and ATP binding still triggers a conformational change in the G domain. In the literature, GTPases that have a G4 motif that seemingly defies abolished nucleotide binding have been reported. For instance, the metal-binding GTPase HypB from *Archeoglobus fulgidus* possesses a G4 motif that has lost its highly conserved aspartate residue (NKVA). Yet, HypB was still shown to be capable of only binding to GDP (Chan *et al*., 2012). Similarly, mutational studies performed on *V. cholerae* FeoB have shown that substituting its aspartate residue (from NKMD to NKMN) only lowers its GTPase activity, but not its ATPase activity (Shin *et al*., 2019). Taken together, modifying the G4 motif alone is insufficient to explain the nucleotide specificity of YchF. Other factors such as the G5 motif may also play a role in modulating nucleotide specificity, as shown in *V. cholerae* FeoB (Shin *et al*., 2019).

5. Conclusion and future direction

I show for the first time, biochemical evidence that YchF operates as an ATP-dependent molecular switch. My findings revealed that YchF exists in two distinct conformational states. YchF adopts a distinct ATP-bound and ADP-bound/*apo* states, similar to the GTP/GDP-bound states observed in other GTPases such as EF-G and HflX (Ticu *et al*., 2009 and Fischer *et al*., 2012). My project also identified that despite modifying the G4 motif in the same YchF scaffold, it did not impact the nucleotide-dependent conformational states that YchF adopts. These new findings show that binding to di/triphosphate nucleotides may not be sufficient to explain YchF's switch-like behaviour. Potentially there are other elements of the G domain that impart adenine nucleotide specificity such as the G5 motif. The mode of nucleotide base recognition may also play a factor in inducing conformational changes and would need to be explored in the future to establish a foothold in elucidating YchF's molecular mechanism.

To expand our current knowledge on the ATP-dependent functional cycle of YchF, I propose a number of projects that can more closely examine its nucleotide specificity. For instance, future projects should attempt to modify the G5 motif, together with the G4 motif to assess if both elements are required to impart adenine nucleotide specificity in YchF. While my project explored the G4 motif of YchF, the G5 motif has remained largely unexplored. Elucidating the contribution of the G5 motif in the nucleotide specificity of YchF can complement other projects that solely focus on the G4 motif.

A G4 motif variant of YchF with GTP-binding specificity would also need to be successfully purified to probe for distinct conformational states. Even though I have demonstrated that YchF_NKMD was found to be insoluble, other G4 motifs from other GTPases could be used in place of NKMD. If a shift in specificity from adenine nucleotide to guanine nucleotide is shown, then perhaps the conformational states the variant adopts should reflect that change.

In this project, only *E. coli* YchF was probed for its structural dynamics. It remains to be seen in other homologs of YchF whether they adopt distinct conformational states, similar to *E. coli* YchF. In particular, rice (*Oryza sativa*) YchF has been reported to have no nucleotide binding preference (Cheung *et al*., 2016) and *T. thermophilus* YchF may potentially be a GTP-specific homolog, based on an available structure (PDB: 2DBY; Kukimoto-Niino *et al*., unpublished).

Understanding how GTPases work as part of the translation machinery can identify their potential as antimicrobial targets. Research into antibiotics that target this unique class of enzymes

typically operate by inhibiting GTP hydrolysis or enzyme dissociation from the ribosome (Walter *et al*., 2012 and Borg *et al*., 2015). For instance, fusidic acid is currently used to treat bacterial infections and works by selectively inhibiting EF-G when it is bound to GDP and the ribosome (Borg *et al*., 2015). This prevents EF-G dissociation from the ribosome, effectively stalling translation. Since YchF also binds to the ribosome, inhibiting its dissociation could be key to disrupting both its molecular switch behavior and impair its ability to regulate the ribosome. Currently, there are no antimicrobial drugs that selectively inhibit YchF's function, making it a promising novel antimicrobial target. In order to assess YchF and its molecular mechanism as an antimicrobial target, understanding its ATP-dependent functional cycle is the first crucial step.

6. References

Abdulkarim, F., Tuohy, T.M.F., Buckingham, R.H., and Hughes, D. 1991. Missense substitutions lethal to essential functions of EF-Tu. Biochimie **73**(12): 1457–1464. doi:10.1016/0300-9084(91)90178-4.

Abel, K., Yoder, M.D., Hilgenfeld, R., and Jurnak, F. 1996. An α to β conformational switch in EF-Tu. Structure **4**(10): 1153–1159. doi:10.1016/S0969-2126(96)00123-2.

Abraham, E.P., and Chain, E. 1940. An Enzyme from Bacteria able to Destroy Penicillin. Nature **146**(3713): 837–837. doi:10.1038/146837a0.

Agrawal, R.K., Heagle, A.B., Penczek, P., Grassucci, R.A., and Frank, J. 1999. EF-G-dependent GTP hydrolysis induces translocation accompanied by large conformational changes in the 70S ribosome. Nat Struct Mol Biol **6**(7): 643–647. doi:10.1038/10695.

Agrawal, R.K., Penczek, P., Grassucci, R.A., and Frank, J. 1998. Visualization of elongation factor G on the *Escherichia coli* 70S ribosome: The mechanism of translocation. Proc Natl Acad Sci U S A **95**(11): 6134–6138. doi:10.1073/pnas.95.11.6134.

Ahmadian, M.R., Stege, P., Scheffzek, K., and Wittinghofer, A. 1997. Confirmation of the arginine-finger hypothesis for the GAP-stimulated GTP-hydrolysis reaction of Ras. Nat Struct Mol Biol **4**(9): 686–689. doi:10.1038/nsb0997-686.

Aínsa, J.A., Blokpoel, M.C.J., Otal, I., Young, D.B., De Smet, K.A.L., and Martín, C. 1998. Molecular Cloning and Characterization of Tap, a Putative Multidrug Efflux Pump Present in *Mycobacterium fortuitum* and *Mycobacterium tuberculosis*. Journal of Bacteriology **180**(22): 5836–5843. doi:10.1128/jb.180.22.5836-5843.1998.

Anand, B., Surana, P., and Prakash, B. 2010. Deciphering the Catalytic Machinery in 30S Ribosome Assembly GTPase YqeH. PLoS One **5**(4): e9944. doi:10.1371/journal.pone.0009944.

Anand, B., Verma, S.K., and Prakash, B. 2006. Structural stabilization of GTP-binding domains in circularly permuted GTPases: Implications for RNA binding. Nucleic Acids Res **34**(8): 2196–2205. doi:10.1093/nar/gkl178.

Andersen, G.R., Thirup, S., Spremulli, L.L., and Nyborg, J. 2000. High resolution crystal structure of bovine mitochondrial EF-tu in complex with GDP1. Journal of Molecular Biology **297**(2): 421–436. doi:10.1006/jmbi.2000.3564.

Åqvist, J., and Kamerlin, S.C.L. 2015. Exceptionally large entropy contributions enable the high rates of GTP hydrolysis on the ribosome. Sci Rep **5**: 15817. doi:10.1038/srep15817.

Armstrong, J.L., Flockhart, R., Veal, G.J., Lovat, P.E., and Redfern, C.P.F. 2010. Regulation of Endoplasmic Reticulum Stress-induced Cell Death by ATF4 in Neuroectodermal Tumor Cells. J Biol Chem **285**(9): 6091–6100. doi:10.1074/jbc.M109.014092.

Ash, M.-R., Maher, M.J., Guss, J.M., and Jormakka, M. 2011. The Initiation of GTP Hydrolysis by the G-Domain of FeoB: Insights from a Transition-State Complex Structure. PLoS One **6**(8): e23355. doi:10.1371/journal.pone.0023355.

Ashe, M.P., De Long, S.K., and Sachs, A.B. 2000. Glucose Depletion Rapidly Inhibits Translation Initiation in Yeast. Mol Biol Cell **11**(3): 833–848. doi:10.1091/mbc.11.3.833.

Babu, C.R., Hilser, V.J., and Wand, A.J. 2004. Direct access to the cooperative substructure of proteins and the protein ensemble via cold denaturation. Nat Struct Mol Biol **11**(4): 352–357. doi:10.1038/nsmb739.

Ban, N., Nissen, P., Hansen, J., Moore, P.B., and Steitz, T.A. 2000. The Complete Atomic Structure of the Large Ribosomal Subunit at 2.4 Å Resolution. Science **289**(5481): 905–920. doi:10.1126/science.289.5481.905.

Becker, M., Gzyl, K.E., Altamirano, A.M., Vuong, A., Urbahn, K., and Wieden, H.-J. 2012. The 70S ribosome modulates the ATPase activity of *Escherichia coli* YchF. RNA Biol **9**(10): 1288–1301. doi:10.4161/rna.22131.

Benveniste, R., and Davies, J. 1973. Aminoglycoside Antibiotic-Inactivating Enzymes in Actinomycetes Similar to Those Present in Clinical Isolates of Antibiotic-Resistant Bacteria. Proc Natl Acad Sci U S A **70**(8): 2276–2280. doi:10.1073/pnas.70.8.2276.

Berg, P., and Offengand, E.J. 1958. An Enzymatic Mechanism for Linking Amino Acids to RNA. Proc Natl Acad Sci U S A **44**(2): 78–86. doi:10.1073/pnas.44.2.78.

Bharat, A., and Brown, E.D. 2014. Phenotypic investigations of the depletion of EngA in *Escherichia coli* are consistent with a role in ribosome biogenesis. FEMS Microbiol Lett **353**(1): 26–32. doi:10.1111/1574-6968.12403.

Bian, R., Zhao, J., Yao, Z., Cai, Y., Shou, C., Lou, D., Zhou, L., and Qian, Y. 2022. Knockdown of Obg-like ATPase 1 enhances sorafenib sensitivity by inhibition of GSK-3β/β-catenin signaling in hepatocellular carcinoma cells. J Gastrointest Oncol **13**(3): 1255–1265. doi:10.21037/jgo-22-458.

Bittner, A.N., Kriel, A., and Wang, J.D. 2014. Lowering GTP Level Increases Survival of Amino Acid Starvation but Slows Growth Rate for *Bacillus subtilis* Cells Lacking (p)ppGpp. J Bacteriol **196**(11): 2067–2076. doi:10.1128/JB.01471-14.

Blanchard, S.C., Gonzalez, R.L., Kim, H.D., Chu, S., and Puglisi, J.D. 2004a. tRNA selection and kinetic proofreading in translation. Nat Struct Mol Biol **11**(10): 1008–1014. doi:10.1038/nsmb831.

Blanchard, S.C., Kim, H.D., Gonzalez, R.L., Puglisi, J.D., and Chu, S. 2004b. tRNA dynamics on the ribosome during translation. Proc Natl Acad Sci U S A **101**(35): 12893–12898. doi:10.1073/pnas.0403884101.

Borg, A., Holm, M., Shiroyama, I., Hauryliuk, V., Pavlov, M., Sanyal, S., and Ehrenberg, M. 2015. Fusidic Acid Targets Elongation Factor G in Several Stages of Translocation on the Bacterial Ribosome. J Biol Chem **290**(6): 3440–3454. doi:10.1074/jbc.M114.611608.

Borges, C.L., Parente, J.A., Pereira, M., and Soares, C.M.D.A. 2007. Identification of the GTPase superfamily in *Mycoplasma synoviae* and *Mycoplasma hyopneumoniae*. Genet. Mol. Biol. **30**(1 suppl): 212–218. doi:10.1590/S1415-47572007000200007.

Bourne, H.R., Sanders, D.A., and McCormick, F. 1991. The GTPase superfamily: conserved structure and molecular mechanism. Nature **349**(6305): 117–127. doi:10.1038/349117a0.

Brandi, L., Marzi, S., Fabbretti, A., Fleischer, C., Hill, W.E., Gualerzi, C.O., and Stephen Lodmell, J. 2004. The Translation Initiation Functions of IF2: Targets for Thiostrepton Inhibition. Journal of Molecular Biology **335**(4): 881–894. doi:10.1016/j.jmb.2003.10.067.

Brandon, H.E. 2021. Biophysical studies of the universally conserved NTPases HflX and YchF. Available from https://opus.uleth.ca/bitstreams/3a34bdd3-cf8e-4842-97c8-ba1e8029ddcb/download [accessed 24 June 2026].

Brenner, S., Barnett, L., Katz, E.R., and Crick, F.H.C. 1967. UGA: A Third Nonsense Triplet in the Genetic Code. Nature **213**(5075): 449–450. doi:10.1038/213449a0.

Brenner, S., Stretton, A.O.W., and Kaplan, S. 1965. Genetic Code: The 'Nonsense' Triplets for Chain Termination and their Suppression. Nature **206**(4988): 994–998. doi:10.1038/206994a0.

Brewster, J.L., de Valoir, T., Dwyer, N.D., Winter, E., and Gustin, M.C. 1993. An Osmosensing Signal Transduction Pathway in Yeast. Science **259**(5102): 1760–1763.

Brodersen, D.E., Clemons, W.M., Carter, A.P., Morgan-Warren, R.J., Wimberly, B.T., and Ramakrishnan, V. 2000. The Structural Basis for the Action of the Antibiotics Tetracycline, Pactamycin, and Hygromycin B on the 30S Ribosomal Subunit. Cell **103**(7): 1143–1154. doi:10.1016/S0092-8674(00)00216-6.

Brown, A., Fernández, I.S., Gordiyenko, Y., and Ramakrishnan, V. 2016. Ribosome-dependent activation of stringent control. Nature **534**(7606): 277–280. doi:10.1038/nature17675.

Brown, A., Shao, S., Murray, J., Hegde, R.S., and Ramakrishnan, V. 2015. Structural basis for stop codon recognition in eukaryotes. Nature **524**(7566): 493–496. doi:10.1038/nature14896.

Brzezinska, M., Benveniste, R., Davies, J., Daniels, P.J.L., and Weinstein, J. 1972. Gentamicin resistance in strains of *Pseudomonas aeruginosa* mediated by enzymic N-acetylation of the deoxystreptamine moiety. Biochemistry **11**(5): 761–766. doi:10.1021/bi00755a013.

Brzovic, P.S., Keeffe, J.R., Nishikawa, H., Miyamoto, K., Fox, D., Fukuda, M., Ohta, T., and Klevit, R. 2003. Binding and recognition in the assembly of an active BRCA1/BARD1 ubiquitin-ligase complex. Proc Natl Acad Sci U S A **100**(10): 5646–5651. doi:10.1073/pnas.0836054100.

Buckstein, M.H., He, J., and Rubin, H. 2008. Characterization of Nucleotide Pools as a Function of Physiological State in *Escherichia coli*. J Bacteriol **190**(2): 718–726. doi:10.1128/JB.01020-07.

Burstein, E.A., Vedenkina, N.S., and Ivkova, M.N. 1973. Fluorescence and the Location of Tryptophan Residues in Protein Molecules. Photochemistry and Photobiology **18**(4): 263–279. doi:10.1111/j.1751-1097.1973.tb06422.x.

Caldon, C.E., and March, P.E. 2003. Function of the universally conserved bacterial GTPases. Current Opinion in Microbiology **6**(2): 135–139. doi:10.1016/S1369-5274(03)00037-7.

Campbell, E.A., Korzheva, N., Mustaev, A., Murakami, K., Nair, S., Goldfarb, A., and Darst, S.A. 2001. Structural Mechanism for Rifampicin Inhibition of Bacterial RNA Polymerase. Cell **104**(6): 901–912. doi:10.1016/S0092-8674(01)00286-0.

Carbone, C.E., Loveland, A.B., Gamper, H.B., Hou, Y.-M., Demo, G., and Korostelev, A.A. 2021. Time-resolved cryo-EM visualizes ribosomal translocation with EF-G and GTP. Nat Commun **12**(1): 7236. doi:10.1038/s41467-021-27415-0.

Casey Cunningham, C. 1992. Actin structural proteins in cell motility. Cancer Metast Rev **11**(1): 69–77. doi:10.1007/BF00047604.

Cashel, M., and Gallant, J. 1969. Two Compounds implicated in the Function of the RC Gene of *Escherichia coli*. Nature **221**(5183): 838–841. doi:10.1038/221838a0.

Chan, K.-H., Li, T., Wong, C.-O., and Wong, K.-B. 2012. Structural Basis for GTP-Dependent Dimerization of Hydrogenase Maturation Factor HypB. PLoS One **7**(1): e30547. doi:10.1371/journal.pone.0030547.

Chappie, J.S., Acharya, S., Leonard, M., Schmid, S.L., and Dyda, F. 2010. G domain dimerization controls dynamin's assembly-stimulated GTPase activity. Nature **465**(7297): 435–440. doi:10.1038/nature09032.

Chau, V., Romero, G., and Biltonen, R.L. 1981. Kinetic studies on the interactions of *Escherichia coli* K12 elongation factor Tu with GDP and elongation factor Ts. Journal of Biological Chemistry **256**(11): 5591–5596. doi:10.1016/S0021-9258(19)69244-6.

Chen, Y.-C., and Chung, Y.-T. 2011. A conserved GTPase YchF of *Vibrio vulnificus* is involved in macrophage cytotoxicity, iron acquisition, and mouse virulence. International Journal of Medical Microbiology **301**(6): 469–474. doi:10.1016/j.ijmm.2011.02.002.

Cheng, J.-Q., Jiang, W., and Hackney, D.D. 1998. Interaction of Mant-Adenosine Nucleotides and Magnesium with Kinesin. Biochemistry **37**(15): 5288–5295. doi:10.1021/bi972742j.

Cheung, M.-Y., Li, X., Ku, Y.-S., Chen, Z., and Lam, H.-M. 2022. Co-crystalization reveals the interaction between AtYchF1 and ppGpp. Front Mol Biosci **9**: 1061350. doi:10.3389/fmolb.2022.1061350.

Cheung, M.-Y., Li, X., Miao, R., Fong, Y.-H., Li, K.-P., Yung, Y.-L., Yu, M.-H., Wong, K.-B., Chen, Z., and Lam, H.-M. 2016. ATP binding by the P-loop NTPase OsYchF1 (an unconventional G protein) contributes to biotic but not abiotic stress responses. Proceedings of the National Academy of Sciences **113**(10): 2648–2653. doi:10.1073/pnas.1522966113.

Choi, E., and Hwang, J. 2018. The GTPase BipA expressed at low temperature in *Escherichia coli* assists ribosome assembly and has chaperone-like activity. J Biol Chem **293**(47): 18404–18419. doi:10.1074/jbc.RA118.002295.

Choi, E., Ryu, E., Kim, D., Byun, J.-W., Kim, K., Lee, M., and Hwang, J. 2025. The dual functions of the GTPase BipA in ribosome assembly and surface structure biogenesis in *Salmonella enterica* serovar Typhimurium. PLoS Pathog **21**(4): e1013047. doi:10.1371/journal.ppat.1013047.

Clanton, D.J., Hattori, S., and Shih, T.Y. 1986. Mutations of the ras gene product p21 that abolish guanine nucleotide binding. Proc Natl Acad Sci U S A **83**(14): 5076–5080. doi:10.1073/pnas.83.14.5076.

Connell, S.R., Takemoto, C., Wilson, D.N., Wang, H., Murayama, K., Terada, T., Shirouzu, M., Rost, M., Schüler, M., Giesebrecht, J., Dabrowski, M., Mielke, T., Fucini, P., Yokoyama, S., and Spahn, C.M.T. 2007. Structural Basis for Interaction of the Ribosome with the Switch Regions of GTP-Bound Elongation Factors. Molecular Cell **25**(5): 751–764. doi:10.1016/j.molcel.2007.01.027.

Connell, S.R., Trieber, C.A., Dinos, G.P., Einfeldt, E., Taylor, D.E., and Nierhaus, K.H. 2003. Mechanism of Tet(O)-mediated tetracycline resistance. EMBO J **22**(4): 945–953. doi:10.1093/emboj/cdg093.

Connell, S.R., Trieber, C.A., Stelzl, U., Einfeldt, E., Taylor, D.E., and Nierhaus, K.H. 2002. The tetracycline resistance protein Tet(○) perturbs the conformation of the ribosomal decoding centre. Molecular Microbiology **45**(6): 1463–1472. doi:10.1046/j.1365-2958.2002.03115.x.

Cornish, P.V., Ermolenko, D.N., Noller, H.F., and Ha, T. 2008. Spontaneous Intersubunit Rotation in Single Ribosomes. Mol Cell **30**(5): 578–588. doi:10.1016/j.molcel.2008.05.004.

Corrigan, R.M., Bellows, L.E., Wood, A., and Gründling, A. 2016. ppGpp negatively impacts ribosome assembly affecting growth and antimicrobial tolerance in Gram-positive bacteria. Proc Natl Acad Sci U S A **113**(12): E1710–E1719. doi:10.1073/pnas.1522179113.

la Cour, T.F., Nyborg, J., Thirup, S., and Clark, B.F. 1985. Structural details of the binding of guanosine diphosphate to elongation factor Tu from *E. coli* as studied by X-ray crystallography. EMBO J **4**(9): 2385–2388. doi:10.1002/j.1460-2075.1985.tb03943.x.

Cruz-Vera, L.R., Galindo, J.M., and Guarneros, G. 2002. Transcriptional analysis of the gene encoding peptidyl-tRNA hydrolase in *Escherichia coli*. Microbiology **148**(11): 3457–3466. doi:10.1099/00221287-148-11-3457.

Danese, I., Haine, V., Delrue, R.-M., Tibor, A., Lestrate, P., Stevaux, O., Mertens, P., Paquet, J.-Y., Godfroid, J., De Bolle, X., and Letesson, J.-J. 2004. The Ton System, an ABC Transporter, and a Universally Conserved GTPase Are Involved in Iron Utilization by *Brucella melitensis* 16M. Infect Immun **72**(10): 5783–5790. doi:10.1128/IAI.72.10.5783-5790.2004.

Das, H.K., and Goldstein, A. 1968. Limited capacity for protein synthesis at zero degrees centigrade in *Escherichia coli*. Journal of Molecular Biology **31**(2): 209–226. doi:10.1016/0022-2836(68)90440-3.

Daviter, T., Wieden, H.-J., and Rodnina, M.V. 2003. Essential Role of Histidine 84 in Elongation Factor Tu for the Chemical Step of GTP Hydrolysis on the Ribosome. Journal of Molecular Biology **332**(3): 689–699. doi:10.1016/S0022-2836(03)00947-1.

deLivron, M.A., and Robinson, V.L. 2008. *Salmonella enterica* Serovar Typhimurium BipA Exhibits Two Distinct Ribosome Binding Modes. J Bacteriol **190**(17): 5944–5952. doi:10.1128/JB.00763-08.

Dell, V.A., Miller, D.L., and Johnson, A.E. 1990. Effects of nucleotide- and aurodox-induced changes in elongation factor Tu conformation upon its interactions with aminoacyl transfer RNA. A fluorescence study. Biochemistry **29**(7): 1757–1763. doi:10.1021/bi00459a014.

Demeshkina, N., Jenner, L., Westhof, E., Yusupov, M., and Yusupova, G. 2012. A new understanding of the decoding principle on the ribosome. Nature **484**(7393): 256–259. doi:10.1038/nature10913.

Dever, T.E., Glynias, M.J., and Merrick, W.C. 1987. GTP-binding domain: three consensus sequence elements with distinct spacing. Proc Natl Acad Sci U S A **84**(7): 1814–1818. doi:10.1073/pnas.84.7.1814.

Dey, S., Biswas, C., and Sengupta, J. 2018. The universally conserved GTPase HflX is an RNA helicase that restores heat-damaged *Escherichia coli* ribosomes. J Cell Biol **217**(7): 2519–2529. doi:10.1083/jcb.201711131.

Diaconu, M., Kothe, U., Schlünzen, F., Fischer, N., Harms, J.M., Tonevitsky, A.G., Stark, H., Rodnina, M.V., and Wahl, M.C. 2005. Structural Basis for the Function of the Ribosomal L7/12 Stalk in Factor Binding and GTPase Activation. Cell **121**(7): 991–1004. doi:10.1016/j.cell.2005.04.015.

Dwyer, D.J., Belenky, P.A., Yang, J.H., MacDonald, I.C., Martell, J.D., Takahashi, N., Chan, C.T.Y., Lobritz, M.A., Braff, D., Schwarz, E.G., Ye, J.D., Pati, M., Vercruysse, M., Ralifo, P.S., Allison, K.R., Khalil, A.S., Ting, A.Y., Walker, G.C., and Collins, J.J. 2014. Antibiotics induce redox-related physiological alterations as part of their lethality. Proc. Natl. Acad. Sci. U.S.A. **111**(20). doi:10.1073/pnas.1401876111.

Eccleston, J.F., Moore, K.J., Morgan, L., Skinner, R.H., and Lowe, P.N. 1993. Kinetics of interaction between normal and proline 12 Ras and the GTPase-activating proteins, p120-GAP and neurofibromin. The significance of the intrinsic GTPase rate in determining the transforming ability of ras. Journal of Biological Chemistry **268**(36): 27012–27019. doi:10.1016/S0021-9258(19)74211-2.

Edmonds, M., Vaughan, M.H., and Nakazato, H. 1971. Polyadenylic acid sequences in the heterogeneous nuclear RNA and rapidly-labeled polyribosomal RNA of HeLa cells: possible evidence for a precursor relationship. Proc Natl Acad Sci U S A **68**(6): 1336–1340. doi:10.1073/pnas.68.6.1336.

Elledge, S.J., and Walker, G.C. 1983. Proteins required for ultraviolet light and chemical mutagenesis: Identification of the products of the *umuC* locus of *Escherichia coli*. Journal of Molecular Biology **164**(2): 175–192. doi:10.1016/0022-2836(83)90074-8.

Elvekrog, M.M., and Gonzalez, R.L. 2013. Conformational selection of translation initiation factor 3 signals proper substrate selection. Nat Struct Mol Biol **20**(5): 628–633. doi:10.1038/nsmb.2554.

Ely, J.O., and Ross, M.H. 1949. Absorption of Ultra-violet Light by Living Cells. Nature **163**(4154): 906–906. doi:10.1038/163906a0.

Endo, Y., Huber, P.W., and Wool, I.G. 1983. The ribonuclease activity of the cytotoxin alpha-sarcin. The characteristics of the enzymatic activity of alpha-sarcin with ribosomes and ribonucleic acids as substrates. Journal of Biological Chemistry **258**(4): 2662–2667. doi:10.1016/S0021-9258(18)32977-6.

Endo, Y., and Tsurugi, K. 1987. RNA N-glycosidase activity of ricin A-chain. Mechanism of action of the toxic lectin ricin on eukaryotic ribosomes. Journal of Biological Chemistry **262**(17): 8128–8130. doi:10.1016/S0021-9258(18)47538-2.

Fan, H., Hahm, J., Diggs, S., Perry, J.J.P., and Blaha, G. 2015. Structural and Functional Analysis of BipA, a Regulator of Virulence in Enteropathogenic *Escherichia coli*. J Biol Chem **290**(34): 20856–20864. doi:10.1074/jbc.M115.659136.

Farewell, A., and Neidhardt, F.C. 1998. Effect of Temperature on In Vivo Protein Synthetic Capacity in *Escherichia coli*. Journal of Bacteriology **180**(17): 4704–4710. doi:10.1128/jb.180.17.4704-4710.1998.

Feig, L.A., Pan, B.T., Roberts, T.M., and Cooper, G.M. 1986. Isolation of ras GTP-binding mutants using an in situ colony-binding assay. Proc Natl Acad Sci U S A **83**(13): 4607–4611. doi:10.1073/pnas.83.13.4607.

Fernebro, J., Blomberg, C., Morfeldt, E., Wolf-Watz, H., Normark, S., and Normark, B.H. 2008. The influence of *in vitro* fitness defects on pneumococcal ability to colonize and to cause invasive disease. BMC Microbiol **8**: 65. doi:10.1186/1471-2180-8-65.

Fischer, E. 1903. Synthese von Polypeptiden. doi:10.1002/cber.19030360356.

Fischer, E., and Fourneau. 1901. Ueber einige Derivate des Glykocolls. doi:10.1002/cber.190103402249.

Fischer, J.J., Coatham, M.L., Eagle Bear, S., Brandon, H.E., De Laurentiis, E.I., Shields, M.J., and Wieden, H.-J. 2012. The ribosome modulates the structural dynamics of the conserved GTPase HflX and triggers tight nucleotide binding. Biochimie **94**(8): 1647–1659. doi:10.1016/j.biochi.2012.04.016.

Fleming, A. 2001. On the antibacterial action of cultures of a penicillium, with special reference to their use in the isolation of *B. influenzae*. 1929. Bull World Health Organ **79**(8): 780–790.

Förster, Th. 1948. Zwischenmolekulare Energiewanderung und Fluoreszenz. Annalen der Physik **437**(1–2): 55–75. doi:10.1002/andp.19484370105.

Frank, J., and Agrawal, R.K. 2000. A ratchet-like inter-subunit reorganization of the ribosome during translocation. Nature **406**(6793): 318–322. doi:10.1038/35018597.

Freestone, P., Nyström, T., Trinei, M., and Norris, V. 1997. The universal stress protein, UspA, of Escherichia coli is phosphorylated in response to stasis. Journal of Molecular Biology **274**(3): 318–324. doi:10.1006/jmbi.1997.1397.

Frolova, L.Y., Tsivkovskii, R.Y., Sivolobova, G.F., Oparina, N.Y., Serpinsky, O.I., Blinov, V.M., Tatkov, S.I., and Kisselev, L.L. 1999. Mutations in the highly conserved GGQ motif of class 1 polypeptide release factors abolish ability of human eRF1 to trigger peptidyl-tRNA hydrolysis. RNA **5**(8): 1014–1020. doi:10.1017/s135583829999043x.

Fujiwara, T., Ito, K., and Nakamura, Y. 2001. Functional mapping of ribosome-contact sites in the ribosome recycling factor: a structural view from a tRNA mimic. RNA **7**(1): 64–70. doi:10.1017/s1355838201001704.

Gabashvili, I.S., Agrawal, R.K., Spahn, C.M.T., Grassucci, R.A., Svergun, D.I., Frank, J., and Penczek, P. 2000. Solution Structure of the *E. coli* 70S Ribosome at 11.5 Å Resolution. Cell **100**(5): 537–549. doi:10.1016/S0092-8674(00)80690-X.

Gale, E.F., and Folkes, J.P. 1953. The assimilation of amino-acids by bacteria. 15. Actions of antibiotics on nucleic acid and protein synthesis in *Staphylococcus aureus*. Biochem J **53**(3): 493–498. doi:10.1042/bj0530493.

Gao, H., Sengupta, J., Valle, M., Korostelev, A., Eswar, N., Stagg, S.M., Roey, P.V., Agrawal, R.K., Harvey, S.C., Sali, A., Chapman, M.S., and Frank, J. 2003. Study of the Structural Dynamics of the *E. coli* 70S Ribosome Using Real-Space Refinement. Cell **113**(6): 789–801. doi:10.1016/S0092-8674(03)00427-6.

Gao, H., Zhou, Z., Rawat, U., Huang, C., Bouakaz, L., Wang, C., Cheng, Z., Liu, Y., Zavialov, A., Gursky, R., Sanyal, S., Ehrenberg, M., Frank, J., and Song, H. 2007a. RF3 Induces Ribosomal Conformational Changes Responsible for Dissociation of Class I Release Factors. Cell **129**(5): 929–941. doi:10.1016/j.cell.2007.03.050.

Gao, N., Zavialov, A.V., Ehrenberg, M., and Frank, J. 2007b. Specific Interaction between EF-G and RRF and Its Implication for GTP-Dependent Ribosome Splitting into Subunits. Journal of Molecular Biology **374**(5): 1345–1358. doi:10.1016/j.jmb.2007.10.021.

Gao, N., Zavialov, A.V., Li, W., Sengupta, J., Valle, M., Gursky, R.P., Ehrenberg, M., and Frank, J. 2005. Mechanism for the Disassembly of the Posttermination Complex Inferred from Cryo-EM Studies. Molecular Cell **18**(6): 663–674. doi:10.1016/j.molcel.2005.05.005.

Gao, Y.-G., Selmer, M., Dunham, C.M., Weixlbaumer, A., Kelley, A.C., and Ramakrishnan, V. 2009. The structure of the ribosome with elongation factor G trapped in the post-translocational state. Science **326**(5953): 694–699. doi:10.1126/science.1179709.

García-Ortega, L., Álvarez-García, E., Gavilanes, J.G., Martínez-del-Pozo, Á., and Joseph, S. 2010. Cleavage of the sarcin–ricin loop of 23S rRNA differentially affects EF-G and EF-Tu binding. Nucleic Acids Res **38**(12): 4108–4119. doi:10.1093/nar/gkq151.

Gasteiger, E., Gattiker, A., Hoogland, C., Ivanyi, I., Appel, R.D., and Bairoch, A. 2003. ExPASy: the proteomics server for in-depth protein knowledge and analysis. Nucleic Acids Res **31**(13): 3784–3788. doi:10.1093/nar/gkg563.

Gavara, N., and Chadwick, R.S. 2016. Relationship between cell stiffness and stress fiber amount, assessed by simultaneous atomic force microscopy and live-cell fluorescence imaging. Biomech Model Mechanobiol **15**(3): 511–523. doi:10.1007/s10237-015-0706-9.

Gavriljuk, K., Gazdag, E.-M., Itzen, A., Kötting, C., Goody, R.S., and Gerwert, K. 2012. Catalytic mechanism of a mammalian Rab·RabGAP complex in atomic detail. Proc Natl Acad Sci U S A **109**(52): 21348–21353. doi:10.1073/pnas.1214431110.

Ghisaidoobe, A.B.T., and Chung, S.J. 2014. Intrinsic Tryptophan Fluorescence in the Detection and Analysis of Proteins: A Focus on Förster Resonance Energy Transfer Techniques. International Journal of Molecular Sciences **15**(12): 22518–22538. doi:10.3390/ijms151222518.

Gilman, A.G. 1984. G proteins and dual control of adenylate cyclase. Cell **36**(3): 577–579. doi:10.1016/0092-8674(84)90336-2.

Goldman, R.A., Hasan, T., Hall, C.C., Strycharz, W.A., and Cooperman, B.S. 1983. Photoincorporation of tetracycline into *Escherichia coli* ribosomes. Identification of the major proteins photolabeled by native tetracycline and tetracycline photoproducts and implications for the inhibitory action of tetracycline on protein synthesis. Biochemistry **22**(2): 359–368. doi:10.1021/bi00271a020.

Gordiyenko, Y., Deroo, S., Zhou, M., Videler, H., and Robinson, C.V. 2008. Acetylation of L12 Increases Interactions in the *Escherichia coli* Ribosomal Stalk Complex. Journal of Molecular Biology **380**(2): 404–414. doi:10.1016/j.jmb.2008.04.067.

Gottesman, M.E. 1967. Reaction of Ribosome-bound Peptidyl Transfer Ribonucleic Acid with Aminoacyl Transfer Ribonucleic Acid or Puromycin. Journal of Biological Chemistry **242**(23): 5564–5571. doi:10.1016/S0021-9258(18)99394-4.

Goyal, A., Belardinelli, R., Maracci, C., Milón, P., and Rodnina, M.V. 2015. Directional transition from initiation to elongation in bacterial translation. Nucleic Acids Res **43**(22): 10700–10712. doi:10.1093/nar/gkv869.

Gradia, D.F., Rau, K., Umaki, A.C.S., de Souza, F.S.P., Probst, C.M., Correa, A., Holetz, F.B., Avila, A.R., Krieger, M.A., Goldenberg, S., and Fragoso, S.P. 2009. Characterization of a novel Obg-like ATPase in the protozoan *Trypanosoma cruzi*. International Journal for Parasitology **39**(1): 49–58. doi:10.1016/j.ijpara.2008.05.019.

Gras, S., Chaumont, V., Fernandez, B., Carpentier, P., Charrier-Savournin, F., Schmitt, S., Pineau, C., Flament, D., Hecker, A., Forterre, P., Armengaud, J., and Housset, D. 2007. Structural insights into a new homodimeric self-activated GTPase family. EMBO Rep **8**(6): 569–575. doi:10.1038/sj.embor.7400958.

Green, M.R., and Sambrook, J. 2020. Precipitation of RNA with Ethanol. Cold Spring Harb Protoc **2020**(3): pdb.prot101717. doi:10.1101/pdb.prot101717.

Grewal, J., Manavathu, E.K., and Taylor, D.E. 1993. Effect of mutational alteration of Asn-128 in the putative GTP-binding domain of tetracycline resistance determinant Tet(O) from *Campylobacter jejuni*. Antimicrob Agents Chemother **37**(12): 2645–2649. doi:10.1128/aac.37.12.2645.

Grigorenko, B.L., Shadrina, M.S., Topol, I.A., Collins, J.R., and Nemukhin, A.V. 2008. Mechanism of the Chemical Step for the Guanosine Triphosphate (GTP) Hydrolysis Catalyzed by Elongation Factor Tu. Biochim Biophys Acta **1784**(12): 1908–1917. doi:10.1016/j.bbapap.2008.08.003.

Gromadski, K.B., Wieden, H.-J., and Rodnina, M.V. 2002. Kinetic Mechanism of Elongation Factor Ts-Catalyzed Nucleotide Exchange in Elongation Factor Tu. Biochemistry **41**(1): 162–169. doi:10.1021/bi015712w.

Guéron, M., and Leroy, J.L. 1978. Molar absorbance of tRNA. Anal Biochem **91**(2): 691–695. doi:10.1016/0003-2697(78)90556-0.

Guerrero, C., Tagwerker, C., Kaiser, P., and Huang, L. 2006. An Integrated Mass Spectrometry-based Proteomic Approach: Quantitative Analysis of Tandem Affinity-purified in vivo Cross-linked Protein Complexes (qtax) to Decipher the 26 s Proteasome-interacting Network. Molecular & Cellular Proteomics **5**(2): 366–378. doi:10.1074/mcp.M500303-MCP200.

Hannemann, L., Suppanz, I., Ba, Q., MacInnes, K., Drepper, F., Warscheid, B., and Koch, H.-G. 2016. Redox Activation of the Universally Conserved ATPase YchF by Thioredoxin 1. Antioxid Redox Signal **24**(3): 141–156. doi:10.1089/ars.2015.6272.

Hardy, S.J.S., Kurland, C.G., Voynow, P., and Mora, G. 1969. Ribosomal proteins of *Escherichia coli*. I. Purification of the 30 S ribosomal proteins. Biochemistry **8**(7): 2897–2905. doi:10.1021/bi00835a031.

Harvey, J.J. 1964. An Unidentified Virus which causes the Rapid Production of Tumours in Mice. Nature **204**(4963): 1104–1105. doi:10.1038/2041104b0.

Hedrick, S.M., Cohen, D.I., Nielsen, E.A., and Davis, M.M. 1984. Isolation of cDNA clones encoding T cell-specific membrane-associated proteins. Nature **308**(5955): 149–153. doi:10.1038/308149a0.

Helgstrand, M., Mandava, C.S., Mulder, F.A.A., Liljas, A., Sanyal, S., and Akke, M. 2007. The Ribosomal Stalk Binds to Translation Factors IF2, EF-Tu, EF-G and RF3 *via* a Conserved Region of the L12 C-terminal Domain. Journal of Molecular Biology **365**(2): 468–479. doi:10.1016/j.jmb.2006.10.025.

Helmstetter, C.E., and Cooper, S. 1968. DNA synthesis during the division cycle of rapidly growing *Escherichia coli* Br. Journal of Molecular Biology **31**(3): 507–518. doi:10.1016/0022-2836(68)90424-5.

Hirashima, A., and Kaji, A. 1972. Factor-dependent release of ribosomes from messenger RNA: Requirement for two heat-stable factors. Journal of Molecular Biology **65**(1): 43–58. doi:10.1016/0022-2836(72)90490-1.

Hiratsuka, T. 1983. New ribose-modified fluorescent analogs of adenine and guanine nucleotides available as subtrates for various enzymes. Biochimica et Biophysica Acta (BBA) - Protein Structure and Molecular Enzymology **742**(3): 496–508. doi:10.1016/0167-4838(83)90267-4.

Hoagland, M.B., Keller, E.B., and Zamecnik, P.C. 1956. Enzymatic carboxyl activation of amino acids. J Biol Chem **218**(1): 345–358.

Hoagland, M.B., Stephenson, M.L., Scott, J.F., Hecht, L.I., and Zamecnik, P.C. 1958. A Soluble Ribonucleic Acid Intermediate In Protein Synthesis. Journal of Biological Chemistry **231**(1): 241–257. doi:10.1016/S0021-9258(19)77302-5.

Holden, M., and Pirie, N.W. 1955. Treatments affecting the ultraviolet absorption spectrum of ribonucleic acid from three sources. Biochimica et Biophysica Acta **16**: 317–321. doi:10.1016/0006-3002(55)90232-8.

Hollander, I.J., Shen, Y.-Q., Heim, J., Demain, A.L., and Wolfe, S. 1984. A Pure Enzyme Catalyzing Penicillin Biosynthesis. Science **224**(4649): 610–612.

Hsu, L.-C., and White, R.L. 1998. BRCA1 is associated with the centrosome during mitosis. Proc Natl Acad Sci U S A **95**(22): 12983–12988. doi:10.1073/pnas.95.22.12983.

Huang, B., Wu, H., Hao, N., Blombach, F., van der Oost, J., Li, X., Zhang, X.C., and Rao, Z. 2010. Functional study on GTP hydrolysis by the GTP-binding protein from *Sulfolobus solfataricus*, a member of the HflX family. J Biochem **148**(1): 103–113. doi:10.1093/jb/mvq039.

Huang, L., Guo, Z., Wang, F., and Fu, L. 2021. KRAS mutation: from undruggable to druggable in cancer. Sig Transduct Target Ther **6**(1): 386. doi:10.1038/s41392-021-00780-4.

Hurwitz, J., Bresler, A., and Diringer, R. 1960. The enzymic incorporation of ribonucleotides into polyribonucleotides and the effect of DNA. Biochemical and Biophysical Research Communications **3**(1): 15–19. doi:10.1016/0006-291X(60)90094-2.

Hutchison, C.A., Chuang, R.-Y., Noskov, V.N., Assad-Garcia, N., Deerinck, T.J., Ellisman, M.H., Gill, J., Kannan, K., Karas, B.J., Ma, L., Pelletier, J.F., Qi, Z.-Q., Richter, R.A., Strychalski, E.A., Sun, L., Suzuki, Y., Tsvetanova, B., Wise, K.S., Smith, H.O., Glass, J.I., Merryman, C., Gibson, D.G., and Venter, J.C. 2016. Design and synthesis of a minimal bacterial genome. Science **351**(6280): aad6253. doi:10.1126/science.aad6253.

Hwang, J., and Inouye, M. 2001. An Essential GTPase, Der, Containing Double GTP-binding Domains from *Escherichia coli* and *Thermotoga maritima*. Journal of Biological Chemistry **276**(33): 31415–31421. doi:10.1074/jbc.M104455200.

Hwang, Y.W., and Miller, D.L. 1987. A mutation that alters the nucleotide specificity of elongation factor Tu, a GTP regulatory protein. Journal of Biological Chemistry **262**(27): 13081–13085. doi:10.1016/S0021-9258(18)45170-8.

Innocenti, M., Tenca, P., Frittoli, E., Faretta, M., Tocchetti, A., Di Fiore, P.P., and Scita, G. 2002. Mechanisms through which Sos-1 coordinates the activation of Ras and Rac. J Cell Biol **156**(1): 125–136. doi:10.1083/jcb.200108035.

Ito, K., Murakami, R., Mochizuki, M., Qi, H., Shimizu, Y., Miura, K., Ueda, T., and Uchiumi, T. 2012. Structural basis for the substrate recognition and catalysis of peptidyl-tRNA hydrolase. Nucleic Acids Res **40**(20): 10521–10531. doi:10.1093/nar/gks790.

Jagath, J.R., Rodnina, M.V., Lentzen, G., and Wintermeyer, W. 1998. Interaction of Guanine Nucleotides with the Signal Recognition Particle from *Escherichia coli*. Biochemistry **37**(44): 15408–15413. doi:10.1021/bi981523a.

Jain, N., Dhimole, N., Khan, A.R., De, D., Tomar, S.K., Sajish, M., Dutta, D., Parrack, P., and Prakash, B. 2009. *E. coli* HflX interacts with 50S ribosomal subunits in presence of nucleotides. Biochemical and Biophysical Research Communications **379**(2): 201–205. doi:10.1016/j.bbrc.2008.12.072.

Janiak, M.J., Small, D.M., and Shipley, G.G. 1979. Temperature and compositional dependence of the structure of hydrated dimyristoyl lecithin. Journal of Biological Chemistry **254**(13): 6068–6078. doi:10.1016/S0021-9258(18)50520-2.

Jenner, L., Starosta, A.L., Terry, D.S., Mikolajka, A., Filonava, L., Yusupov, M., Blanchard, S.C., Wilson, D.N., and Yusupova, G. 2013. Structural basis for potent inhibitory activity of the antibiotic tigecycline during protein synthesis. Proc Natl Acad Sci U S A **110**(10): 3812–3816. doi:10.1073/pnas.1216691110.

Jevons, M.P. 1961. "Celbenin" - resistant Staphylococci. Br Med J **1**(5219): 124–125. doi:10.1136/bmj.1.5219.124-a.

Jeyabal, P.V., Rubio, V., Chen, H., Zhang, J., and Shi, Z.-Z. 2014. Regulation of cell-matrix adhesion by OLA1, the Obg-like ATPase 1. Biochem Biophys Res Commun **444**(4): 568–574. doi:10.1016/j.bbrc.2014.01.099.

Jia, L., Mao, Y., Ji, Q., Dersh, D., Yewdell, J.W., and Qian, S.-B. 2020. Decoding mRNA translatability and stability from the 5′ UTR. Nat Struct Mol Biol **27**(9): 814–821. doi:10.1038/s41594-020-0465-x.

Jiang, H., Milanov, M., Jüngert, G., Angebauer, L., Flender, C., Smudde, E., Gather, F., Vogel, T., Jessen, H.J., and Koch, H.-G. 2024. Control of a chemical chaperone by a universally conserved ATPase. iScience **27**(7): 110215. doi:10.1016/j.isci.2024.110215.

Jørgensen, R., Ortiz, P.A., Carr-Schmid, A., Nissen, P., Kinzy, T.G., and Andersen, G.R. 2003. Two crystal structures demonstrate large conformational changes in the eukaryotic ribosomal translocase. Nat Struct Mol Biol **10**(5): 379–385. doi:10.1038/nsb923.

Karimi, R., Pavlov, M.Y., Buckingham, R.H., and Ehrenberg, M. 1999. Novel Roles for Classical Factors at the Interface between Translation Termination and Initiation. Molecular Cell **3**(5): 601–609. doi:10.1016/S1097-2765(00)80353-6.

Khan, P., Idrees, D., Moxley, M.A., Corbett, J.A., Ahmad, F., von Figura, G., Sly, W.S., Waheed, A., and Hassan, Md.I. 2014. Luminol-Based Chemiluminescent Signals: Clinical and Non-clinical Application and Future Uses. Appl Biochem Biotechnol **173**(2): 333–355. doi:10.1007/s12010-014-0850-1.

Khodursky, A.B., Zechiedrich, E.L., and Cozzarelli, N.R. 1995. Topoisomerase IV is a target of quinolones in *Escherichia coli*. Proc Natl Acad Sci U S A **92**(25): 11801–11805. doi:10.1073/pnas.92.25.11801.

Kira, Y., and Nishikawa, M. 2008. The identification and characterization of a new GTP-binding protein (Gbp45) involved in cell proliferation and death related to mitochondrial function. Cell Mol Biol Lett **13**(4): 570. doi:10.2478/s11658-008-0023-8.

Kiss, E., Huguet, T., Poinsot, V., and Batut, J. 2004. The *typA* Gene is Required for Stress Adaptation as Well as for Symbiosis of *Sinorhizobium meliloti* 1021 with Certain Medicago truncatula Lines. MPMI **17**(3): 235–244. doi:10.1094/MPMI.2004.17.3.235.

Kjeldgaard, M., Nissen, P., Thirup, S., and Nyborg, J. 1993. The crystal structure of elongation factor EF-Tu from *Thermus aquaticus* in the GTP conformation. Structure **1**(1): 35–50. London, England : 1993. doi:10.1016/0969-2126(93)90007-4.

Koch, M., Flür, S., Kreutz, C., Ennifar, E., Micura, R., and Polacek, N. 2015. Role of a ribosomal RNA phosphate oxygen during the EF-G–triggered GTP hydrolysis. Proc Natl Acad Sci U S A **112**(20): E2561–E2568. doi:10.1073/pnas.1505231112.

Koller-Eichhorn, R., Marquardt, T., Gail, R., Wittinghofer, A., Kostrewa, D., Kutay, U., and Kambach, C. 2007. Human OLA1 Defines an ATPase Subfamily in the Obg Family of GTP-binding Proteins. Journal of Biological Chemistry **282**(27): 19928–19937. doi:10.1074/jbc.M700541200.

Koopman, W.J.H., Verkaart, S., Visch, H.-J., van der Westhuizen, F.H., Murphy, M.P., van den Heuvel, L.W.P.J., Smeitink, J.A.M., and Willems, P.H.G.M. 2005. Inhibition of complex I of the electron transport chain causes O2−·-mediated mitochondrial outgrowth. American Journal of Physiology-Cell Physiology **288**(6): C1440–C1450. doi:10.1152/ajpcell.00607.2004.

Korostelev, A., Asahara, H., Lancaster, L., Laurberg, M., Hirschi, A., Zhu, J., Trakhanov, S., Scott, W.G., and Noller, H.F. 2008. Crystal structure of a translation termination complex formed with release factor RF2. Proc Natl Acad Sci U S A **105**(50): 19684–19689. doi:10.1073/pnas.0810953105.

Koutmou, K.S., McDonald, M.E., Brunelle, J.L., and Green, R. 2014. RF3:GTP promotes rapid dissociation of the class 1 termination factor. RNA **20**(5): 609–620. doi:10.1261/rna.042523.113.

Kriel, A., Bittner, A.N., Kim, S.H., Liu, K., Tehranchi, A.K., Zou, W.Y., Rendon, S., Chen, R., Tu, B.P., and Wang, J.D. 2012. Direct Regulation of GTP Homeostasis by (p)ppGpp: A

Critical Component of Viability and Stress Resistance. Mol Cell **48**(2): 231–241. doi:10.1016/j.molcel.2012.08.009.

Kumar, V., Chen, Y., Ero, R., Ahmed, T., Tan, J., Li, Z., Wong, A.S.W., Bhushan, S., and Gao, Y.-G. 2015. Structure of BipA in GTP form bound to the ratcheted ribosome. Proc Natl Acad Sci U S A **112**(35): 10944–10949. doi:10.1073/pnas.1513216112.

La Teana, A., Gualerzi, C.O., and Dahlberg, A.E. 2001. Initiation factor IF 2 binds to the alpha-sarcin loop and helix 89 of *Escherichia coli* 23S ribosomal RNA. RNA **7**(8): 1173–1179. doi:10.1017/s1355838201010366.

Lancaster, L., Kiel, M.C., Kaji, A., and Noller, H.F. 2002. Orientation of Ribosome Recycling Factor in the Ribosome from Directed Hydroxyl Radical Probing. Cell **111**(1): 129–140. doi:10.1016/S0092-8674(02)00938-8.

Land, M., Hauser, L., Jun, S.-R., Nookaew, I., Leuze, M.R., Ahn, T.-H., Karpinets, T., Lund, O., Kora, G., Wassenaar, T., Poudel, S., and Ussery, D.W. 2015. Insights from 20 years of bacterial genome sequencing. Funct Integr Genomics **15**(2): 141–161. doi:10.1007/s10142-015-0433-4.

Landwehr, V., Milanov, M., Angebauer, L., Hong, J., Jüngert, G., Hiersemenzel, A., Siebler, A., Schmit, F., Öztürk, Y., Dannenmaier, S., Drepper, F., Warscheid, B., and Koch, H.-G. 2021a. The Universally Conserved ATPase YchF Regulates Translation of Leaderless mRNA in Response to Stress Conditions. Front Mol Biosci **8**: 643696. doi:10.3389/fmolb.2021.643696.

Landwehr, V., Milanov, M., Hong, J., and Koch, H.-G. 2021b. The Role of the Universally Conserved ATPase YchF/Ola1 in Translation Regulation during Cellular Stress. Microorganisms **10**(1): 14. doi:10.3390/microorganisms10010014.

Langmuir, I. 1918. The Adsorption Of Gases On Plane Surfaces Of Glass, Mica And Platinum. J. Am. Chem. Soc. **40**(9): 1361–1403. doi:10.1021/ja02242a004.

Lartigue, C., Vashee, S., Algire, M.A., Chuang, R.-Y., Benders, G.A., Ma, L., Noskov, V.N., Denisova, E.A., Gibson, D.G., Assad-Garcia, N., Alperovich, N., Thomas, D.W., Merryman, C., Hutchison, C.A., Smith, H.O., Venter, J.C., and Glass, J.I. 2009. Creating Bacterial Strains from Genomes That Have Been Cloned and Engineered in Yeast. Science **325**(5948): 1693–1696. doi:10.1126/science.1173759.

Lehman, I.R., Bessman, M.J., Simms, E.S., and Kornberg, A. 1958. Enzymatic Synthesis of Deoxyribonucleic Acid. Journal of Biological Chemistry **233**(1): 163–170. doi:10.1016/S0021-9258(19)68048-8.

Leipe, D.D., Wolf, Y.I., Koonin, E.V., and Aravind, L. 2002. Classification and evolution of P-loop GTPases and related ATPases. Journal of Molecular Biology **317**(1): 41–72. doi:10.1006/jmbi.2001.5378.

Li, L., Rybak, M.Y., Lin, J., and Gagnon, M.G. 2024. The ribosome termination complex remodels release factor RF3 and ejects GDP. Nat Struct Mol Biol **31**(12): 1909–1920. doi:10.1038/s41594-024-01360-0.

Li, P., Nijhawan, D., Budihardjo, I., Srinivasula, S.M., Ahmad, M., Alnemri, E.S., and Wang, X. 1997. Cytochrome c and dATP-Dependent Formation of Apaf-1/Caspase-9 Complex Initiates an Apoptotic Protease Cascade. Cell **91**(4): 479–489. doi:10.1016/S0092-8674(00)80434-1.

Li, W., Atkinson, G.C., Thakor, N.S., Allas, Ü., Lu, C., Chan, K.-Y., Tenson, T., Schulten, K., Wilson, K.S., Hauryliuk, V., and Frank, J. 2013. Mechanism of Tetracycline Resistance by Ribosomal Protection Protein Tet(O). Nat Commun **4**: 1477. doi:10.1038/ncomms2470.

Liljas, A., Ehrenberg, M., and Åqvist, J. 2011. Comment on "The Mechanism for Activation of GTP Hydrolysis on the Ribosome." Science **333**(6038): 37–37. doi:10.1126/science.1202472.

Lin, Z., Li, R., Han, Z., Liu, Y., Gao, L., Huang, S., Miao, Y., and Miao, R. 2023. The Universally Conserved Unconventional G Protein YchF Is Critical for Growth and Stress Response. Life (Basel) **13**(4): 1058. doi:10.3390/life13041058.

Liu, J., Yang, Q., Xiao, K.C., Dobleman, T., Hu, S., and Xiao, G.G. 2020. Obg-like ATPase 1 inhibited oral carcinoma cell metastasis through TGFβ/SMAD2 axis in vitro. BMC Mol and Cell Biol **21**(1): 65. doi:10.1186/s12860-020-00311-z.

Liu, W., and Northup, J.K. 1998. The helical domain of a G protein α subunit is a regulator of its effector. Proc Natl Acad Sci U S A **95**(22): 12878–12883. doi:10.1073/pnas.95.22.12878.

Liu, Y., Fiskum, G., and Schubert, D. 2002. Generation of reactive oxygen species by the mitochondrial electron transport chain. Journal of Neurochemistry **80**(5): 780–787. doi:10.1046/j.0022-3042.2002.00744.x.

Liu, Y., Kong, X.-X., He, J.-J., Xu, Y.-B., Zhang, J.-K., Zou, L.-Y., Ding, K.-F., and Xu, D. 2022. OLA1 promotes colorectal cancer tumorigenesis by activation of HIF1α/CA9 axis. BMC Cancer **22**: 424. doi:10.1186/s12885-022-09508-1.

Llop, A., Bibak, S., Cantos, R., Salinas, P., and Contreras, A. 2023. The ribosome assembly GTPase EngA is involved in redox signaling in cyanobacteria. Front. Microbiol. **14**. doi:10.3389/fmicb.2023.1242616.

Lopez, J.M., Dromerick, A., and Freese, E. 1981. Response of Guanosine 5′-Triphosphate Concentration to Nutritional Changes and Its Significance for *Bacillus subtilis* Sporulation. J Bacteriol **146**(2): 605–613. doi:10.1128/jb.146.2.605-613.1981.

Loveland, A.B., Bah, E., Madireddy, R., Zhang, Y., Brilot, A.F., Grigorieff, N., and Korostelev, A.A. 2016. Ribosome•RelA structures reveal the mechanism of stringent response activation. eLife **5**: e17029. doi:10.7554/eLife.17029.

Loveland, A.B., Demo, G., Grigorieff, N., and Korostelev, A.A. 2017. Ensemble cryo-EM elucidates the mechanism of translation fidelity. Nature **546**(7656): 113–117. doi:10.1038/nature22397.

Lucas-Lenard, J., and Lipmann, F. 1966. Separation of three microbial amino acid polymerization factors. Proc Natl Acad Sci U S A **55**(6): 1562–1566. doi:10.1073/pnas.55.6.1562.

Luo, S., Zhu, M., and Fu, C. 2025. The Obg-like ATPase Ola1 prevents excessive mitochondrial reactive oxygen species by inhibiting MAPK/Pmk1 signaling in fission yeast. Microbiological Research **299**: 128259. doi:10.1016/j.micres.2025.128259.

Maillard, J., Klehs, K., Rumble, C., Vauthey, E., Heilemann, M., and Fürstenberg, A. 2021. Universal quenching of common fluorescent probes by water and alcohols. Chem. Sci. **12**(4): 1352–1362. doi:10.1039/D0SC05431C.

Manavathu, E.K., Fernandez, C.L., Cooperman, B.S., and Taylor, D.E. 1990. Molecular studies on the mechanism of tetracycline resistance mediated by Tet(O). Antimicrob Agents Chemother **34**(1): 71–77. doi:10.1128/aac.34.1.71.

Maracci, C., Peske, F., Dannies, E., Pohl, C., and Rodnina, M.V. 2014. Ribosome-induced tuning of GTP hydrolysis by a translational GTPase. Proc Natl Acad Sci U S A **111**(40): 14418–14423. doi:10.1073/pnas.1412676111.

Marlovits, T.C., Haase, W., Herrmann, C., Aller, S.G., and Unger, V.M. 2002. The membrane protein FeoB contains an intramolecular G protein essential for Fe(II) uptake in bacteria. Proceedings of the National Academy of Sciences **99**(25): 16243–16248. doi:10.1073/pnas.242338299.

Martemyanov, K.A., and Gudkov, A.T. 2000. Domain III of Elongation Factor G from *Thermus thermophilus* Is Essential for Induction of GTP Hydrolysis on the Ribosome. Journal of Biological Chemistry **275**(46): 35820–35824. doi:10.1074/jbc.M002656200.

Matsuzawa, A., Kanno, S., Nakayama, M., Mochiduki, H., Wei, L., Shimaoka, T., Furukawa, Y., Kato, K., Shibata, S., Yasui, A., Ishioka, C., and Chiba, N. 2014. The BRCA1/BARD1-Interacting Protein OLA1 Functions in Centrosome Regulation. Molecular Cell **53**(1): 101–114. doi:10.1016/j.molcel.2013.10.028.

Maxwell, I.H. 1967. Partial removal of bound transfer RNA from polysomes engaged in protein synthesis *in vitro* after addition of tetracycline. Biochimica et Biophysica Acta (BBA) - Nucleic Acids and Protein Synthesis **138**(2): 337–346. doi:10.1016/0005-2787(67)90494-7.

McClure, W.R., and Cech, C.L. 1978. On the mechanism of rifampicin inhibition of RNA synthesis. Journal of Biological Chemistry **253**(24): 8949–8956. doi:10.1016/S0021-9258(17)34269-2.

McCord, J.M., and Fridovich, I. 1969. Superoxide Dismutase. Journal of Biological Chemistry **244**(22): 6049–6055. doi:10.1016/S0021-9258(18)63504-5.

McGowan, J.E., Jr. 1983. Antimicrobial Resistance in Hospital Organisms and Its Relation to Antibiotic Use. Rev Infect Dis **5**(6): 1033–1048. doi:10.1093/clinids/5.6.1033.

McGrath, J.P., Capon, D.J., Goeddel, D.V., and Levinson, A.D. 1984. Comparative biochemical properties of normal and activated human ras p21 protein. Nature **310**(5979): 644–649. doi:10.1038/310644a0.

McQuillen, K., Roberts, R.B., and Britten, R.J. 1959. Synthesis of Nascent Protein by Ribosomes in *Escherichia coli*. Proceedings of the National Academy of Sciences of the United States of America **45**(9): 1437–1447.

Milburn, M.V., Tong, L., deVos, A.M., Brünger, A., Yamaizumi, Z., Nishimura, S., and Kim, S.-H. 1990. Molecular Switch for Signal Transduction: Structural Differences between Active and Inactive Forms of Protooncogenic ras Proteins. Science **247**(4945): 939–945.

Miller, D.L. 1972. Elongation Factors EF Tu and EF G Interact at Related Sites on Ribosomes. Proc Natl Acad Sci U S A **69**(3): 752–755. doi:10.1073/pnas.69.3.752.

Miller, G.H., Doukas, P.H., and Seydel, J.K. 1972. Sulfonamide structure-activity relation in a cell-free system. Correlation of inhibition of folate synthesis with antibacterial activity and physicochemical parameters. J. Med. Chem. **15**(7): 700–706. doi:10.1021/jm00277a002.

Miller, O.L., Hamkalo, B.A., and Thomas, C.A. 1970. Visualization of Bacterial Genes in Action. Science **169**(3943): 392–395.

Milón, P., Carotti, M., Konevega, A.L., Wintermeyer, W., Rodnina, M.V., and Gualerzi, C.O. 2010. The ribosome-bound initiation factor 2 recruits initiator tRNA to the 30S initiation complex. EMBO Rep **11**(4): 312–316. doi:10.1038/embor.2010.12.

Milón, P., Maracci, C., Filonava, L., Gualerzi, C.O., and Rodnina, M.V. 2012. Real-time assembly landscape of bacterial 30S translation initiation complex. Nat Struct Mol Biol **19**(6): 609–615. doi:10.1038/nsmb.2285.

Mishra, R., Gara, S.K., Mishra, S., and Prakash, B. 2005. Analysis of GTPases carrying hydrophobic amino acid substitutions in lieu of the catalytic glutamine: Implications for GTP hydrolysis. Proteins: Structure, Function, and Bioinformatics **59**(2): 332–338. doi:10.1002/prot.20413.

Moazed, D., Robertson, J.M., and Noller, H.F. 1988. Interaction of elongation factors EF-G and EF-Tu with a conserved loop in 23S RNA. Nature **334**(6180): 362–364. doi:10.1038/334362a0.

Mohr, D., Wintermeyer, W., and Rodnina, M.V. 2002. GTPase Activation of Elongation Factors Tu and G on the Ribosome. Biochemistry **41**(41): 12520–12528. doi:10.1021/bi026301y.

Monro, R.E., Cerná, J., and Marcker, K.A. 1968. Ribosome-catalyzed peptidyl transfer: substrate specificity at the P-site. Proc Natl Acad Sci U S A **61**(3): 1042–1049. doi:10.1073/pnas.61.3.1042.

More, N., Daniel, R.M., and Petach, H.H. 1995. The effect of low temperatures on enzyme activity. Biochem J **305**(Pt 1): 17–20. doi:10.1042/bj3050017.

Morimoto, T., Loh, P.C., Hirai, T., Asai, K., Kobayashi, K., Moriya, S., and Ogasawara, N. 2002. Six GTP-binding proteins of the Era/Obg family are essential for cell growth in *Bacillus subtilis*. Microbiology (Reading) **148**(Pt 11): 3539–3552. Reading, England. doi:10.1099/00221287-148-11-3539.

Müller, J.M., Moos, K., Baar, T., Maier, K.C., Zumer, K., and Tresch, A. 2024. Nuclear export is a limiting factor in eukaryotic mRNA metabolism. PLOS Computational Biology **20**(5): e1012059. doi:10.1371/journal.pcbi.1012059.

Müller, M., Schmidt, O., Angelova, M., Faserl, K., Weys, S., Kremser, L., Pfaffenwimmer, T., Dalik, T., Kraft, C., Trajanoski, Z., Lindner, H., and Teis, D. 2015. The coordinated action of

the MVB pathway and autophagy ensures cell survival during starvation. eLife **4**. doi:10.7554/elife.07736.

Murray, D.K., and Bremer, H. 1996. Control of spoT-dependent ppGpp Synthesis and Degradation in *Escherichia coli*. Journal of Molecular Biology **259**(1): 41–57. doi:10.1006/jmbi.1996.0300.

Nakamoto, T., Fox, C.F., and Weiss, S.B. 1964. Enzymatic Synthesis of Ribonucleic Acid. Journal of Biological Chemistry **239**(1): 167–174. doi:10.1016/S0021-9258(18)51765-8.

Natchiar, S.K., Myasnikov, A.G., Kratzat, H., Hazemann, I., and Klaholz, B.P. 2017. Visualization of chemical modifications in the human 80S ribosome structure. Nature **551**(7681): 472–477. doi:10.1038/nature24482.

Neuhoff, V., Arold, N., Taube, D., and Ehrhardt, W. 1988. Improved staining of proteins in polyacrylamide gels including isoelectric focusing gels with clear background at nanogram sensitivity using Coomassie Brilliant Blue G-250 and R-250. Electrophoresis **9**(6): 255–262. doi:10.1002/elps.1150090603.

Neyfakh, A.A., Borsch, C.M., and Kaatz, G.W. 1993. Fluoroquinolone resistance protein NorA of *Staphylococcus aureus* is a multidrug efflux transporter. Antimicrob Agents Chemother **37**(1): 128–129. doi:10.1128/aac.37.1.128.

Niemann, H.H., Knetsch, M.L.W., Scherer, A., Manstein, D.J., and Kull, F.J. 2001. Crystal structure of a dynamin GTPase domain in both nucleotide-free and GDP-bound forms. EMBO J **20**(21): 5813–5821. doi:10.1093/emboj/20.21.5813.

Nirenberg, M., and Leder, P. 1964. RNA Codewords and Protein Synthesis. Science **145**(3639): 1399–1407.

Nirenberg, M.W., and Matthaei, J.H. 1961. The Dependence of Cell- Free Protein Synthesis in *E. coli* upon Naturally Occurring or Synthetic Polyribonucleotides. Proceedings of the National Academy of Sciences of the United States of America **47**(10): 1588–1602.

Nissen, P., Kjeldgaard, M., Thirup, S., Polekhina, G., Reshetnikova, L., Clark, B.F.C., and Nyborg, J. 1995. Crystal Structure of the Ternary Complex of Phe-tRNA^{Phe}, EF-Tu, and a GTP Analog. Science **270**(5241): 1464–1472.

Noller, H.F., Lancaster, L., Zhou, J., and Mohan, S. 2017. The ribosome moves: RNA mechanics and translocation. Nat Struct Mol Biol **24**(12): 1021–1027. doi:10.1038/nsmb.3505.

Nurk, S., Koren, S., Rhie, A., Rautiainen, M., Bzikadze, A.V., Mikheenko, A., Vollger, M.R., Altemose, N., Uralsky, L., Gershman, A., Aganezov, S., Hoyt, S.J., Diekhans, M., Logsdon, G.A., Alonge, M., Antonarakis, S.E., Borchers, M., Bouffard, G.G., Brooks, S.Y., Caldas, G.V., Chen, N.-C., Cheng, H., Chin, C.-S., Chow, W., de Lima, L.G., Dishuck, P.C., Durbin, R., Dvorkina, T., Fiddes, I.T., Formenti, G., Fulton, R.S., Fungtammasan, A., Garrison, E., Grady, P.G.S., Graves-Lindsay, T.A., Hall, I.M., Hansen, N.F., Hartley, G.A., Haukness, M., Howe, K., Hunkapiller, M.W., Jain, C., Jain, M., Jarvis, E.D., Kerpedjiev, P., Kirsche, M., Kolmogorov, M., Korlach, J., Kremitzki, M., Li, H., Maduro, V.V., Marschall, T., McCartney, A.M., McDaniel, J., Miller, D.E., Mullikin, J.C., Myers, E.W., Olson, N.D., Paten, B., Peluso, P., Pevzner, P.A., Porubsky, D., Potapova, T., Rogaev, E.I., Rosenfeld, J.A., Salzberg, S.L., Schneider, V.A., Sedlazeck, F.J., Shafin, K., Shew, C.J., Shumate, A., Sims, Y., Smit, A.F.A., Soto, D.C., Sović, I., Storer, J.M., Streets, A., Sullivan, B.A., Thibaud-Nissen, F., Torrance, J., Wagner, J., Walenz, B.P., Wenger, A., Wood, J.M.D., Xiao, C., Yan, S.M., Young, A.C., Zarate, S., Surti, U., McCoy, R.C., Dennis, M.Y., Alexandrov, I.A., Gerton, J.L., O'Neill, R.J., Timp, W., Zook, J.M., Schatz, M.C., Eichler, E.E., Miga, K.H., and Phillippy, A.M. 2022. The complete sequence of a human genome. Science **376**(6588): 44–53. doi:10.1126/science.abj6987.

Ogle, J.M., Brodersen, D.E., Clemons, W.M., Tarry, M.J., Carter, A.P., and Ramakrishnan, V. 2001. Recognition of Cognate Transfer RNA by the 30S Ribosomal Subunit. Science **292**(5518): 897–902. doi:10.1126/science.1060612.

Ogle, J.M., Murphy, F.V., Tarry, M.J., and Ramakrishnan, V. 2002. Selection of tRNA by the Ribosome Requires a Transition from an Open to a Closed Form. Cell **111**(5): 721–732. doi:10.1016/S0092-8674(02)01086-3.

Ohta, T., and Thach, R.E. 1968. Binding of Formylmethionyl-tRNA and Aminoacyl-tRNA to Ribosomes. Nature **219**(5151): 238–243. doi:10.1038/219238a0.

Pai, E.F., Krengel, U., Petsko, G.A., Goody, R.S., Kabsch, W., and Wittinghofer, A. 1990. Refined crystal structure of the triphosphate conformation of H-ras p21 at 1.35 A resolution: implications for the mechanism of GTP hydrolysis. EMBO J **9**(8): 2351–2359. doi:10.1002/j.1460-2075.1990.tb07409.x.

Pape, T., Wintermeyer, W., and Rodnina, M. 1999. Induced fit in initial selection and proofreading of aminoacyl-tRNA on the ribosome. EMBO J **18**(13): 3800–3807. doi:10.1093/emboj/18.13.3800.

Pape, T., Wintermeyer, W., and Rodnina, M.V. 1998. Complete kinetic mechanism of elongation factor Tu-dependent binding of aminoacyl-tRNA to the A site of the E. coli ribosome. EMBO J **17**(24): 7490–7497. doi:10.1093/emboj/17.24.7490.

Penman, S. 1966. RNA metabolism in the HeLa cell nucleus. Journal of Molecular Biology **17**(1): 117-IN4. doi:10.1016/S0022-2836(66)80098-0.

Peske, F., Kuhlenkoetter, S., Rodnina, M.V., and Wintermeyer, W. 2014. Timing of GTP binding and hydrolysis by translation termination factor RF3. Nucleic Acids Res **42**(3): 1812–1820. doi:10.1093/nar/gkt1095.

Peske, F., Rodnina, M.V., and Wintermeyer, W. 2005. Sequence of Steps in Ribosome Recycling as Defined by Kinetic Analysis. Molecular Cell **18**(4): 403–412. doi:10.1016/j.molcel.2005.04.009.

del Peso Santos, T., Alvarez, L., Sit, B., Irazoki, O., Blake, J., Warner, B.R., Warr, A.R., Bala, A., Benes, V., Waldor, M.K., Fredrick, K., and Cava, F. 2021. BipA exerts temperature-dependent translational control of biofilm-associated colony morphology in *Vibrio cholerae*. eLife **10**: e60607. doi:10.7554/eLife.60607.

Petrychenko, V., Peng, B.-Z., de A P Schwarzer, A.C., Peske, F., Rodnina, M.V., and Fischer, N. 2021. Structural mechanism of GTPase-powered ribosome-tRNA movement. Nat Commun **12**(1): 5933. doi:10.1038/s41467-021-26133-x.

Pfennig, P., and Flower, A. 2001. BipA is required for growth of Escherichia coli K12 at low temperature. Mol Gen Genomics **266**(2): 313–317. doi:10.1007/s004380100559.

Pioletti, M., Schlünzen, F., Harms, J., Zarivach, R., Glühmann, M., Avila, H., Bashan, A., Bartels, H., Auerbach, T., Jacobi, C., Hartsch, T., Yonath, A., and Franceschi, F. 2001. Crystal structures of complexes of the small ribosomal subunit with tetracycline, edeine and IF3. EMBO J **20**(8): 1829–1839. doi:10.1093/emboj/20.8.1829.

Privé, G.G., Milburn, M.V., Tong, L., de Vos, A.M., Yamaizumi, Z., Nishimura, S., and Kim, S.H. 1992. X-ray crystal structures of transforming p21 ras mutants suggest a transition-state stabilization mechanism for GTP hydrolysis. Proc Natl Acad Sci U S A **89**(8): 3649–3653. doi:10.1073/pnas.89.8.3649.

Proshkin, S., Rahmouni, R., Mironov, A., and Nudler, E. 2010. Cooperation between Translating Ribosomes and RNA Polymerase in Transcription Elongation. Science **328**(5977): 504–508. doi:10.1126/science.1184939.

Ranu, R.S., and Wool, I.G. 1975. Discrimination between eukaryotic and prokaryotic, and formylated and non-formylated, initiator tRNAs by eukaryotic initiation factor EIF-3. Nature **257**(5527): 616–618. doi:10.1038/257616a0.

Record, M.T., Lohman, T.M., and Haseth, P. de. 1976. Ion effects on ligand-nucleic acid interactions. Journal of Molecular Biology **107**(2): 145–158. doi:10.1016/S0022-2836(76)80023-X.

Reinstein, J., Schlichting, I., and Wittinghofer, A. 1990. Structurally and catalytically important residues in the phosphate binding loop of adenylate kinase of *Escherichia coli*. Biochemistry **29**(32): 7451–7459. doi:10.1021/bi00484a014.

Rheinberger, H.J., Sternbach, H., and Nierhaus, K.H. 1981. Three tRNA binding sites on *Escherichia coli* ribosomes. Proc Natl Acad Sci U S A **78**(9): 5310–5314. doi:10.1073/pnas.78.9.5310.

Rissone, P., Severino, A., Pastor, I., and Ritort, F. 2024. Universal cold RNA phase transitions. Proceedings of the National Academy of Sciences **121**(34): e2408313121. doi:10.1073/pnas.2408313121.

Ritossa, F. 1962. A new puffing pattern induced by temperature shock and DNP in *Drosophila*. Experientia **18**(12): 571–573. doi:10.1007/BF02172188.

Robertson, C.I., Gaffney, D.P., Chrin, L.R., and Berger, C.L. 2005. Structural Rearrangements in the Active Site of Smooth-Muscle Myosin. Biophysical Journal **89**(3): 1882–1892. doi:10.1529/biophysj.105.059840.

Robinson, V.L., Hwang, J., Fox, E., Inouye, M., and Stock, A.M. 2002. Domain Arrangement of Der, a Switch Protein Containing Two GTPase Domains. Structure **10**(12): 1649–1658. doi:10.1016/S0969-2126(02)00905-X.

Rodnina, M.V. 2018. Translation in Prokaryotes. Cold Spring Harb Perspect Biol **10**(9): a032664. doi:10.1101/cshperspect.a032664.

Rosler, K.S., Mercier, E., Andrews, I.C., and Wieden, H.-J. 2015. Histidine 114 Is Critical for ATP Hydrolysis by the Universally Conserved ATPase YchF. J Biol Chem **290**(30): 18650–18661. doi:10.1074/jbc.M114.598227.

Rovera, G., Berman, S., and Baserga, R. 1970. Pulse Labeling of RNA of Mammalian Cells. Proc Natl Acad Sci U S A **65**(4): 876–883. doi:10.1073/pnas.65.4.876.

Rundlet, E.J., Holm, M., Schacherl, M., Natchiar, S.K., Altman, R.B., Spahn, C.M.T., Myasnikov, A.G., and Blanchard, S.C. 2021. Structural basis of early translocation events on the ribosome. Nature **595**(7869): 741–745. doi:10.1038/s41586-021-03713-x.

Sakmann, B., and Neher, E. 1984. Patch Clamp Techniques for Studying Ionic Channels in Excitable Membranes. Annual Review of Physiology **46**(Volume 46,): 455–472. doi:10.1146/annurev.ph.46.030184.002323.

Sanchez, C.J., Mende, K., Beckius, M.L., Akers, K.S., Romano, D.R., Wenke, J.C., and Murray, C.K. 2013. Biofilm formation by clinical isolates and the implications in chronic infections. BMC Infect Dis **13**: 47. doi:10.1186/1471-2334-13-47.

Saraste, M., Sibbald, P.R., and Wittinghofer, A. 1990. The P-loop — a common motif in ATP- and GTP-binding proteins. Trends in Biochemical Sciences **15**(11): 430–434. doi:10.1016/0968-0004(90)90281-F.

Sashital, D.G., Greeman, C.A., Lyumkis, D., Potter, C.S., Carragher, B., and Williamson, J.R. 2014. A combined quantitative mass spectrometry and electron microscopy analysis of ribosomal 30S subunit assembly in *E. coli*. eLife **3**: e04491. doi:10.7554/eLife.04491.

Schmeing, T.M., Voorhees, R.M., Kelley, A.C., Gao, Y.-G., Murphy, F.V., Weir, J.R., and Ramakrishnan, V. 2009a. The crystal structure of the ribosome bound to EF-Tu and aminoacyl-tRNA. Science **326**(5953): 688–694. doi:10.1126/science.1179700.

Schmeing, T.M., Voorhees, R.M., Kelley, A.C., Gao, Y.-G., Murphy, F.V., Weir, J.R., and Ramakrishnan, V. 2009b. The crystal structure of the ribosome bound to EF-Tu and aminoacyl-tRNA. Science **326**(5953): 688–694. doi:10.1126/science.1179700.

Schmitt, E., Mechulam, Y., Fromant, M., Plateau, P., and Blanquet, S. 1997. Crystal structure at 1.2 A resolution and active site mapping of Escherichia coli peptidyl-tRNA hydrolase. EMBO J **16**(15): 4760–4769. doi:10.1093/emboj/16.15.4760.

Schneckenburger, H. 2019. Förster resonance energy transfer–what can we learn and how can we use it? Methods Appl. Fluoresc. **8**(1): 013001. doi:10.1088/2050-6120/ab56e1.

Schüller, C., Brewster, J.L., Alexander, M.R., Gustin, M.C., and Ruis, H. 1994. The HOG pathway controls osmotic regulation of transcription via the stress response element (STRE) of the

Saccharomyces cerevisiae CTT1 gene. EMBO J **13**(18): 4382–4389. doi:10.1002/j.1460-2075.1994.tb06758.x.

Scolnick, E.M., Papageorge, A.G., and Shih, T.Y. 1979. Guanine nucleotide-binding activity as an assay for src protein of rat-derived murine sarcoma viruses. Proc Natl Acad Sci U S A **76**(10): 5355–5359. doi:10.1073/pnas.76.10.5355.

Scrima, A., and Wittinghofer, A. 2006. Dimerisation-dependent GTPase reaction of MnmE: how potassium acts as GTPase-activating element. EMBO J **25**(12): 2940–2951. doi:10.1038/sj.emboj.7601171.

Scully, R., Anderson, S.F., Chao, D.M., Wei, W., Ye, L., Young, R.A., Livingston, D.M., and Parvin, J.D. 1997. BRCA1 is a component of the RNA polymerase II holoenzyme. Proc Natl Acad Sci U S A **94**(11): 5605–5610. doi:10.1073/pnas.94.11.5605.

Selmer, M., Al-Karadaghi, S., Hirokawa, G., Kaji, A., and Liljas, A. 1999. Crystal Structure of *Thermotoga maritima* Ribosome Recycling Factor: A tRNA Mimic. Science **286**(5448): 2349–2352. doi:10.1126/science.286.5448.2349.

Semmelrock, J., and Wieden, H.-J. 2026. The universally conserved NTPase OLA1. Biochem. Cell Biol. **104**: 1–18. doi:10.1139/bcb-2025-0347.

Setlow, R.B., and Setlow, J.K. 1962. Evidence that ultraviolet-induced thymine dimers in DNA cause biological damage. Proc Natl Acad Sci U S A **48**(7): 1250–1257. doi:10.1073/pnas.48.7.1250.

Shan, S., and Walter, P. 2003. Induced nucleotide specificity in a GTPase. Proceedings of the National Academy of Sciences **100**(8): 4480–4485. doi:10.1073/pnas.0737693100.

Shaw, G., and Kamen, R. 1986. A conserved AU sequence from the 3′ untranslated region of GM-CSF mRNA mediates selective mRNA degradation. Cell **46**(5): 659–667. doi:10.1016/0092-8674(86)90341-7.

Shen, L.L., Kohlbrenner, W.E., Weigl, D., and Baranowski, J. 1989. Mechanism of quinolone inhibition of DNA gyrase: Appearance of unique norfloxacin binding sites in enzyme-DNA complexes. Journal of Biological Chemistry **264**(5): 2973–2978. doi:10.1016/S0021-9258(19)81708-8.

Shi, X., Khade, P.K., Sanbonmatsu, K.Y., and Joseph, S. 2012. Functional Role of the Sarcin-Ricin Loop of the 23S rRNA in the Elongation Cycle of Protein Synthesis. J Mol Biol **419**(3–4): 125–138. doi:10.1016/j.jmb.2012.03.016.

Shields, M.J., Fischer, J.J., and Wieden, H.-J. 2009. Toward Understanding the Function of the Universally Conserved GTPase HflX from *Escherichia coli*: A Kinetic Approach. Biochemistry **48**(45): 10793–10802. doi:10.1021/bi901074h.

Shin, M., Mey, A.R., and Payne, S.M. 2019. Vibrio cholerae FeoB contains a dual nucleotide-specific NTPase domain essential for ferrous iron uptake. Proceedings of the National Academy of Sciences **116**(10): 4599–4604. doi:10.1073/pnas.1817964116.

Shorey, R.L., Ravel, J.M., Garner, C.W., and Shive, W. 1969. Formation and Properties of the Aminoacyl Transfer Ribonucleic Acid-Guanosine Triphosphate-Protein Complex. Journal of Biological Chemistry **244**(17): 4555–4564. doi:10.1016/S0021-9258(18)93662-8.

Silva, D.-A., Weiss, D.R., Pardo Avila, F., Da, L.-T., Levitt, M., Wang, D., and Huang, X. 2014. Millisecond dynamics of RNA polymerase II translocation at atomic resolution. Proc. Natl. Acad. Sci. U.S.A. **111**(21): 7665–7670. doi:10.1073/pnas.1315751111.

Silverman, J.A., Perlmutter, N.G., and Shapiro, H.M. 2003. Correlation of Daptomycin Bactericidal Activity and Membrane Depolarization in *Staphylococcus aureus*. Antimicrob Agents Chemother **47**(8): 2538–2544. doi:10.1128/AAC.47.8.2538-2544.2003.

Smith, T.L., Pearson, M.L., Wilcox, K.R., Cruz, C., Lancaster, M.V., Robinson-Dunn, B., Tenover, F.C., Zervos, M.J., Band, J.D., White, E., and Jarvis, W.R. 1999. Emergence of Vancomycin Resistance in *Staphylococcus aureus*. N Engl J Med **340**(7): 493–501. doi:10.1056/NEJM199902183400701.

Song, H., Mugnier, P., Das, A.K., Webb, H.M., Evans, D.R., Tuite, M.F., Hemmings, B.A., and Barford, D. 2000. The crystal structure of human eukaryotic release factor eRF1--mechanism of stop codon recognition and peptidyl-tRNA hydrolysis. Cell **100**(3): 311–321. doi:10.1016/s0092-8674(00)80667-4.

Song, L.F., Rabara, D., Bali, S.K., Pei, J., Lau, E.Y., Kirshner, D., Lightstone, F.C., McCormick, F., Stephen, A.G., and Yang, Y. 2025. How KRAS Mutations Impair Intrinsic GTP Hydrolysis: Experimental and Computational Investigations. J. Chem. Inf. Model. **65**(23): 12822–12833. doi:10.1021/acs.jcim.5c02061.

Spahn, C.M.T., Beckmann, R., Eswar, N., Penczek, P.A., Sali, A., Blobel, G., and Frank, J. 2001a. Structure of the 80S Ribosome from *Saccharomyces cerevisiae*—tRNA-Ribosome and Subunit-Subunit Interactions. Cell **107**(3): 373–386. doi:10.1016/S0092-8674(01)00539-6.

Spahn, C.M.T., Blaha, G., Agrawal, R.K., Penczek, P., Grassucci, R.A., Trieber, C.A., Connell, S.R., Taylor, D.E., Nierhaus, K.H., and Frank, J. 2001b. Localization of the Ribosomal Protection Protein Tet(O) on the Ribosome and the Mechanism of Tetracycline Resistance. Molecular Cell **7**(5): 1037–1045. doi:10.1016/S1097-2765(01)00238-6.

Spencer, A.C., and Spremulli, L.L. 2004. Interaction of mitochondrial initiation factor 2 with mitochondrial fMet-tRNA. Nucleic Acids Res **32**(18): 5464–5470. doi:10.1093/nar/gkh886.

Stark, H., Rodnina, M.V., Rinke-Appel, J., Brimacombe, R., Wintermeyer, W., and Heel, M. van. 1997. Visualization of elongation factor Tu on the *Escherichia coli* ribosome. Nature **389**(6649): 403–406. doi:10.1038/38770.

Stark, H., Rodnina, M.V., Wieden, H.-J., van Heel, M., and Wintermeyer, W. 2000. Large-Scale Movement of Elongation Factor G and Extensive Conformational Change of the Ribosome during Translocation. Cell **100**(3): 301–309. doi:10.1016/S0092-8674(00)80666-2.

Summer, H., Grämer, R., and Dröge, P. 2009. Denaturing Urea Polyacrylamide Gel Electrophoresis (Urea PAGE). J Vis Exp (32): 1485. doi:10.3791/1485.

Sun, H., Luo, X., Montalbano, J., Jin, W., Shi, J., Sheikh, M.S., and Huang, Y. 2010. DOC45, a Novel DNA Damage–Regulated Nucleocytoplasmic ATPase That Is Overexpressed in Multiple Human Malignancies. Molecular Cancer Research **8**(1): 57–66. doi:10.1158/1541-7786.MCR-09-0278.

Sun, J., Conn, C.S., Han, Y., Yeung, V., and Qian, S.-B. 2011. PI3K-mTORC1 Attenuates Stress Response by Inhibiting Cap-independent Hsp70 Translation. Journal of Biological Chemistry **286**(8): 6791–6800. doi:10.1074/jbc.M110.172882.

Suwastika, I.N., Denawa, M., Yomogihara, S., Im, C.H., Bang, W.Y., Ohniwa, R.L., Bahk, J.D., Takeyasu, K., and Shiina, T. 2014. Evidence for lateral gene transfer (LGT) in the evolution of eubacteria-derived small GTPases in plant organelles. Front Plant Sci **5**: 678. doi:10.3389/fpls.2014.00678.

Taylor, D.E., Jerome, L.J., Grewal, J., and Chang, N. 1995. Tet(O), a protein that mediates ribosomal protection to tetracycline, binds, and hydrolyses GTP. Can. J. Microbiol. **41**(11): 965–970. doi:10.1139/m95-134.

Teplyakov, A., Obmolova, G., Chu, S.Y., Toedt, J., Eisenstein, E., Howard, A.J., and Gilliland, G.L. 2003. Crystal Structure of the YchF Protein Reveals Binding Sites for GTP and Nucleic Acid. J Bacteriol **185**(14): 4031–4037. doi:10.1128/JB.185.14.4031-4037.2003.

Teusink, B., Passarge, J., Reijenga, C.A., Esgalhado, E., van der Weijden, C.C., Schepper, M., Walsh, M.C., Bakker, B.M., van Dam, K., Westerhoff, H.V., and Snoep, J.L. 2000. Can yeast glycolysis be understood in terms of in vitro kinetics of the constituent enzymes? Testing biochemistry. European Journal of Biochemistry **267**(17): 5313–5329. doi:10.1046/j.1432-1327.2000.01527.x.

Thakor, N.S., Nechifor, R., Scott, P.G., Keelan, M., Taylor, D.E., and Wilson, K.S. 2008. Chimeras of bacterial translation factors Tet(O) and EF-G. FEBS Letters **582**(9): 1386–1390. doi:10.1016/j.febslet.2008.03.023.

Thompson, R.C., and Karim, A.M. 1982. The accuracy of protein biosynthesis is limited by its speed: high fidelity selection by ribosomes of aminoacyl-tRNA ternary complexes containing GTP[gamma S]. Proc Natl Acad Sci U S A **79**(16): 4922–4926. doi:10.1073/pnas.79.16.4922.

Ticu, C., Nechifor, R., Nguyen, B., Desrosiers, M., and Wilson, K.S. 2009. Conformational changes in switch I of EF-G drive its directional cycling on and off the ribosome. EMBO J **28**(14): 2053–2065. doi:10.1038/emboj.2009.169.

Tomar, S.K., Dhimole, N., Chatterjee, M., and Prakash, B. 2009. Distinct GDP/GTP bound states of the tandem G-domains of EngA regulate ribosome binding. Nucleic Acids Res **37**(7): 2359–2370. doi:10.1093/nar/gkp107.

Tomar, S.K., Kumar, P., and Prakash, B. 2011. Deciphering the catalytic machinery in a universally conserved ribosome binding ATPase YchF. Biochemical and Biophysical Research Communications **408**(3): 459–464. doi:10.1016/j.bbrc.2011.04.052.

Trieber, C.A., Burkhardt, N., Nierhaus, K.H., and Taylor, D.E. 1998. Ribosomal Protection from Tetracycline Mediated by Tet(O): Tet(O) Interaction with Ribosomes Is GTP-Dependent. **379**(7): 847–856. doi:10.1515/bchm.1998.379.7.847.

Tsai, A., Petrov, A., Marshall, R.A., Korlach, J., Uemura, S., and Puglisi, J.D. 2012. Heterogeneous pathways and timing of factor departure during translation initiation. Nature **487**(7407): 390–393. doi:10.1038/nature11172.

Uematsu, S., and Qian, S.-B. 2025. Interpreting ribosome dynamics during mRNA translation. J Biol Chem **301**(8): 110469. doi:10.1016/j.jbc.2025.110469.

Uppal, S., Maurya, S.R., Hire, R.S., and Jawali, N. 2011. Cyclic AMP Receptor Protein Regulates cspE, an Early Cold-Inducible Gene, in *Escherichia coli*. Journal of Bacteriology **193**(22): 6142–6151. doi:10.1128/jb.05728-11.

Valle, M., Zavialov, A., Li, W., Stagg, S.M., Sengupta, J., Nielsen, R.C., Nissen, P., Harvey, S.C., Ehrenberg, M., and Frank, J. 2003a. Incorporation of aminoacyl-tRNA into the ribosome as seen by cryo-electron microscopy. Nat Struct Mol Biol **10**(11): 899–906. doi:10.1038/nsb1003.

Valle, M., Zavialov, A., Sengupta, J., Rawat, U., Ehrenberg, M., and Frank, J. 2003b. Locking and Unlocking of Ribosomal Motions. Cell **114**(1): 123–134. doi:10.1016/S0092-8674(03)00476-8.

Verstraeten, N., Fauvart, M., Versées, W., and Michiels, J. 2011. The universally conserved prokaryotic GTPases. Microbiol Mol Biol Rev **75**(3): 507–542, second and third pages of table of contents. doi:10.1128/MMBR.00009-11.

Vesper, O., Amitai, S., Belitsky, M., Byrgazov, K., Kaberdina, A.C., Engelberg-Kulka, H., and Moll, I. 2011. Selective Translation of Leaderless mRNAs by Specialized Ribosomes Generated by MazF in *Escherichia coli*. Cell **147**(1): 147–157. doi:10.1016/j.cell.2011.07.047.

Vestergaard, B., Van, L.B., Andersen, G.R., Nyborg, J., Buckingham, R.H., and Kjeldgaard, M. 2001. Bacterial Polypeptide Release Factor RF2 Is Structurally Distinct from Eukaryotic eRF1. Molecular Cell **8**(6): 1375–1382. doi:10.1016/S1097-2765(01)00415-4.

Vetter, I.R., and Wittinghofer, A. 2001. The Guanine Nucleotide-Binding Switch in Three Dimensions. Science **294**(5545): 1299–1304. doi:10.1126/science.1062023.

Vithani, N., Batra, S., Prakash, B., and Nair, N.N. 2017. Elucidating the GTP Hydrolysis Mechanism in FeoB: A Hydrophobic Amino-Acid Substituted GTPase. ACS Catal. **7**(1): 902–906. doi:10.1021/acscatal.6b03365.

Voorhees, R.M., Schmeing, T.M., Kelley, A.C., and Ramakrishnan, V. 2010. The mechanism for activation of GTP hydrolysis on the ribosome. Science **330**(6005): 835–838. doi:10.1126/science.1194460.

Walker, J.E., Saraste, M., Runswick, M.J., and Gay, N.J. 1982. Distantly related sequences in the alpha- and beta-subunits of ATP synthase, myosin, kinases and other ATP-requiring enzymes and a common nucleotide binding fold. EMBO J **1**(8): 945–951. doi:10.1002/j.1460-2075.1982.tb01276.x.

Walter, J.D., Hunter, M., Cobb, M., Traeger, G., and Spiegel, P.C. 2012. Thiostrepton inhibits stable 70S ribosome binding and ribosome-dependent GTPase activation of elongation factor G and elongation factor 4. Nucleic Acids Res **40**(1): 360–370. doi:10.1093/nar/gkr623.

Wang, G.L., and Semenza, G.L. 1995. Purification and Characterization of Hypoxia-inducible Factor 1. Journal of Biological Chemistry **270**(3): 1230–1237. doi:10.1074/jbc.270.3.1230.

Wei, C.M., Gershowitz, A., and Moss, B. 1975. Methylated nucleotides block 5' terminus of HeLa cell messenger RNA. Cell **4**(4): 379–386. doi:10.1016/0092-8674(75)90158-0.

Weiser, J.N., Ferreira, D.M., and Paton, J.C. 2018. *Streptococcus pneumoniae*: transmission, colonization and invasion. Nat Rev Microbiol **16**(6): 355–367. doi:10.1038/s41579-018-0001-8.

Weixlbaumer, A., Petry, S., Dunham, C.M., Selmer, M., Kelley, A.C., and Ramakrishnan, V. 2007. Crystal structure of the ribosome recycling factor bound to the ribosome. Nat Struct Mol Biol **14**(8): 733–737. doi:10.1038/nsmb1282.

Wenk, M., Ba, Q., Erichsen, V., MacInnes, K., Wiese, H., Warscheid, B., and Koch, H.-G. 2012. A Universally Conserved ATPase Regulates the Oxidative Stress Response in *Escherichia coli*. J Biol Chem **287**(52): 43585–43598. doi:10.1074/jbc.M112.413070.

Wilden, B., Savelsbergh, A., Rodnina, M.V., and Wintermeyer, W. 2006. Role and timing of GTP binding and hydrolysis during EF-G-dependent tRNA translocation on the ribosome. Proc Natl Acad Sci U S A **103**(37): 13670–13675. doi:10.1073/pnas.0606099103.

Wimberly, B.T., Brodersen, D.E., Clemons, W.M., Morgan-Warren, R.J., Carter, A.P., Vonrhein, C., Hartsch, T., and Ramakrishnan, V. 2000. Structure of the 30S ribosomal subunit. Nature **407**(6802): 327–339. doi:10.1038/35030006.

Wise, E.M., and Park, J.T. 1965. Penicillin: its basic site of action as an inhibitor of a peptide cross-linking reaction in cell wall mucopeptide synthesis. Proc Natl Acad Sci U S A **54**(1): 75–81. doi:10.1073/pnas.54.1.75.

Wu, D., Huang, H., Chen, T., Gai, X., Li, Q., Wang, C., Yao, J., Liu, Y., Cai, S., and Yu, X. 2023. The BRCA1/BARD1 complex recognizes pre-ribosomal RNA to facilitate homologous recombination. Cell Discov **9**(1): 99. doi:10.1038/s41421-023-00590-8.

Yanagi, Y., Yoshikai, Y., Leggett, K., Clark, S.P., Aleksander, I., and Mak, T.W. 1984. A human T cell-specific cDNA clone encodes a protein having extensive homology to immunoglobulin chains. Nature **308**(5955): 145–149. doi:10.1038/308145a0.

Yokoyama, T., Shaikh, T.R., Iwakura, N., Kaji, H., Kaji, A., and Agrawal, R.K. 2012. Structural insights into initial and intermediate steps of the ribosome-recycling process. EMBO J **31**(7): 1836–1846. doi:10.1038/emboj.2012.22.

Yoshida, H., Kojima, T., Yamagishi, J., and Nakamura, S. 1988. Quinolone-resistant mutations of the *gyrA* gene of *Escherichia coli*. Mol Gen Genet **211**(1): 1–7. doi:10.1007/BF00338386.

Yu, T., Li, X., Dong, W., Zhou, Q., Li, Q., Du, Z., and Zeng, F. 2025. Conserved GTPase OLA1 promotes efficient translation on D/E-rich mRNA. Nat Commun **16**(1): 1549. doi:10.1038/s41467-025-56797-8.

Yusupov, M.M., Yusupova, G.Zh., Baucom, A., Lieberman, K., Earnest, T.N., Cate, J.H.D., and Noller, H.F. 2001. Crystal Structure of the Ribosome at 5.5 Å Resolution. Science **292**(5518): 883–896. doi:10.1126/science.1060089.

Yusupova, G., Jenner, L., Rees, B., Moras, D., and Yusupov, M. 2006. Structural basis for messenger RNA movement on the ribosome. Nature **444**(7117): 391–394. doi:10.1038/nature05281.

Zavialov, A.V., Buckingham, R.H., and Ehrenberg, M. 2001. A Posttermination Ribosomal Complex Is the Guanine Nucleotide Exchange Factor for Peptide Release Factor RF3. Cell **107**(1): 115–124. doi:10.1016/S0092-8674(01)00508-6.

Zhang, J., Rubio, V., Lieberman, M.W., and Shi, Z.-Z. 2009a. OLA1, an Obg-like ATPase, suppresses antioxidant response via nontranscriptional mechanisms. Proc Natl Acad Sci U S A **106**(36): 15356–15361. doi:10.1073/pnas.0907213106.

Zhang, J., Rubio, V., Zheng, S., and Shi, Z. 2009b. Knockdown of OLA1, a regulator of oxidative stress response, inhibits motility and invasion of breast cancer cells. J Zhejiang Univ Sci B **10**(11): 796–804. doi:10.1631/jzus.B0910009.

Zhou, J., Lancaster, L., Trakhanov, S., and Noller, H.F. 2012. Crystal structure of release factor RF3 trapped in the GTP state on a rotated conformation of the ribosome. RNA **18**(2): 230–240. doi:10.1261/rna.031187.111.

7. Appendix

Table A1. Fusion proteins used in this thesis.

Fusion protein	Source	Amino acid sequence[a]
N-terminal 6xHis tag WT *E. coli* YchF	Becker *et al*., 2012	MGSSHHHHHHSSGLVPRGSHMGFKCGIVGLPNVGKSTLFN ALTKAGIEAANFPFCTIEPNTGVVPMPDPRLDQLAEIVKPQR TLPTTMEFVDIAGLVKGASKGEGLGNQFLTNIRETEAIGHV VRCFENDNIIHVSGKVNPADDIEVINTELALADLDTCERAIH RVQKKAKGGDKDAKAELAVLEKCLPQLENAGMLRALDLS AEEKAAIRYLSFLTLKPTMYIA**NVNE**DGFENNPYLDQVREI AAKEGSVVVPVCAAVEADIAELDDEERDEFMQELGLEEPG LNRVIRAGYKLLNLQTYFTAGVKEVRAWTIPVGATAPQAA GKIHTDFEKGFIRAQTISFEDFITYKGEQGAKEAGKMRAEG KDYIVKDGDVMNFLFNV*
N-terminal 6xHis tag *E. coli* YchF_NLSE	Pageni, unpublished	MGSSHHHHHHSSGLVPRGSHMGFKCGIVGLPNVGKSTLFN ALTKAGIEAANFPFCTIEPNTGVVPMPDPRLDQLAEIVKPQR TLPTTMEFVDIAGLVKGASKGEGLGNQFLTNIRETEAIGHV VRCFENDNIIHVSGKVNPADDIEVINTELALADLDTCERAIH RVQKKAKGGDKDAKAELAVLEKCLPQLENAGMLRALDLS AEEKAAIRYLSFLTLKPTMYIA**NLSE**DGFENNPYLDQVREI AAKEGSVVVPVCAAVEADIAELDDEERDEFMQELGLEEPG LNRVIRAGYKLLNLQTYFTAGVKEVRAWTIPVGATAPQAA GKIHTDFEKGFIRAQTISFEDFITYKGEQGAKEAGKMRAEG KDYIVKDGDVMNFLFNV*
N-terminal 6xHis tag *E. coli* YchF_NKMD	Pageni, unpublished	MGSSHHHHHHSSGLVPRGSHMGFKCGIVGLPNVGKSTLFN ALTKAGIEAANFPFCTIEPNTGVVPMPDPRLDQLAEIVKPQR TLPTTMEFVDIAGLVKGASKGEGLGNQFLTNIRETEAIGHV VRCFENDNIIHVSGKVNPADDIEVINTELALADLDTCERAIH RVQKKAKGGDKDAKAELAVLEKCLPQLENAGMLRALDLS AEEKAAIRYLSFLTLKPTMYIA**NKMD**DGFENNPYLDQVREI AAKEGSVVVPVCAAVEADIAELDDEERDEFMQELGLEEPG LNRVIRAGYKLLNLQTYFTAGVKEVRAWTIPVGATAPQAA GKIHTDFEKGFIRAQTISFEDFITYKGEQGAKEAGKMRAEG KDYIVKDGDVMNFLFNV*
N-terminal 6xHis tag *E. coli* YchF_NLSS	Pageni, unpublished	MGSSHHHHHHSSGLVPRGSHMGFKCGIVGLPNVGKSTLFN ALTKAGIEAANFPFCTIEPNTGVVPMPDPRLDQLAEIVKPQR TLPTTMEFVDIAGLVKGASKGEGLGNQFLTNIRETEAIGHV VRCFENDNIIHVSGKVNPADDIEVINTELALADLDTCERAIH RVQKKAKGGDKDAKAELAVLEKCLPQLENAGMLRALDLS AEEKAAIRYLSFLTLKPTMYIA**NLSE**DGFENNPYLDQVREI AAKEGSVVVPVCAAVEADIAELDDEERDEFMQELGLEEPG LNRVIRAGYKLLNLQTYFTAGVKEVRAWTIPVGATAPQAA GKIHTDFEKGFIRAQTISFEDFITYKGEQGAKEAGKMRAEG KDYIVKDGDVMNFLFNV*

[a] The asterisk at the end of each protein sequence indicates the stop codon.

Objective 1. Nucleotide binding

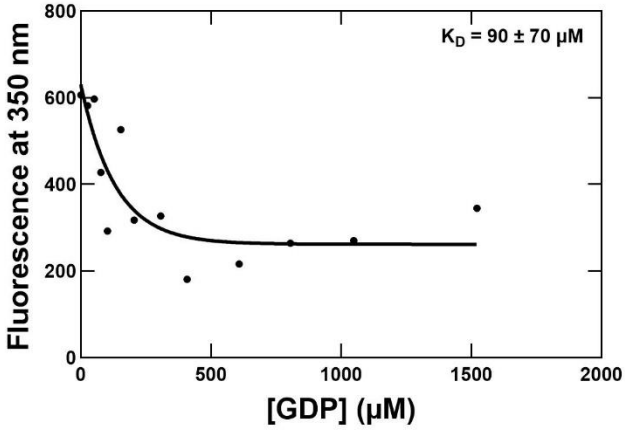

Figure A1. Assessing the inner filter effect on nucleotide binding. Tryptophan (1 µM) was prepared in TAKM7 buffer and was titrated with increasing concentrations of GDP (0-1500 µM) in a cuvette with 1 mm pathlength. The sample was equilibrated for 1 minute at room temperature, then excited at 280 nm to obtain the emission spectra. YchF dilution at each titration step was accounted for in the final calculations, as was the excitation of the nucleotide.